FIRE RESISTANCE OF COMPOSITE SLABS WITH STEEL DECKING AND THERMAL INSULATION

OTÁVIO GANDOLPHI DO NASCIMENTO RIBEIRO

Dissertation presented to the Escola Superior de Tecnologia e Gestão of the Instituto Politécnico de Bragança – ESTIG – IPB to obtain a master's degree in Construction Engineering.

Supervision of:

Prof. Dr. Paulo Alexandre Gonçalves Piloto

Prof. Dr. Gustavo De Miranda Saleme Gidrao

Braganca, 2025

FIRE RESISTANCE OF COMPOSITE SLABS WITH STEEL DECKING AND THERMAL INSULATION

OTÁVIO GANDOLPHI DO NASCIMENTO RIBEIRO

Supervisors:

Prof. Dr. Paulo Alexandre Gonçalves Piloto

Prof. Dr. Gustavo De Miranda Saleme Gidrao

May 11, 2025

“Somos a soma das
experiencias de todos aqueles
que vieram antes, é um
privilegio e uma
responsabilidade.”

(Otávio Ribeiro)

Obrigado, Bragança.

ACKNOWLEDGMENTS

First and foremost, I would like to express my profound gratitude to my family, the foundation and unwavering support of this journey. To my mother, Luciana do Nascimento, for her unconditional love and strength that has always guided me; to my father, Jean Ribeiro, for his wisdom and steadfast encouragement; and to my brother, Vinicius Gandolphi, for his camaraderie and motivation throughout. A special acknowledgement is also extended to Maria Rozane, for her patience, emotional support, and understanding during my prolonged absences, which were indispensable to the completion of this endeavour.

Secondly, I extend my sincere appreciation to my supervisors, Professor Paulo Piloto and Professor Gustavo Gidrão. To Professor Gustavo, for serving as an exemplary figure in my academic career, embodying the dedication and excellence I strive to emulate. To Professor Paulo Piloto, not only for his scholarly guidance but also for his invaluable support during my stay in Portugal, as well as the mentorship that has profoundly shaped my development as a researcher.

I must also acknowledge those who enriched my experience in Portugal, making it both memorable and culturally transformative. I am grateful to my friends who shared daily life with me: Guilherme Marconato and Athos Costa, my flatmates and companions through challenges, and to my dear friends Gabriela Lyra and Larissa Araújo, for their emotional support and the cross-cultural exchanges that broadened my perspective. This extends to all others whom space constraints prevent me from naming individually.

A distinct recognition is owed to the staff of the Polytechnic Institute of Bragança, particularly Tereza and Arminda from the library, whose kindness, efficiency, and unwavering assistance—even during demanding periods—were a constant source of reassurance.

Lastly, I express my gratitude to the institutions that enabled this Master's degree: the Polytechnic Institute of Bragança, for providing an exceptional academic environment, and the Federal University of Technology – Paraná (UTFPR), especially the COECI Guarapuava, for entrusting me with the opportunity to pursue this Master's in Construction Engineering.

This achievement is, above all, a reflection of the collective support I have received. To all, my eternal gratitude.

RESUMO

Esta pesquisa é sobre o comportamento termomecânico de lajes mistas aço-concreto com perfis trapezoidais e reentrantes sob condições de incêndio, com ênfase em estratégias de isolamento térmico passivo (proteção de aço e lã mineral) para aprimorar a segurança estrutural e reduzir impactos ambientais. O estudo integrou modelagem numérica bidimensional (ANSYS, Mechanical APDL), com validação usando resultados experimentais (testes em forno em escala real) e a apresentação de uma nova proposta de métodos simplificados para o Eurocódigo 4, visando preencher lacunas normativas relacionadas a geometrias complexas.

As simulações numéricas incorporaram mecanismos não lineares de transferência de calor (condução, convecção, radiação) e consideraram a existência de uma camada de ar entre a chapa de aço e o concreto, resultante da expansão térmica que promove a separação durante os ensaios. A validação do modelo numérico demonstrou concordância com dados experimentais, comprovando a precisão dos modelos. Sistemas com proteção de chapa de aço podem ser utilizados nas nervuras para reduzir significativamente a temperatura na face não exposta, aumentando a resistência ao fogo pelo critério de isolamento térmico (I). Já a lã mineral destacou-se como solução mais eficaz, garantindo maior resistência ao fogo e permitindo redução no consumo de concreto, o que contribuiu para a diminuição de emissões de CO_2.

Para o critério de capacidade estrutural (R), lajes com isolamento passivo mantiveram capacidade resistente superior em comparação a sistemas convencionais, mesmo após exposição prolongada ao fogo ISO 834. A calibração de coeficientes empíricos revisados para o Eurocódigo 4, que incorporaram o efeito de separação (camada de ar) e geometrias não convencionais, melhorou a precisão das previsões termo-estruturais, alinhando métodos analíticos a resultados experimentais.

Concluiu-se que a integração de isolamento térmico passivo e modelagem refinada oferece soluções equilibradas entre segurança contra incêndio, eficiência material e sustentabilidade. Recomenda-se o uso de geometrias otimizadas com isolamento adequado em edifícios de média a alta altura, garantindo resistência ao fogo conforme requisitos normpassivos e reduzindo o impacto ambiental associado à produção de concreto.

Palavras-Chave: Lajes mistas aço-concreto, resistência ao fog, Eurocódigo 4, Método dos elementos finitos, camada de ar, coeficientes empíricos, redução de CO_2, resistência ao fogo.

ABSTRACT

This study investigated the thermomechanical behaviour of steel-concrete composite slabs with trapezoidal and re-entrant profiles under fire conditions, with emphasis on passive thermal insulation strategies (steel shields and mineral wool) to enhance structural safety and reduce environmental impacts. The research integrated two-dimensional numerical modelling (*ANSYS, Mechanical APDL*), numerical validation (real-scale furnace tests), and a presentation of a new proposal to the simplified method in Eurocode 4, aiming to address normative gaps related to complex geometries and air gaps.

Numerical simulations incorporated nonlinear heat transfer mechanisms (conduction, convection, radiation) and accounted for an air gap between the steel and concrete, resulting from the thermal expansion verified during the experimental tests. The numerical validation demonstrated agreement with experimental results, confirming model accuracy. Systems with steel shields in the ribs significantly reduced temperatures on the unexposed face, enhancing the fire resistance regarding to insulation criterion (*I*). Mineral wool proved to be the most effective solution, ensuring prolonged fire resistance and enabling reduced concrete consumption, thereby contributing to lower CO_2 emissions.

For the structural capacity criterion (*R*), slabs with passive insulation maintained superior load-bearing capacity compared to conventional systems, even after prolonged standard ISO834 fire exposure. The calibration of revised empirical coefficients for Eurocode 4, incorporating the air gap effect and non-conventional geometries, improved the accuracy of thermal-structural predictions, aligning analytical methods with experimental results.

The study concluded that integrating passive thermal insulation and refined modelling offers balanced solutions between fire safety, material efficiency, and sustainability. The use of optimised geometries with appropriate insulation is recommended for medium to high-rise buildings, ensuring compliance with fire resistance requirements while reducing the environmental impact associated with concrete production.

Keywords: Steel-concrete composite slabs, fire resistance, Eurocode 4, Finite element method, air gap, empirical coefficients, CO_2 reduction, fire resistance.

LIST OF FIGURES

LIST OF TABLES

INDEX

1. INTRODUCTION

1.1. Contextualization

Fire safety aims to protect human life and property by reducing the risks of fatalities, injuries, material losses, and environmental damage resulting from accidental fires [1,2]. Since fire incidents in buildings can occur at any moment, it is impossible to eliminate their consequences after ignition. Therefore, preventive measures are crucial to ensure the survival of occupants and rescue teams, mitigating structural damage that may compromise the building's integrity (such as the spread of smoke and toxic gases), and preventing premature collapse or the spread of fire to neighbouring constructions [1,3]. It is vital, therefore, to ensure that structural components, such as concrete and steel, retain their mechanical strength during a fire, thus maintaining stability until safe evacuation can be achieved [1,3].

The construction industry is continually seeking innovative techniques, materials, and methodologies. Beyond functionality, durability, and safety, economic considerations play a pivotal role, driving the relentless pursuit of safer and more cost-effective alternatives [4]. Furthermore, the sector is under increasing pressure to reduce CO_2 emissions, with cement production alone responsible for approximately 9% of global carbon emissions [5,6]. Despite the availability of advanced technologies and diverse market solutions, cost-benefit analysis remains a critical determinant of project viability. Among these solutions, composite steel deck slabs stand out as a more efficient, sustainable, and lightweight structural option compared to conventional reinforced concrete slabs.

Composite steel deck slabs represent a highly efficient and lightweight structural solution compared to conventional reinforced concrete slabs. Owing to these advantages, this slab system has been extensively adopted in steel-framed building projects, particularly high-rise construction [7]. The system comprises a thin cold-rolled steel sheet, typically ranging in thickness from 0.6 to 1.2 mm, which serves as permanent formwork during concrete placement [8]. The concrete layer is generally reinforced with a lightweight anti-crack mesh and may incorporate additional reinforcement bars, often positioned within the ribs of the profiled steel deck. Crucially, the profiled steel deck functions as continuous positive reinforcement under sagging moments, thereby

obviating the need for temporary formwork and conventional reinforced concrete bars (rebar) [9].

Composite steel deck slabs offer notable advantages, including reduced concrete consumption, resulting in a lighter self-weight of the structure and shorter construction timelines, as the steel deck serves as permanent formwork. However, the unprotected steel deck within these slabs presents a significant drawback regarding fire resistance. When directly exposed to fire, the structural stability of the steel deck may be compromised due to a temperature-induced reduction in strength and stiffness [10]. This issue arises because the steel components are integral to the slabs' load-bearing capacity, which is critical for maintaining structural stability during a fire event. Furthermore, these slabs play a vital role in limiting fire propagation between building compartments, underscoring the importance of addressing their fire performance.

According to M. Crisinel and D. O'Leary [11], the first composite slab system was developed in the late 1930s for high-rise buildings. Owing to their efficiency and structural advantages, such slabs were rapidly adopted in steel-framed construction projects, including high-rise, low-rise, and industrial buildings. For decades, composite slabs were predominantly utilised in North America, with their use expanding significantly across Europe from the 1980s onwards. However, as noted by Cooke G. M. E. [12], widespread adoption in Europe occurred only after the 1980s, once sufficient empirical data had validated their performance and safety in practical applications.

In 2018, J. Jiang et al. [13] highlighted that reducing the use of concrete and shortening the construction period are advantages of this solution, as the steel plate replaces traditional formwork. Composite slabs employ cold-formed steel plates, which serve as formwork during construction and subsequently as reinforcement. The concrete is typically enhanced with a light crack-resistant mesh and may include steel bars arranged in the ribs. This solution has gained popularity in Europe due to its efficiency in terms of strength, stiffness and speed of execution.

Composite structures, particularly those made of steel, suffer significant losses in strength and stiffness at elevated temperatures, and may collapse if fire safety measures are not integrated into the design. Fire protection is crucial for building safety, aiming to reduce the risks of fatalities, injuries, material losses and environmental damage caused by accidental fires [2]. Protecting the structure and the building's contents is equally vital to prevent the spread of fire and structural collapse, ensuring that the structure endures long enough to safely evacuate occupants [3]. Property protection begins with the

preservation of the structure, the construction, and the building's contents. This is important to prevent the fire from spreading and causing structural collapse. In some countries, limiting environmental damage during large-scale fires is also necessary. The primary ecological concerns are pollution from firefighting water and the emissions of gaseous pollutants present in the smoke [2].

Composite slab models vary according to the intended service life, required strength, and stiffness. The steel sheeting profiles can be trapezoidal or re-entrant [14] (Figure 1.1). In addition to these more traditional profiles, studies conducted by Fourie [15] (Figure 1.2) employ a profile comprising two distinct regions: a larger trapezoidal region and a smaller re-entrant region. In these profiles, the sheeting may be exposed to environmental conditions, raising concerns regarding external influences, such as fire.

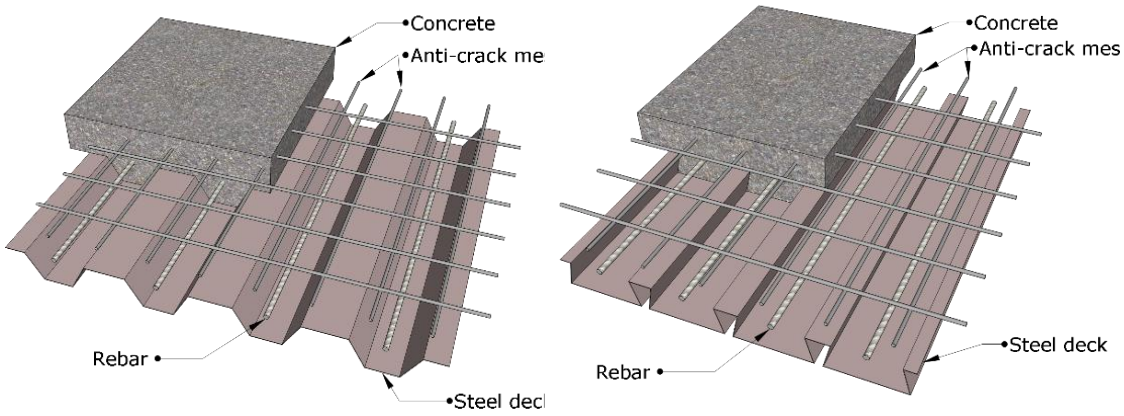

(a) (b)

Figure 1.1: Usual layout of composite slab profiles: (a) Trapezoidal, (b) Re-entrant. [4]

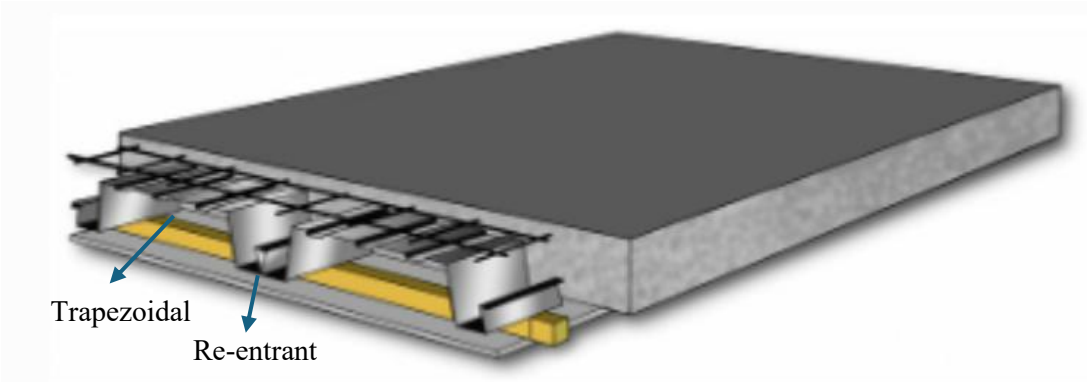

Figure 1.2: Layout of composite slab profiles used by Fourie [15].

The fire resistance classification of structural elements, as defined by Jiang et al.

[16], is determined by standardised tests that expose the element to a predefined temperature curve (such as ISO 834 [1]), evaluating criteria such as load-bearing capacity (R), thermal insulation (I), and integrity (E). These parameters guide designs to balance structural protection, fire containment, and occupant safety, underscoring the importance of solutions that combine durability, efficiency, and thermal resilience [1,2,16]. However, current normative methods, such as Annex B of prEN 1994-1-2, [17], exhibit significant limitations. For instance, they neglect the air gap effect (~0.5 mm), caused by the thermal expansion between steel and concrete, which reduces heat transfer and compromises accurate temperature prediction [13].

Furthermore, recent studies emphasise the importance of incorporating the cooling phase into structural analysis, as failures in frame connections and composite slabs are frequently observed during this stage, potentially leading to delayed collapses [25,93]. Gernay and Franssen [18] demonstrated that neglecting this phase results in overestimation of residual strength, while Ramesh et al. [19] and Choe et al. [20] linked beam-column connection failures to progressive slab collapse and fire spread between floors.

The thermal behaviour of composite slabs is influenced by heat distribution through conduction, convection, and radiation. Energy transferred via radiation and convection requires detailed analysis, as it determines the fraction absorbed by the steel sheeting and concrete. For non-conventional profiles, such as those proposed by Fourie [15], the simplified methods of PR EN 1994-1-2 [17] become inadequate, as they do not account for complex geometries or passive insulation strategies. Experiments conducted by Fourie [15] with steel shields demonstrated reductions of 16–41% in unexposed surface temperatures and a 19.35% reduction in concrete usage, validating the efficacy of innovative solutions.

Numerical simulations in ANSYS, validated with experimental data [15], revealed that insulation using steel shields or mineral wool significantly enhances load-bearing capacity under fire conditions. However, to replicate realistic scenarios, it is essential to incorporate a 0.5 mm air gap in models to simulate debonding between the sheeting and concrete during fire exposure [21]. This approach, not yet supported by the Eurocode prEN1994-1-2 [17], necessitates the calibration of new coefficients (*bi* for steel deck temperature and *ci* for reinforcement temperatures), as proposed by Piloto et al. [7] and Jiang et al. [13].

In summary, the absence of regulatory guidelines for innovative profiles, the

oversight of critical phenomena (such as cooling phases and air gaps), and the need for updated simplified methods highlight gaps in the fire safety of composite slabs. This research aims to address these gaps through numerical simulations, numerical validation, and the development of a new proposal with adjusted coefficients, contributing to more robust and resilient structural designs.

The scope of this investigation entails two-dimensional numerical simulations to evaluate the thermal behaviour of steel deck slabs, as proposed by Fourie [15], under passive thermal insulation conditions via a steel shield and mineral wool. Results derived from the numerical simulations, validated against experimental data, were critical for approximating new coefficients capable of informing design requirements in accordance with Eurocode 4 [17]. Furthermore, the study demonstrates performance enhancements across three vector dimensions: (i) the thermal insulation capacity of the system; (ii) the load-bearing structural performance; and (iii) sustainability criteria, wherein the practical efficacy of these insulants enables a significant reduction in material usage during the construction of such slabs.

1.2. Objectives

This research aims to advance the understanding of fire-resistant design methodologies for steel-concrete composite slabs through a holistic investigation encompassing numerical modelling, experimental validation, and sustainability assessment. The study addresses critical gaps in existing regulatory frameworks by integrating innovative thermal insulation strategies and refining predictive models for fire performance. The specific objectives are delineated as follows:

1. Thermal Behaviour Analysis:
    - To evaluate the transient thermal analysis of composite slabs under ISO 834 standard fire exposure, with emphasis on heat transfer mechanisms (conduction, convection, radiation) and temperature-dependent material degradation.
    - To quantify the influence of air gaps (~0.5 mm) arising from differential thermal expansion between steel decking and concrete on heat flux distribution and insulation performance.
2. Numerical Model Validation:

- To develop and validate two-dimensional finite element models in ANSYS, Mechanical APDL, incorporating advanced boundary conditions for radiative and convective heat transfer, comparing against full-scale experimental furnace tests conducted by Fourie (2020).
- To assess the accuracy of numerical simulations by benchmarking temperature profiles against experimental results, focusing on critical regions such as the steel deck's lower flange, web, and unexposed concrete surfaces.

3. Simplified Design Methodology Development:
    - To develop a new proposal with revised analytical coefficients (ai, bi, ci) for Eurocode 4 Annex B, enabling accurate predictions of fire resistance (insulation *I*) and load-bearing capacity degradation (criterion *R*) for composite slabs with passive insulation systems.
    - To extend Eurocode provisions to account for non-conventional profiles, and insulation strategies such as steel shields and mineral wool panels.
4. Insulation System Efficacy:
    - To compare the fire resistance enhancement offered by steel shields and mineral wool insulation in terms of:
        - Temperature mitigation at unexposed surfaces.
        - Structural ability preservation under sagging moments.
        - Delayed debonding at steel-concrete interfaces.
    - To evaluate the mechanical stability of insulation systems under prolonged thermal exposure, including anchorage robustness and thermal expansion effects.
5. Sustainability Integration:
    - To quantify reductions in concrete consumption and embodied carbon achievable through optimised slab geometries and insulation strategies, aligning with global decarbonisation targets.
    - To propose design recommendations balancing fire safety, structural efficiency, and environmental responsibility for high-rise and industrial applications.

1.3. Dissertation structure

This dissertation is structured to systematically address the research objectives through eight chapters, as outlined below:

- Chapter 1: Introduction

  Establishes the contextual framework for fire safety in composite slabs, highlighting the imperative for preventive measures, material efficiency, and regulatory advancements. Key challenges, including CO_2 emissions from concrete production and limitations in Eurocode methodologies, are introduced.
- Chapter 2: Literature Review

  Critically examines historical developments, experimental methodologies, and numerical advancements in composite slab fire investigations. Identifies gaps in current standards, particularly regarding cooling-phase phenomena, air gap effects, and insulation system integration.
- Chapter 3: Methodology for Thermal Analysis

  Details the finite element modelling approach using ANSYS, Mechanical APDL, including governing equations, mesh optimisation, and boundary condition definitions. Explains the weighted residual method (WRM) and describes the use of the finite element (PLANE55, LINK31, LINK34) for heat transfer analysis.
- Chapter 4: Development of the Numerical Model

  Presents geometric configurations, material properties, and parametric studies for composite slabs with trapezoidal and re-entrant profiles. Describes insulation system integration (steel shields, mineral wool) and validation against experimental datasets.
- Chapter 5: Simplified Calculation Methods

  Proposes refined Eurocode 4 coefficients for fire resistance prediction, incorporating air gap effects and insulation strategies. Derives quadratic relationships between the effective slab thickness and insulation performance.
- Chapter 6: Numerical and Analytical Results

  Compares temperature distributions, fire resistance durations, and load-bearing capacity degradation across insulation systems. Validates numerical models against experimental data and introduces revised empirical coefficients.
- Chapter 7: Mechanical Performance

  Evaluates structural resilience under fire exposure through bending moment

analysis. Quantifies CO_2 emission reductions achievable via material optimisation and insulation-driven concrete savings.

- Chapter 8: Conclusion

  Synthesises key findings, emphasising fire resistance enhancements, sustainability gains, and practical design recommendations. Discusses limitations and proposes future research directions, including 3D modelling and cyclic thermal durability studies.

- References

  Comprehensive compilation of academic literature, standards, and technical reports cited throughout the dissertation.

- Appendices

  Appendices of the 21 simulations conducted in the study, containing the boundary conditions, material types, finite element mesh, and results for the insulation and bearing capacity performance criteria.

This structure ensures a logical progression from theoretical foundations to practical applications, enabling researchers to implement findings in both academic research and industrial design contexts.

2. LITERATURE REVIEW

2.1. State of the art

The behaviour of composite structures, particularly concrete-steel composite slabs, has emerged as a significant research field, driven by a series of experimental studies on isolated components and the ongoing development of numerical models for system analysis. Building on this research, methodologies have been established to predict the fire resistance duration of these elements under standard fire conditions (e.g., ISO 834), advancing structural design practices and enhancing the safety of human lives and infrastructure.

Advances in computational technology have prioritised sophisticated structural analysis methods, which offer a superior cost-benefit ratio and yield results comparable to experimental testing. Consequently, refining numerical techniques is critical to improve the accuracy of structural assessments in fire scenarios. Furthermore, enhanced analytical precision enables structural optimisation, reducing material consumption in construction while maintaining performance. This approach supports sustainability objectives by minimising embodied carbon and associated CO_2 emissions.

The following section provides a concise literature review of studies on concrete-steel composite slabs under fire exposure. It examines the historical context, current advancements, and critical analyses of fire incident statistics in built environments. Additionally, it explores sustainable design solutions that balance fire resistance, structural integrity, and environmental responsibility.

2.1.1. Experimental test

In 1961, the International Standards Organisation (ISO) constituted a committee to establish specifications for fire resistance testing methodologies. This initiative synthesised the American ASTM E119 (1918) and British BS 476 (1932) temperature-time curves, culminating in the first harmonised model for a standardised fire exposure regime [22].

The resultant standard fire curve was formally promulgated in 1975 through ISO 834 Fire Endurance Testing – Building Elements. This framework underwent subsequent

refinement, with the inaugural edition of ISO 834-1 [1] superseding the original standard in 1999. Key revisions included adjustments to permissible deviations between furnace temperature profiles and the nominal fire curve, alongside updated specifications for instrumentation and measurement protocols.

The standard ISO 834 prescribes three discrete criteria for evaluating fire resistance under standardised time-temperature conditions: load-bearing capacity (R), denoting structural integrity under applied loads; integrity (E), preventing flame or smoke penetration; and thermal insulation (I), which imposes temperature limits on the unexposed slab surface to mitigate fire propagation.

As noted by Cooke [12], such fire testing procedures remain resource-intensive, constrained by logistical challenges such as extended concrete curing periods and the operational demands of full-scale furnace experiments. This historical progression underscores the iterative development of fire safety standards, balancing empirical validation with the practical exigencies of construction material behaviour under thermal loading.

In Europe, the European Convention for Steel Construction (ECCS) [23] pioneered the formalisation of calculation methodologies for composite slab design under fire conditions. In 1983, the ECCS published foundational calculation rules for the practical design of steel-concrete composite slabs with profiled steel decks subjected to standardised fire exposure. These performance criteria were derived from a streamlined interpretation of the ISO 834 fire resistance principles, catalysing subsequent academic and industrial efforts to refine both simplified analytical and advanced numerical modelling approaches.

While composite slabs had been utilised in North America since the 1970s, their adoption in the United Kingdom gained significant traction in 1980. However, European regulatory bodies raised concerns regarding the paucity of empirical data on composite slab fire resistance, which fell short of the stringent fire safety benchmarks mandated by emerging European standards [24]. This deficiency prompted an extensive programme of large-scale fire testing commencing post-1982, aimed at generating robust experimental datasets to validate design methodologies and ensure compliance with performance requirements.

The ECCS framework, by harmonising theoretical and empirical insights, marked a pivotal advancement in standardising fire-safe composite slab design across Europe. This initiative addressed regulatory apprehensions and stimulated further research into

optimising thermo-structural models, thereby enhancing the reliability and applicability of composite systems in fire-prone built environments.

Following investigations into fire resistance during 1988, G. Cooke et al. [12] sought to demonstrate the feasibility of composite slabs achieving a 90-minute fire resistance rating without requiring supplementary insulation on the exposed slab surface, utilising solely a steel reinforcement grid positioned at the slab's upper face. Prior to this research, adherence to this fire resistance criterion necessitated the incorporation of conventional reinforcing bars. The study drew upon experimental data derived from fire tests conducted by the Construction Industry Research & Information Association (CIRIA) between 1983 and 1985, and by the British Steel Corporation (BSC) between 1984 and 1986. Analysis of these test outcomes substantiated that including negative moment reinforcement grids at the slab's upper surface enabled the attainment of the stipulated 90-minute fire resistance threshold. Additionally, the experimental trials revealed that slabs incorporating recessed profiled geometry exhibited superior thermal insulation and shielding performance compared to those with trapezoidal profiles, underscoring the influence of geometric configuration on fire-resistant behaviour.

Between 1995 and 2003, the Building Research Establishment (BRE) conducted a series of full-scale fire tests at the Cardington laboratory, as comprehensively documented in 1999 [25]. These experiments involved an eight-storey steel and composite construction building, subjected to varied fire scenarios, with dimensions of 21 m × 45 m and a total height of 33 m. Mechanical loading was applied through distributed sandbags in addition to the structure's self-weight. As no structural collapse was observed during the trials, the findings validated the conservative nature of Eurocode fire design methodologies. The primary objective of these tests was to generate representative fire performance data to support the validation and verification of advanced computational programmes for numerical analysis of structural behaviour under fire conditions. The study concluded that the structural configuration demonstrated adequate fire safety performance, indicating that a standard office building—modelled through the applied load distribution—would exhibit comparable fire resistance characteristics. Furthermore, the experimental results provided critical insights into the behaviour of slab-to-beam and beam-to-column connections under thermal loading, contributing to the refinement of analytical and numerical modelling approaches for fire-resistant structural design.

In 1998, C. Both [26] conducted a comprehensive experimental investigation aimed at establishing accessible calculation methodologies and enhancing understanding of fire

behaviour and failure mechanisms, with a focus on continuous composite slabs. The study concluded that the proposed thermal model effectively characterised two- and three-dimensional heat transfer within composite slabs under fire conditions. Furthermore, it highlighted opportunities to refine the fire resistance assessment guidelines outlined in Eurocode 4 at the time, suggesting substantial potential for improvement.

In 1999, Abdel-Halim et al. [27] examined the performance of composite slabs subjected to fire, with particular emphasis on the influence of supplementary reinforcement on fire resistance. The experimental programme compared failure modes related to insulation and integrity criteria. In the first test, insulation failure occurred at 86 minutes, while the second test exhibited insulation failure at 80 minutes. Integrity failure was observed after 192 minutes in the first test and 180 minutes in the second. The study concluded that the separation of the steel decking from the concrete during fire exposure negated its contribution to the slab's thermal resistance, underscoring the importance of considering this detachment in design evaluations.

In 1999, Bailey et al. [28] reported findings from two full-scale experimental tests conducted by the Building Research Establishment (BRE) in the UK, which revealed that structural performance under fire conditions deviated from the assumptions of prescriptive fire resistance codes. The results demonstrated that the codes' provisions were unduly conservative, as the structural elements exhibited enhanced robustness compared to predictions. The tests further highlighted discrepancies between the observed fire behaviour and outcomes derived from standard small-scale fire resistance tests, emphasising the limitations of conventional testing methodologies. The study concluded that composite slab systems exhibited favourable fire resistance characteristics, challenging existing code-based expectations.

In a 2019 investigation, Piloto et al. [24] analysed the fire performance of composite slabs incorporating a profiled steel plate. The structural configuration comprised a steel deck overlaid with a concrete layer to resist negative bending moments and mitigate concrete cracking, supplemented by a steel mesh in the upper region. Individual reinforcing bars were positioned between the deck's ribs to enhance resistance to positive bending. Notably, the steel plate functioned as primary tensile reinforcement under fire exposure, with its direct interaction with fire conditions forming a critical aspect of the study. This composite system, widely employed in buildings requiring regulated fire resistance, was evaluated using the ISO 834 standard fire curve. Two specimens were tested to assess integrity (E) and insulation (I) criteria, with a specific focus on insulation

resistance classification. The investigation revealed that PR EN 1994-1-2 overestimates the fire resistance of such composite slabs, potentially yielding non-conservative predictions.

In 2020, Fourier [15] conducted an experimental investigation to evaluate the thermal performance of composite slabs with integrated steel reinforcements under fire conditions. The study employed a full-scale furnace test setup, exposing a composite slab specimen—comprising a profiled steel deck, concrete fill, and strategically placed steel shields—to the ISO 834 standard fire curve. Thermocouples were embedded within the concrete and steel components at critical depths to monitor temperature gradients and heat flux distribution. Fourier's work specifically examined the efficacy of steel shields in mitigating heat transfer through the thinnest regions of the slab (i.e., between decking ribs), a design feature intended to delay insulation failure. The results demonstrated that the steel shields reduced peak temperatures at the unexposed surface by approximately 15–20% compared to conventional configurations, thereby extending the insulation resistance period. However, challenges were noted regarding the mechanical stability of the shields during prolonged fire exposure, as thermal expansion caused partial detachment from the decking. This study highlighted the potential of innovative shielding systems to enhance fire resistance while underscoring the need for robust anchoring solutions to ensure long-term performance under thermal stress.

Bolina et al. [29] in 2021 investigated the thermal behaviour of reinforced concrete composite slabs under fire conditions, with the objective of comparing cross-sectional temperature distributions derived from experimental, numerical, and analytical methodologies. The study encompassed eight full-scale fire tests, during which specimens were exposed to the ISO 834 standard fire curve. Experimental data were utilised to calibrate numerical models developed in ABAQUS software, and both approaches were subsequently evaluated against the analytical method prescribed by PR EN 1994-1-2 [17]. Key findings revealed that steel deck detachment occurred within the initial five minutes of fire exposure, leading to a premature loss of composite action. This observation indicated that the structural benefits associated with composite slab behaviour were largely absent during the majority of the fire resistance period. The authors concluded that the assumptions underlying Table D.6 of PR EN 1994-1-2 [17], which governs the calculation of composite slab resistance, required revision to account for the early degradation of steel-concrete interaction. The study underscored the limitations of current Eurocode provisions in predicting real-world thermal performance and emphasised the

necessity of integrating empirical observations into design frameworks.

2.1.2. Numerical simulations

Between 1983 and 1985, the Construction Industry Research and Information Association (CIRIA), commissioned by leading UK steel deck manufacturers, conducted a comprehensive fire-testing programme. The study employed six loaded composite slab specimens (one full-scale and five reduced-scale), incorporating steel reinforcement meshes, to evaluate fire performance. Key findings indicated that prevailing design recommendations were overly conservative, with slabs featuring dovetail profiled steel decks demonstrating significantly enhanced fire resistance compared to trapezoidal profiles [12].

In 1990, Hamerlinck et al. [30] addressed the limitations of ISO 834-based experimental analyses—notably their prohibitive cost and duration—and the excessive conservatism of the ECCS 1984 [31] structural safety model. They developed a coupled thermal-mechanical simulation framework to predict the behaviour of concrete-steel composite slabs under fire conditions. The model was validated via experimental testing on twelve specimens with varied steel profile geometries and consistent concrete thicknesses, integrated cross-sectional thermal-mechanical analyses, and global structural response assessments. Validation trials at the Institute for Building Materials and Structures (TNO) confirmed that numerical predictions of temperature evolution exhibited a strong correlation with experimental data.

In 1991, Hamerlinck [32] methodologically delineated the analytical frameworks underpinning his fire-exposure models for composite slabs, emphasising the segregation of heat transfer mechanisms and mechanical response calculations. The study incorporated numerical validation, confirming negligible divergence between predicted and empirical data. The thermal model dissected two critical phenomena: (i) conductive heat propagation within the slab matrix, and (ii) convective-radiative boundary interactions at exposed surfaces.

Subsequently, Both [33] (1996) advanced a thermally explicit numerical model to simulate temperature distributions in concrete-steel composite slabs under fire conditions. Twelve parametric tests evaluated the influence of steel deck geometry and concrete thickness on thermal performance. The framework considers:

1. Zinc layer fusion effects, modelled via temperature-dependent emissivity adjustments to account for phase transitions in the steel deck coating.
2. Moisture evaporation dynamics, addressed through a temperature-specific heat correlation to replicate transient hygrothermal behaviour in concrete.

According to the author, the model presented satisfactory results since it showed similarities with the results obtained in the experimental tests.

In 1997, Both [34] formulated a finite element model using DIANA software to assess the thermomechanical response of Slim Floor systems under fire exposure. The study identified a critical threshold at 100°C, where hygrothermal degradation (moisture evaporation) within the concrete matrix induced debonding at the steel-concrete interface. This interfacial separation necessitated the incorporation of radiative-convective heat transfer mechanisms within the resultant air gap, refining the model's fidelity to physical behaviour.

Subsequently, Lamont et al. [35] (2001) employed the finite element software HADAPT to conduct 2D non-linear transient thermal analyses, benchmarking results against the Cardington fire test series. The numerical framework replicated concrete temperature evolution in alignment with experimental data for an initial period. Notably, experimental trials exhibited a transient thermal plateau at 100°C, attributed to latent heat absorption during moisture vaporisation, which reduced heating rates. Conversely, simulations displayed sustained temperature escalation, lacking this stabilisation. The authors justified this discrepancy to the differential moisture content between modelled and Cardington test concrete specimens.

In 2004, Lamont et al. [14] conducted a finite element analysis using ABAQUS to investigate the thermomechanical behaviour of a five-storey steel-concrete composite structure under two distinct fire scenarios: (i) a short-duration, high-intensity fire and (ii) a prolonged, lower-intensity fire. Numerical models were validated against experimental data from the Cardington test series. The study revealed that short-duration, high-intensity fires induce rapid structural degradation, characterised by accelerated deformation rates leading to premature collapse. This finding contradicted conventional structural assessments based on temperature-time curve integration, which prioritise cumulative thermal exposure.

Conversely, prolonged fires with reduced peak temperatures resulted in elevated steel and concrete temperatures over extended durations. While such scenarios produced greater ultimate material temperatures, the delayed thermal penetration mitigated

immediate displacement risks. The authors posited that short-duration fires pose a critical threat to structural integrity due to their capacity to exceed deformation thresholds before thermal equilibration, whereas prolonged fires permit gradual load redistribution, deferring failure mechanisms [14].

In 2017, Jiang et al. [36] undertook a parametric numerical study to evaluate factors influencing the fire resistance of composite slabs under thermal insulation criteria (I). The research introduced a revised analytical formulation incorporating explicit moisture content parameters to quantify fire resistance, addressing limitations in existing predictive models. Through systematic analysis of 54 composite slab configurations, the authors identified concrete thickness and hygrothermal properties (moisture content) as the predominant determinants of insulation performance. These findings underscored the necessity of integrating transient moisture dynamics into fire resistance calculations, challenging conventional assumptions prioritising geometric or material composition factors alone.

In recent years, advancements in finite element analysis software have facilitated the development of diverse thermal and structural models to predict the thermo-structural behaviour of steel-concrete composite slabs under fire conditions.

In 2018, Piloto et al. [37] conducted an investigation into the fire resistance of composite concrete slabs incorporating profiled steel decks with an upper steel mesh and reinforcing bars positioned between deck ribs. The primary objective of this study was to formulate a two-dimensional numerical model utilising MATLAB and ANSYS software to assess the fire resistance of varied composite slab configurations in alignment with thermal insulation criteria. The study evaluated the insulation criterion (I) through numerical simulations and simplified computational methodologies, with validation provided by experimental fire tests. Results indicated that fire resistance (I) significantly increases with concrete thickness, across both approaches. However, the numerical method yielded conservative predictions of fire resistance (I) relative to established standards, thereby demonstrating enhanced reliability in ensuring structural stability. Consequently, the authors proposed a novel analytical framework incorporating a quadratic relationship between fire resistance and the effective thickness of composite slabs, offering improved predictive accuracy for engineering applications. This revised approach underscores the necessity of integrating refined computational methodologies to better align theoretical models with empirical performance data in fire safety engineering.

In 2019, P.A.G. Piloto et al. [21,38] conducted a study using ANSYS and MATLAB software to perform numerical simulations of a standardised fire, incorporating three-dimensional numerical validated models to assess load-bearing (R) and thermal insulation (I) criteria. The study aimed to evaluate the influence of applied loads on the structural resistance criterion (R) and the relationship between concrete thickness and insulation performance (I). For the thermal analysis, the authors modelled the phenomenon wherein rapid heating and expansion of the steel deck during fire exposure induces separation from the concrete layer, introducing an alternative computational approach incorporating air gaps at the steel-concrete interface. This interfacial separation, termed the "air-gap" effect, was found to significantly influence fire resistance predictions. The authors concluded that conventional standardised formulations overestimate the composite slab's actual fire resistance, while simulations assuming perfect steel-concrete contact conversely underestimate performance. This discrepancy arises due to the insulating properties of the air gap, which enhances the composite system's thermal resistance. Furthermore, the proposed revised formulation for insulation criterion (I) demonstrated a quadratic correlation between fire resistance and the slab's effective thickness, offering improved alignment with experimental observations.

Concurrently in 2019, Balsa et al. [39] advanced the validation of thermo-mechanical numerical models through ANSYS-based refinements, substituting solid finite elements with shell elements to represent the air layer between steel and concrete. This new modelling technique reduced computational processing time significantly by minimising nodal density within the thermal model. The revised approach also enhanced predictive accuracy for insulation criterion (I), yielding results within 3.88% of experimental values when simulating a 0.50 mm air gap. The study highlighted the efficacy of shell elements in balancing computational efficiency with precision, particularly in capturing critical interfacial thermal behaviours under fire conditions.

In 2021, P.A.G. Piloto and Balsa et al. [40] conducted a study investigating the influence of varied steel deck geometries on the thermal performance of composite slabs under standard fire conditions through computational simulations. Employing the MATLAB Partial Differential Equations (PDE) Toolbox, three-dimensional finite element models were developed to simulate full-scale fire testing scenarios. The resultant data informed the formulation of a novel analytical methodology as an alternative to the PR EN 1994-1-2 standard for predicting temperature distributions within slab

components, including the lower and upper flanges, web, and reinforcement bars. The proposed method enhances temperature estimation accuracy across discrete time intervals (45, 60, 90, and 120 minutes) by calibrating analytical expressions against numerical reference values. However, the use on the Generalised Reduced Gradient (GRG) optimisation method to derive empirical coefficients introduces uncertainty regarding the attainment of optimal or quasi-optimal solutions, highlighting potential limitations in the model's generalisability.

Concurrently, Bolina et al. [29] (2021) examined the thermal behaviour of steel-concrete composite slabs subjected to standardised fire exposure, comparing cross-sectional temperature distributions derived from experimental, numerical, and analytical approaches. Numerical models, developed using ABAQUS software, were calibrated against eight full-scale fire tests conducted by the authors. Discrepancies were observed between the temperature predictions of the PR EN 1994-1-2 [17] analytical method and those obtained via numerical and experimental methodologies, particularly for the steel deck. While limited convergence between analytical and empirical-numerical results was noted for the steel deck, significant deviations persisted for concrete, reinforcement bars, and thermal insulation components. Consequently, the authors proposed a revised analytical framework incorporating a novel approximation for rebar temperature estimation and an additional factor to evaluate thermal insulation performance, addressing identified gaps in existing standards.

These studies collectively emphasise the critical need for refining analytical models to account for material-specific thermal interactions and advocate for iterative validation against empirical data to enhance predictive reliability in fire safety engineering.

2.1.3. Demand for Sustainable Construction

Since the Industrial Revolution, the annual increases in energy consumption and greenhouse gas emissions from human production activities have led to global warming. According to the Fifth Assessment Report by the Intergovernmental Panel on Climate Change (IPCC), the global average temperature rose by approximately 0.8 °C between 1880 and 2012. Following this trend, the global average temperature is projected to increase by 3 ± 1.5 °C by the end of this century, which may result in sea-level rise and extreme temperature events, threatening species survival [91].

The construction industry accounts for 40% of global energy consumption and 36% of carbon emissions, respectively [42]. Among industrial sectors, construction is the largest carbon emitter due to the energy-intensive nature of its materials [43]. The production of building materials generates most carbon emissions (64.5%) over a building's lifecycle. Specifically, the production and use of steel and concrete are the primary contributors to emissions associated with this sector. Notably, steel's recyclability is superior to that of concrete, and the quantity of steel used is significantly lower than that of concrete. Consequently, concrete is the largest contributor to carbon emissions over a building's lifecycle. To mitigate the carbon footprint of construction, replacing concrete with low-energy materials is imperative.

2.1.4. Fire accidents statistics

Fires pose a critical global threat, with over 300 000 annual fatalities attributed to fire-induced burns, predominantly in low- and middle-income countries (LMICs) [44]. Residential fires account for 80% of fire-related deaths in the United States, occurring every 85 seconds [45,46], while 78% of unintentional fire fatalities in London arise from residential incidents [47]. Human behaviour, particularly unsafe practices, is a primary causative factor [48], exacerbated by evacuation challenges in densely populated residential complexes [49,46]. Despite 75% of fires being preventable [50], inadequate fire alarm systems and insufficient preventative measures persist as key vulnerabilities, with 39% of fires in China (2007–2010) originating in residential settings [51].

Mitigating fire-related injuries necessitates systematic strategies, including public safety campaigns, evacuation training, and legislative reforms [52,53]. Architectural design prioritising fire-resistant features and robust alarm systems is critical to safeguarding occupants [54]. To address gaps in current safety frameworks, a comprehensive review of risk factors and preventative measures is urgently required, particularly for residential buildings [55]. Such efforts align with global sustainability agendas, aiming to reduce human casualties and economic losses while enhancing community resilience [56].

2.2.Characterisation of composite slabs

A steel-concrete composite slab is a structural system comprising interconnected materials that synergistically contribute to load-bearing capacity. The slabs consist of a thin cold-rolled steel sheet, typically with thicknesses ranging from 0.6 to 1.2 mm, over which concrete is poured [8], reinforcing bars and a light reinforcement mesh. The system is characterised by a reinforced concrete layer cast atop a steel deck, which may incorporate additional rebar within the ribbed sections (Figure 1.1). The steel deck fulfills three critical functions: temporary working platform, permanent formwork, and positive moment reinforcement. This configuration ensures structural light weight, offering enhanced efficiency and cost-effectiveness compared to conventional slabs. Composite slabs are integral to the global stability of buildings under fire conditions and must comply with regulatory standards [28].

Key advantages include reduced concrete usage, lowering self-weight, and accelerated construction timelines due to the steel deck's dual role as formwork. However, the presence of an unprotected steel deck in composite slabs represents a significant disadvantage in terms of fire resistance. When directly exposed to fire, the steel deck's structural stability can be compromised due to the temperature-induced reduction in strength and stiffness [10]. This issue arises because the steel components are primarily responsible for the load-bearing capacity of the composite slabs, which are crucial for maintaining the structure's stability during a fire. Additionally, these slabs play a vital role in preventing the spread of fire to other compartments within the building.

2.2.1. Application Fields

Composite steel-concrete slabs are widely adopted across construction sectors due to their structural efficiency, economic viability, and adaptability to architectural and logistical demands. Their use spans commercial, industrial, residential, and institutional projects, driven by their capacity to balance load-bearing performance with rapid construction timelines [57].

Composite slabs are extensively utilised across diverse sectors due to their adaptability and efficiency. In commercial and office developments, these elements enable long spans with minimal intermediate supports, which is ideal for flexible layouts in urban high-rises, while retail and leisure sectors benefit from rapid installation via steel decking acting as permanent formwork. Industrial and logistics facilities leverage their

high load-bearing capacity to sustain heavy machinery and embedded services, aligning with prefabricated construction principles to minimise waste. Residential applications exploit their lightweight nature for expedited construction in dense urban areas, compatible with hybrid systems (e.g., steel-masonry) and heritage retrofitting. Educational infrastructure prioritises its vibration-damping properties and adaptability, facilitating acoustic insulation or underfloor heating integration without structural compromise [58].

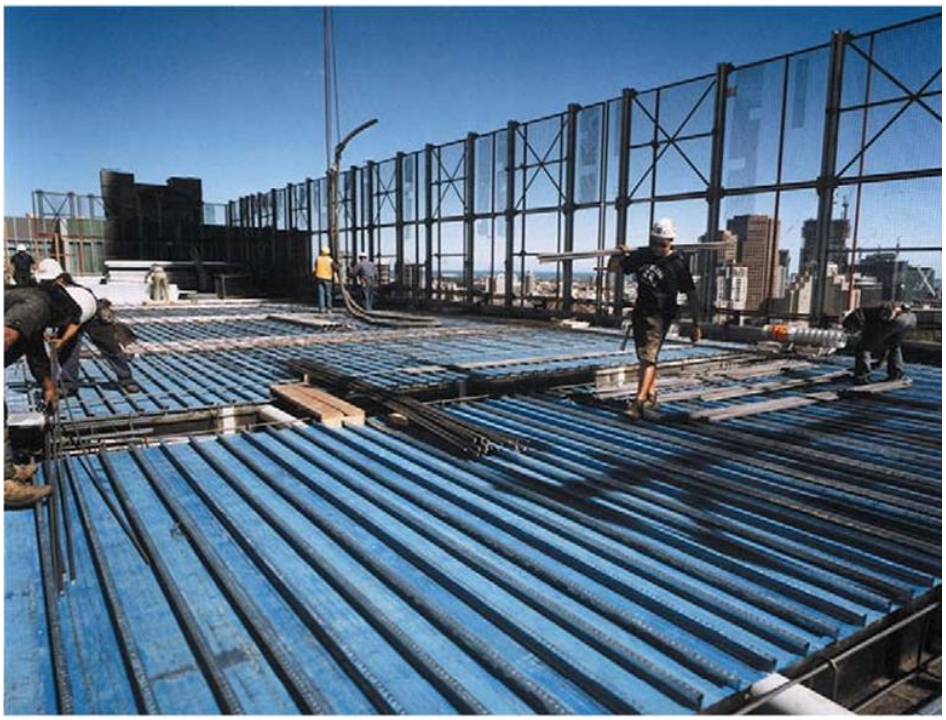

Figure 2.1: Composite floor in construction for a high-rise office and residential complex in Melbourne [58].

Challenges persist in environments requiring stringent acoustic performance or specialised load distributions. The geometric profile of steel decking, for example, may necessitate additional damping layers to mitigate noise transmission in residential or mixed-use developments. Similarly, asymmetrical loading conditions in industrial settings demand careful consideration of shear connector spacing and concrete thickness to prevent premature deflection.

Emerging trends focus on material innovation and sustainability. Advances in steel profiling, such as cellular voids or hybrid rib geometries, enhance shear bonding while accommodating service integrations within reduced slab depths. Recyclability of steel components aligns with circular economy principles, reducing embodied carbon in line

with global sustainability agendas.

In summary, composite slabs address competing demands of structural performance, construction efficiency, and environmental responsibility. Their adoption reflects a balance between empirical engineering principles and innovative solutions tailored to evolving architectural, logistical, and regulatory priorities.

2.2.2. Fire Safety Verification of Steel-Deck Composite Slabs

In the context of elucidating the historical development of structural safety considerations during fire events, the European Convention for Constructional Steelwork (ECCS) first introduced foundational principles in Europe through its publications. Subsequent contributions by researchers, including Hamerlinck R. and Booth K. [30], informed the formulation of PR EN 1994-1-2 [17], which outlines methodologies for determining the fire resistance of structural components. Compliance with fire safety requirements, as stipulated by building regulations, necessitates adherence to these standards.

Traditionally, fire resistance evaluations have relied on fire testing of individual structural elements, such as beams and columns. For composite slabs, fire ratings are typically derived from standardised furnace tests, which assess three critical criteria: insulation (I), integrity (E), and load-bearing capacity (R). Fire resistance classifications are expressed in incremental intervals of 30 minutes, ranging from 15 to 240 minutes, with extended durations applicable to scenarios requiring higher fire ratings [59]. These classifications ensure structural elements meet prescribed performance thresholds under defined thermal exposure conditions.

The European Standard EN 13501-2 [59] establishes the criteria and fire rating system for the fire rating of building products and structural elements. The classification, denoted as REI, specifies the duration (in minutes) during which the three fundamental criteria—load-bearing capacity (R), integrity (E), and thermal insulation (I)—are collectively satisfied. Crucially, the standard clarifies that these criteria need not be met simultaneously; depending on the functional role of the structural component, compliance with two criteria (RE) or solely the load-bearing criterion (R) may suffice.

To ensure structural integrity and prevent collapse during fire events, experimental testing under controlled thermal conditions is mandated. Such tests are conducted in

accordance with the standardised heating curve defined by ISO 834 [1], which quantifies fire resistance as the time (in minutes) until structural failure occurs. National building codes prescribe minimum fire resistance durations for specific building elements, while EN 13501-2 [59] provides a harmonised framework for fire ratings. This framework serves as a critical reference for both commercial design applications and academic research to optimise current fire safety methodologies, as exemplified in this thesis.

The present study focuses on evaluating fire resistance under the thermal insulation criterion (I), alongside the performance of temperature-affected components in maintaining load-bearing capacity. The subsequent subsections detail the three fire resistance criteria (REI) as applied to composite slab systems, elucidating their interdependencies and operational significance in fire safety engineering.

2.2.2.1. Insulation proposal

To extend the load-bearing capacity time (R), Fourie (2020) [15] proposed a novel type of insulation for composite slabs with steel decking, as illustrated in Figure 2.2.

(a)

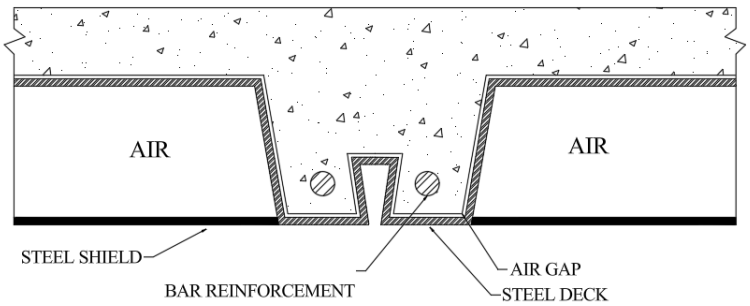

(b)

Figure 2.2. Slab model presented by Fourie [15]. (a) Slab before test 2 (b) Schematic representation.

The insulation consists of a steel plate, referred to as a steel shield, attached to both ends of the lower regions of the rib, creating an area shielded from direct exposure to fire.

To analyse the thermal behaviour of this new proposal, Fourie (2020) [15] conducted two experimental tests, where the difference between the tests lies in the presence of the steel shield. Thermocouples were placed on the lower, web, upper, and rebar, with a fire duration of 90 minutes for test 1 and 80 minutes for test 2. The results indicate that including steel shields reduces the unexposed surface average temperature by 16% to 41% [8]. This reduction contributes to a 19.35% decrease in concrete usage [15].

2.3. Fire resistance criteria

Composite slabs must comply with fire safety standards outlined in building codes, which typically require fire resistance durations of 30, 60, 90 minutes, or longer. The fire rating of these structural components is generally determined through standard fire resistance testing [9-26-60] and must account for three key criteria: stability (R), integrity (E), and insulation (I). The fire resistance rating of the slab is defined by the shortest time at which failure occurs in any of these three categories (R, E, or I), even if the other criteria remain intact for a significantly longer period [32].

The European standard EN 13501-2 [59] establishes the framework for defining fire resistance classification criteria and performance ratings applicable to construction materials and structural components. This standard further specifies that the three principal criteria (e.g., load-bearing capacity, integrity, and insulation) need not be simultaneously satisfied for all structural elements. Compliance with fire safety requirements may instead be achieved through the fulfilment of two or even a single criterion, contingent upon the functional role and performance expectations of the component under assessment.

2.3.1. Load-bearing Capacity (R)

Load-Bearing Resistance (R) is defined as the capacity of a structural element to withstand applied loads without collapse or excessive deformation. When membrane action is disregarded [32], three primary failure modes govern structural performance:

flexural failure, longitudinal shear failure, and vertical shear failure. Compliance with the functional adequacy criterion under fire exposure is specified by the international standard EN 1363-1 [9], which establishes permissible limits for maximum deflection (D_{limit}) and maximum deflection rate ($\frac{dD}{dt}$)$_{\text{limit}}$ as follows:

$$D_{limit} = \frac{L^2}{400d} \text{ [mm]} \tag{2.1}$$

$$\left(\frac{dD}{dt}\right)_{limit} = \frac{L^2}{9000d} \text{ [mm/min]} \tag{2.2}$$

Here, L denotes the span of the slab [mm], d represents the distance from the extreme compression fiber to the extreme tensile fiber of the cross-section under ambient conditions [mm], and t is the fire-exposure duration [min].

The revised 2020 edition of EN 1363-1 [9] introduces updated failure criteria for load-bearing resistance. Structural failure is deemed to occur under either of the following conditions:

1. The maximum displacement exceeds 1.5 x D_{limit}, or
2. Concurrently, the maximum displacement reaches D_{limit} *and* the deflection rate attains $(dD/dt)_{limit.}$

These dual criteria ensure a comprehensive evaluation of structural capacity under fire conditions, addressing both instantaneous deformation thresholds and progressive deformation rates.

2.3.2. Fire resistance by Insulation (I)

The current computational framework for assessing the fire resistance by insulation criterion (*I*) of composite slabs is rooted in the idealised representation of the composite steel-concrete 2D cross-section. This simplification enables transient heat transfer modelling, where the fire performance of unprotected concrete and steel composite structures (i.e., those lacking external thermal insulation on the fire-exposed face) is defined by slab-specific geometric parameters, such as rib height, sheet thickness, and concrete cover.

Fire resistance by insulation 'I' corresponds to the ability of the element to limit the evolution on the unexposed face. The limit is set to an average increase of 140 ºC or a

localised maximum 180 ºC rise, above the initial average temperature [61]. This methodology inherently relies on tracking the temperature evolution on the unexposed side.

The equations (2.3) and (2.4) express the application of the criterion.

$$T_{MAX} = 180 + \theta_0 \ [°C] \tag{2.3}$$

or

$$T_{AVE} = 140 + \theta_0 \ [°C] \tag{2.4}$$

2.3.3. Integrity (E)

The integrity criterion (*E*), as defined in EN 1363-1 [9], evaluates the ability of a structural element to prevent the passage of flames or hot gases through cracks, fissures, or other discontinuities during fire exposure. For *in situ* cast concrete slabs, compliance with this criterion is typically inherent due to the monolithic nature of the concrete matrix, which provides intrinsic crack resistance under thermally induced deformations, coupled with adherence to joint sealing protocols. In composite steel/concrete slabs, the integrity condition (*E*) is presumptively satisfied by the continuous steel deck, which acts as a flame and gas barrier, provided the steel sheet retains its structural continuity and load-transfer capacity during fire exposure.

Failure of the integrity criterion occurs if sustained flaming, flame penetration, or structural discontinuity (e.g., cracks exceeding allowable limits) is observed on the unexposed surface, as per standardised test procedures. Critical failure modes include rupture of the steel deck due to thermal buckling or oxidation, or delamination at the steel-concrete interface, compromising the slab's ability to resist gas infiltration.

2.4. Heat transfer and thermal actions

Heat transfer is a process that investigates the transfer of energy between material elements driven by temperature gradients. Heat can be transferred through three mechanisms: conduction, convection, and radiation. Consequently, the temperature distribution within a system depends on the combined effects of these three heat transfer modes [62].

The action of fire on a structure elevates the temperature of structural elements, reducing their stiffness and load-bearing capacity, which may lead to collapse [63]. Therefore, it is essential to determine the transient evolution of the thermal field and simultaneously assess the fire resistance time.

When analysing the rate of temperature evolution in structural elements, it is crucial to quantify the heat flux impacting these components. EN 1991-1-2 [64] defines thermal actions for temperature analysis. The net heat flux density characterises this effect ($\dot{h}_{net}$ $[W/m^2]$) when applied on the element's boundary surface, assuming two different types of heat flux: radiative heat flux ($\dot{h}_{net,r}$) and convective heat flux ($\dot{h}_{net,c}$) from the fire environment.

For standard fire scenarios, the temperature-time curve (ISO 834) [1] is adopted, where the absorbed heat flux density is determined using both heat transfer mechanisms. Surface heat fluxes are calculated using Equation 2.5, which accounts for convective and radiative heat transfer.

$$\dot{h}_{net} = \dot{h}_{net,c} + \dot{h}_{net,r} \tag{2.5}$$

The following subsections present the formulations employed to determine each component of the equation and briefly describe the three modes of heat transfer.

2.4.1. Conduction

Heat conduction is fundamentally governed by atomic and molecular interactions, as these mechanisms drive thermal energy transfer at microscopic scales. Interparticle energy exchange occurs when a higher-energy object transfers energy to a lower-energy particle within an adjacent material [34].

This mode of heat transfer manifests in solids, gases, and liquids. In fluids (gases and liquids), conduction results from molecular collisions and diffusive motion during random particle movement. In solids, it arises from lattice vibrations (phonons) and the migration of free electrons. The heat transfer rate is influenced by the medium's temperature gradient, geometry, thickness, and intrinsic material properties. Specifically, thermal conductivity across a planar section is directly proportional to the temperature difference between the layer and the heat transfer interface, and inversely proportional to

the layer's thickness [35]. This relationship is governed by Fourier's law (1822), which models conductive heat transfer and is expressed in differential form as Equation (2.6):

$$\dot{h}_{cd} = -\lambda \cdot \frac{d\theta}{dx} \tag{2.6}$$

In Equation (2.6), $d\theta/dx$ represents the temperature gradient in the direction of heat flow [K/m], which quantifies the material's ability to conduct heat along the x-axis, and λ denotes the thermal conductivity of the material [W/m·K]. Since heat flux is a vector quantity, the three-dimensional formulation of Fourier's law is expressed a equation (2.7).

$$\vec{h}_{cd} = -\lambda \cdot \vec{\nabla}\theta \tag{2.7}$$

Where $\nabla\theta$ is the temperature gradient vector, describing the spatial variation of temperature across all three-dimensional axes.

2.4.2. Convection

Convection is the heat transfer mechanism driven by fluid motion, defined as the energy exchange between a solid surface and an adjacent moving fluid (gas or liquid) at their interface, involving advection and diffusion processes. This phenomenon depends on both molecular conduction within the fluid and its macroscopic motion [14]. Convective heat transfer may be considered in forced convection, where fluid flow is mechanically induced (e.g., fans, pumps, or atmospheric winds), and natural convection, where flow arises from density gradients caused by temperature variations in the fluid [65]. Due to the inherent complexity of convective effects, Newton's law of cooling provides a simplified expression for the convective heat transfer rate, proportional to the temperature difference between the surface and the fluid.

According to EN 1991-1-2 [64], the net convective heat flux from the fluid is calculated using the equation:

$$\dot{h}_{net,c} = \alpha_c(\theta_s - \theta_\infty) \tag{2.8}$$

Where α_c is the convective heat transfer coefficient [W/m²·K], applicable to nominal temperature-time curves; θ_s is the surface temperature of the solid body [°C]; and θ_∞ is the ambient fluid or gas temperature [°C]. As specified in PR EN 1994-1-2 [17], the net convective heat flux on the unexposed surface of separating elements should adopt $\alpha_c = 4$ [W/m^2]. When accounting for combined radiation effects, this coefficient is adjusted to $\alpha_c = 9$ [W/m^2]. For fire-exposed surfaces, the convective heat transfer coefficient is prescribed as $\alpha_c = 25$ [W/m^2] for elements subjected to the standard fire curve ISO 834 [1] or external fire curves, and $\alpha_c = 50$ [W/m^2] for surfaces exposed to hydrocarbon fire curves, such as those involving liquid fuel combustion.

2.4.3. Radiation

Radiation heat transfer is defined as the transmission of energy via electromagnetic waves resulting from changes in the electronic configurations of atoms or molecules. All bodies continuously emit energy through electromagnetic radiation, though the magnitude of this energy depends on the body's temperature and surface properties [37]. The Stefan-Boltzmann law quantifies the maximum emissive power E [W/m^2] of a surface.

The idealised thermal radiator, termed a blackbody, emits thermal radiation proportional to the fourth power of its absolute temperature. The upper limit of emissive power is described by Stefan-Boltzmann law:

$$E_b = \sigma \cdot \theta^4 \tag{2.9}$$

Where θ is the absolute surface temperature [K], and σ is the Stefan-Boltzmann constant $\sigma = 5.67 \cdot 10^{-8}$ [W/$m^2 \cdot K^4$], characterising the ideal blackbody.

Blackbody radiation is fundamental to radiative heat transfer. While blackbodies possess unique properties, their superior emissive capacity is most critical. To model radiation from real surfaces, a dimensionless parameter called emissivity (ε) is introduced. Emissivity quantifies a surface's ability to emit or absorb thermal energy relative to a blackbody.

Emissivity typically depends on wavelength, surface temperature, and emission angle. For simplicity, surfaces with wavelength-independent emissivity are termed grey

bodies. In fire engineering, emissivity (ε) — a dimensionless coefficient ranging from 0 to 1 (where 1 represents a blackbody) — is used to adapt Equation (2.10) for practical applications:

$$E_b = \varepsilon\sigma \cdot \theta^4 \tag{2.10}$$

Per Eurocode 1 – Part 1-2 [64], the net radiative heat flux $\dot{h}_{net,r}$ in [W/m^2] on fire-exposed structural surfaces is calculated as:

$$\dot{h}_{net,r} = \emptyset\varepsilon_f \cdot \varepsilon_m \cdot \sigma[(\theta_r + 273)^4 - (\theta_m + 273)^4] \tag{2.11}$$

Where:

$\emptyset$: View factor (geometric configuration factor between surfaces);

ε_f: Emissivity of the fire;

ε_m: Emissivity of the exposed structural element;

θ_r: Effective radiation temperature of the fire environment [°C];

θ_m: Surface temperature of the irradiated element [°C].

2.4.4. View factor

Radiation is the primary heat transfer mechanism that increases the slab's temperature in fire analysis, particularly under high-temperature conditions. To calculate radiative heat transfer ($\dot{h}_{net,r}$), the flame's position and the thermal energy-receiving element, known as the view factor ($\emptyset$), must be considered.

The view factor is a dimensionless parameter that quantifies the proportion of thermal radiation absorbed by a fire-exposed surface. It directly depends on the geometric configuration between the radiating and receiving surfaces [66]. Although its determination is complex, technical literature simplifies specific cases, such as composite slabs with steel decking in fire scenarios, due to practical variability.

According to PR EN 1994-1-2 [17], the view factor calculation is based on Hottel's crossed-string method (1950) [67]. For composite slabs, the view factor of the steel deck'sb lower flange is taken as $\emptyset_{lower} = 1$, as there is no radiation obstruction.

However, the view factors for the web and upper flange of the steel deck are less

than 1.0 due to the obstacle from the slab's ribs. Equations (2.12) and (2.13) and Figure 2.3 provide mathematical relationships to calculate these factors based on the profile's geometric dimensions.

$$\emptyset_{UPPER} = \frac{\left(\sqrt{h_2^2 + \left(L_3 + \frac{L_1 - L_2}{2}\right)^2} - \sqrt{h_2^2 + \left(\frac{L_1 - L_2}{2}\right)^2}\right)}{L_3} \tag{2.12}$$

$$\emptyset_{WEB} = \frac{\left(\sqrt{h_2^2 + \left(\frac{L_1 - L_2}{2}\right)^2} + (L_3 + L_1 - L_2) - \sqrt{h_2^2 + \left(L_3 + \frac{L_1 - L_2}{2}\right)^2}\right)}{2\sqrt{h_2^2 + \left(\frac{L_1 - L_2}{2}\right)^2}} \tag{2.13}$$

In accordance with this methodology, Figure 2.3 illustrates the geometric parameters required to determine the view factor ($\emptyset$) in composite slabs with steel decking.

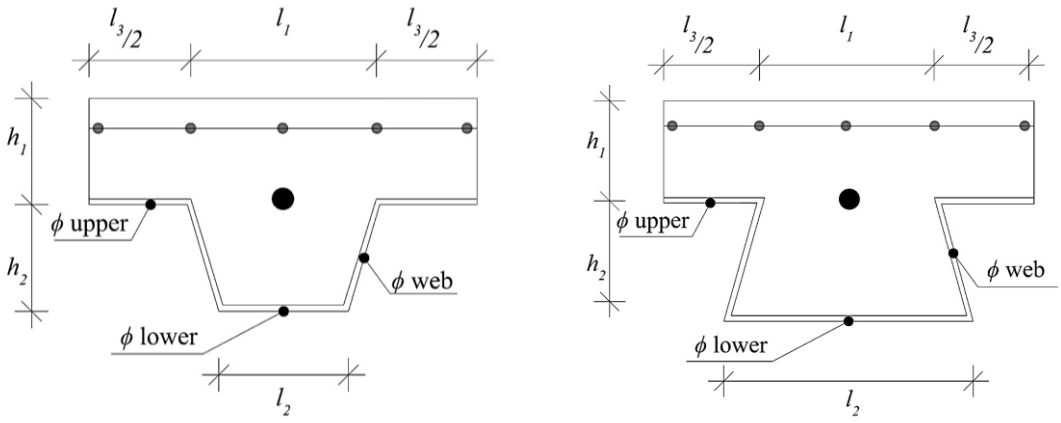

Figure 2.3: Parameters for determining the view factors: (a) Trapezoidal profile, (b) Re-entrant profile [4].

2.5. Thermal properties of materials

Heat transfer studies require thermal properties such as density, thermal conductivity, and specific heat. As this research aims to numerically simulate the solution of the second-order heat differential equation to predict temperature distribution in composite slabs, it is critical to understand how thermal properties and boundary

conditions influence the thermal performance of these elements.

To optimise the thermal model's accuracy, material properties must be defined realistically and as temperature-dependent. Given that composite slabs are heterogeneous structures at both global and local scales, nonlinear heat transfer across the cross-section is an intrinsic characteristic. Consequently, temperature changes during a fire event induce variations in specific heat, thermal conductivity, and material density.

Thermal properties describe the mechanical response of materials to temperature variations and directly impact numerical simulation outcomes, as they dictate the structure's thermal behaviour.

In the numerical model, the properties of concrete, steel, and mineral wool follow the formulations of Eurocodes 2, 3, and 5, as specified in EN 1992-1-2 [68], EN 1993-1-2 [69], and EN 1995-1-2 [70], respectively. The analytical model was developed in accordance with PR EN 1994-1-2 [17]. Additionally, since the air gap between the steel plate and concrete is considered, the thermal properties of air are also included.

2.5.1. Steel

The thermal properties stand for both steel elements (steel deck and rebars). This variation may be determined through equations available in Eurocode 3 Part 1-2 [69], presented in the following topics.

1. Emissivity Coefficient: Surface emissivity values for various steel types are detailed in Table 2.1, providing critical information for thermal analysis.

Table 2.1 — Values of surface emissivity ε_m

Type of steel	ε_m ($\leq 500^{o}C$)	ε_m ($> 500^{o}C$)
Carbon steel	0.7	0.7
HDG steel [a]	0.35	0.7

[a] Steel that has been hot–dip galvanised according to EN ISO 1461[71]and with steel composition according to Category A or B of EN ISO 14713 – 2:2020 [72].

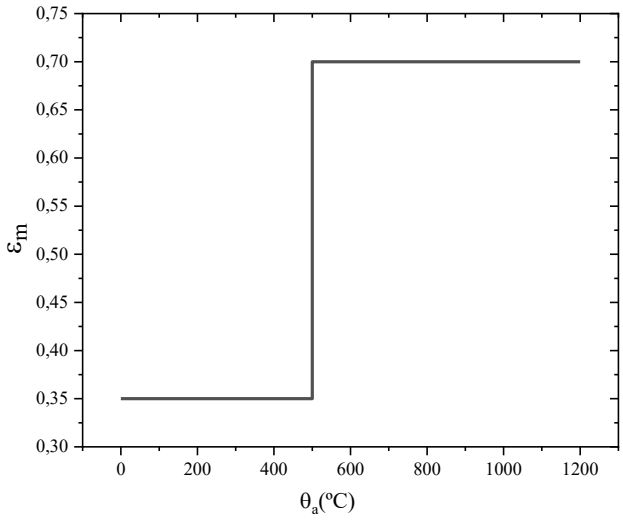

Figure 2.4: Emissivity ε_m for HGD steel.

2. Thermal Conductivity: The thermal conductivity is defined for different temperature ranges:

   - For temperatures between 20°C and 800°C:

$$\lambda_a = 54 - 3.33 * 10^{-2} * \theta_a [\text{W/mK}] \quad (2.14)$$

   - For temperatures between 800°C and 1,200°C:

$$\lambda_a = 27.3 \, [\text{W/mK}] \quad (2.15)$$

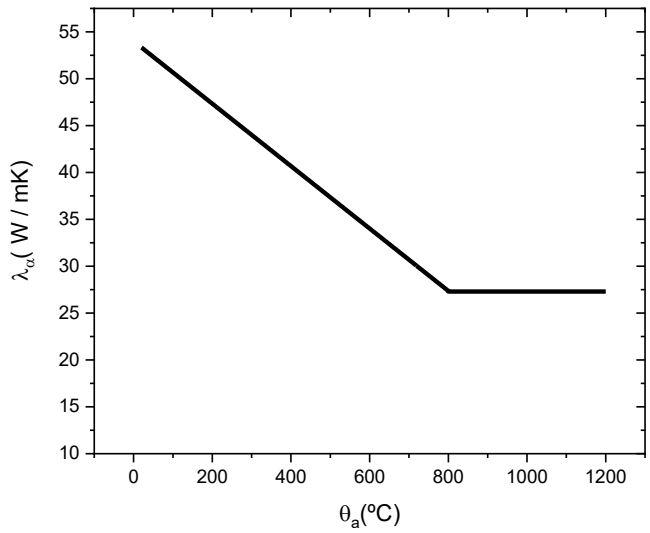

Figure 2.5: Thermal Conductivity (λ_a) of steel

3. Specific Heat: The specific heat varies with temperature, ensuring accurate thermal modelling.
    - Figure 2.6 illustrates the specific heat behaviour of steel as temperature increases. Between 0°C and 700°C, the average specific heat is ~600 J/kgK, corresponding to the Ferrite (alpha iron) phase. Beyond this range, a phase transition begins, involving molecular rearrangement that shifts the crystalline structure from body-centered cubic (BCC) to face-centered cubic (FCC), marking the Ferrite-to-Austenite (gamma iron) transformation. This process requires significant energy input [73,74].
    - The temperature range for phase transformation depends on steel properties, such as carbon content. In civil construction, the Austenite phase demands caution, as reaching this state can increase ductility and flexibility depending on cooling rates, potentially compromising structural load-bearing capacity.

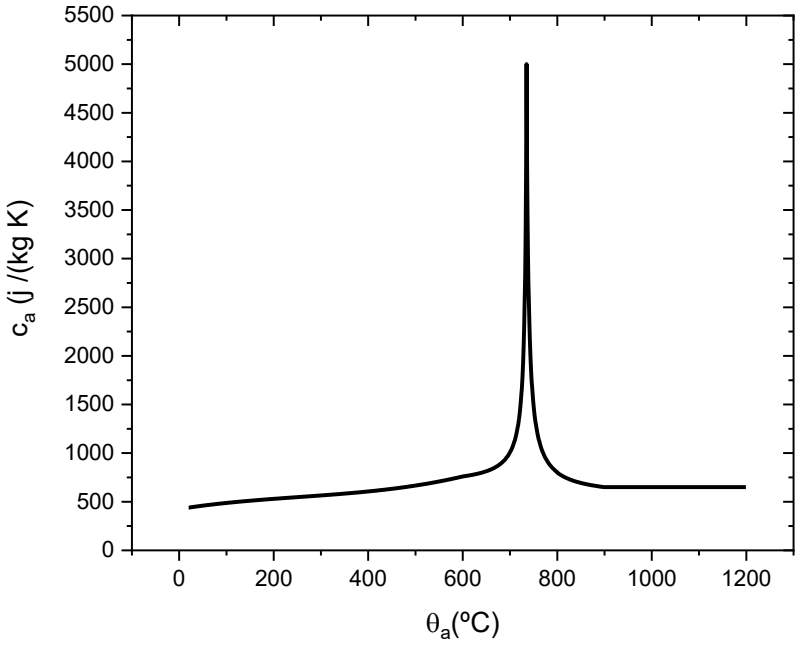

Figure 2.6: Specific Heat(C_a) of steel

4. Density: The density is taken as $\rho_a = 7850$ kg/m^3, considered independent of temperature for practical purposes.

The mechanical properties are defined for both types of steel (deck and rebar).

- **Strength and Stiffness**: The strength and stiffness of steel are assessed for heating rates ranging from 2 to 50 K/min, with stress-strain relationships provided in Table 5.2 [17], enabling a comprehensive understanding of material behaviour under thermal stress, presented in Figure 2.7.

Strain Range	Stress σ	Tangent modulus
I / elastic $\varepsilon \le \varepsilon_{ap,\theta}$	$E_{a,\theta}\varepsilon_{a,\theta}$	$E_{a,\theta}$
II / transit elliptical $\varepsilon_{ap,\theta} \le \varepsilon$ $\varepsilon \le \varepsilon_{ay,\theta}$	$\left(f_{ap,\theta}-c\right)+\frac{b}{a}\sqrt{a^2-\left(\varepsilon_{ay,\theta}-\varepsilon_{a,\theta}\right)^2}$ with $a^2=\left(\varepsilon_{av,\theta}-\varepsilon_{ap,\theta}\right)\left(\varepsilon_{av,\theta}-\varepsilon_{ap,\theta}+c/E_{a,\theta}\right)b^2$ $b^2=E_{a,\theta}\left(\varepsilon_{ay,\theta}-\varepsilon_{ap,\theta}\right)c+c^2$ $c=\frac{\left(f_{ay,\theta}-f_{ap},\theta\right)^2}{E_{a,\theta}\left(\varepsilon_{ay,\theta}-\varepsilon_{ap,\theta}\right)-2\left(f_{ay,\theta}-f_{ap,\theta}\right)}$	$\frac{b\left(\varepsilon_{ay,\theta}-\varepsilon_{a},\theta\right)}{a\sqrt{a^2-\left(\varepsilon_{ay,\theta}-\varepsilon_{a,\theta}\right)^2}}$
III / plastic $\varepsilon_{ay,\theta} \le \varepsilon$ $\varepsilon \le \varepsilon_{au,\theta}$	$f_{ay,\theta}$	0

Figure 2.7 – Relation between the carious parameters of the mathematical model by PR EN 1994-1-2 [17].

- **Reduction Factors**: Effective yield strength and other relevant parameters are illustrated in Figure 2.8, providing a visual representation of how fire conditions impact the mechanical properties of steel. The reduction factors used in that research are presented in table 2.2.

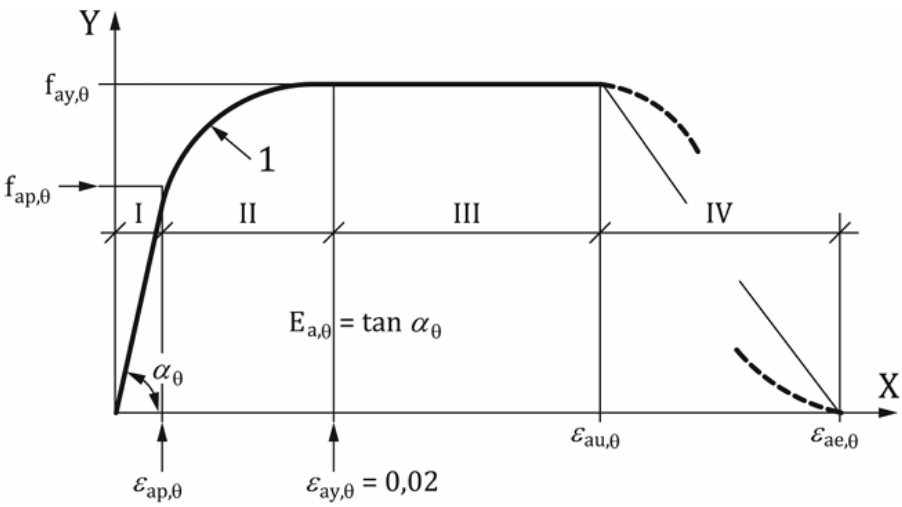

Figure 2.8 - Mathematical model for stress-strain relationships of structural steel at elevated temperatures [17].

Table 2.2 – Reduction factors for steel in hot rolled stage [17].

Steel Temperature θ_a [ºC]	$k_{y,i}$
20	1.00
100	1.00
200	1.00
300	1.00
400	1.00
500	0.78
600	0.47
700	0.23
800	0.11
900	0.04
1100	0.02
1200	0

2.5.2. Concrete

To determine the thermal properties of concrete in accordance with Eurocode 2 [68], the equations presented in the following sections are applied.

1. Emissivity Coefficient:

- Value: The emissivity coefficient for a concrete surface should be considered as 0.7.

2. Thermal Conductivity (λ_c):

- For normal weight concrete, the thermal conductivity, λc, varies with temperature and is calculated as follows:
    - When θc ≤ 140 °C:

$$\lambda c = 2 - 0.2451\left(\frac{\theta c}{100}\right) + 0.0107\left(\frac{\theta c}{100}\right)^2 [W/(m.K)] \quad (2.16)$$

- For 140 °C < θc ≤ 160 °C:

$$\lambda c = -0.02604 * \theta c + 5.324[W/(m.K)] \quad (2.17)$$

- When θc ≥ 160 °C:

$$\lambda c = 1.36 - 0.136\left(\frac{\theta c}{100}\right) + 0.0057\left(\frac{\theta c}{100}\right)^2 [W/(m.K)] \quad (2.18)$$

- For lightweight concrete:
  - 20 °C ≤ θc ≤ 800 °C:

$$\lambda c = 1 - \left(\frac{\theta c}{1600}\right)[W/(m.K)] \quad (2.19)$$

  - θc > 800 °C:

$$\lambda c = 0.5[W/(m.K)] \quad (2.20)$$

Figure 2.9 represents the thermal conductivity for the normal (NWC) and light weight concrete (LWC).

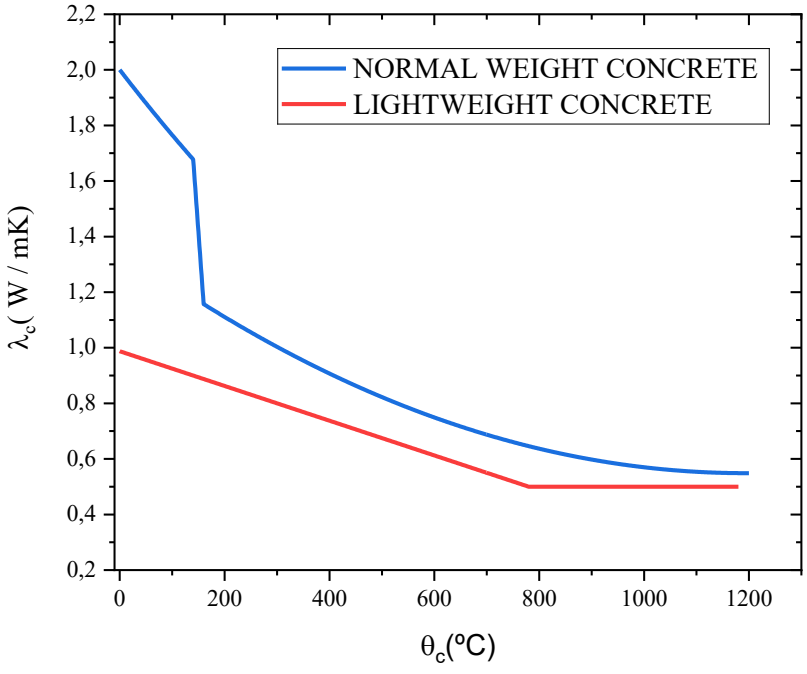

Figure 2.9: Thermal Conductivity (λ_c) of concrete

3. Specific Heat (c_c):

- For normal and lightweight concrete with 0% moisture:
  - 20 °C ≤ θc ≤ 100 °C:

$$c_c = 900\ (\frac{J}{kg * K}) \quad (2.21)$$

  - 100 °C < θc ≤ 200 °C:

$$c_c = 900 + (\theta_c - 100)(\frac{J}{kg * K}) \quad (2.22)$$

  - 200 °C < θc ≤ 400 °C:

$$c_c = 1000 + \frac{\theta_c - 200}{2}(\frac{J}{kg * K}) \quad (2.23)$$

  - 400 °C < θc ≤ 1200 °C:

$$c_c = 1100\ (\frac{J}{kg * K}) \quad (2.24)$$

- Moisture content impact:
  - Specific heat values change according to the concrete's moisture content: At 3% moisture, used in this research. That value its for a range of temperature 100 º C by 115 º C, and a linear regression to the range 200 °C < θc ≤ 400 °C**.**

$$c_c = 2020\ (\frac{J}{kg * K}) \quad (2.25)$$

Figure 2.10 represents the variation of this property with temperature.

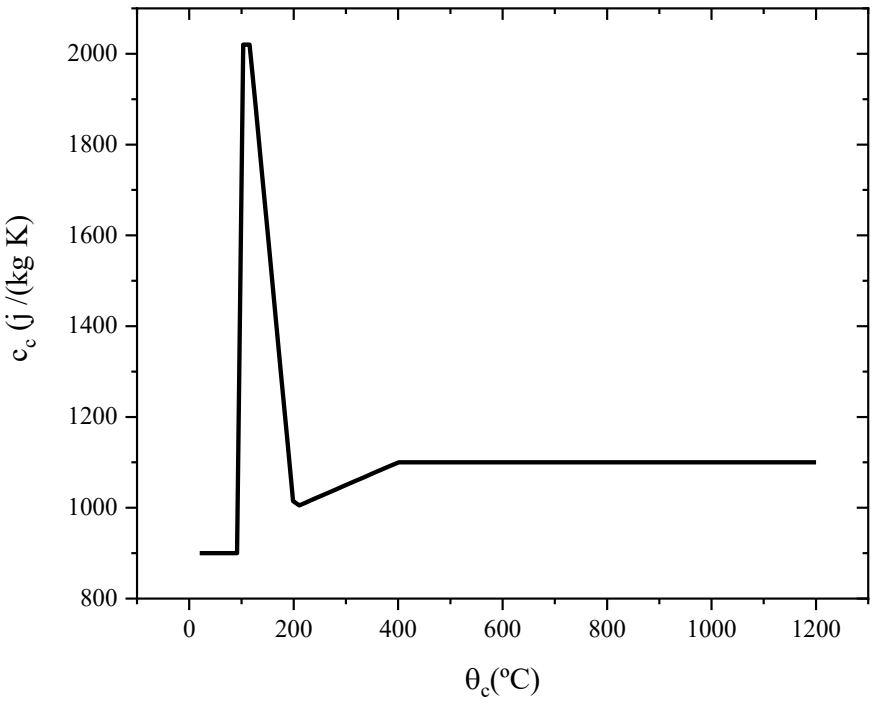

Figure 2.10: Specific Heat(C_c) of concrete with **moisture = 3%**

4. Density (ρ_c):

- Density variation with temperature for normal weight concrete (NWC) is as follows:

  - 20 °C ≤ θc ≤ 115 °C:

$$\rho(\theta c) = \rho(20°C)[kg/m^3] \tag{2.26}$$

  - 115 °C < θc ≤ 200 °C:

$$\rho(\theta c) = \rho(20°C) * (1 - 0.02 * \frac{\theta c - 115}{85}) \left[\frac{kg}{m^3}\right] \tag{2.27}$$

  - 200 °C < θc ≤ 400 °C:

$$\rho(\theta c) = \rho(20°C) * (0.98 - 0.03 * \frac{\theta c - 200}{200}) \left[\frac{kg}{m^3}\right] \tag{2.28}$$

  - 400 °C < θc ≤ 1200 °C:

$$\rho(\theta c) = \rho(20°C) * (0.95 - 0.07 * \frac{\theta c - 400}{800}) \left[\frac{kg}{m^3}\right] \tag{2.29}$$

Figure 2.11 represents the variation of density with temperature.

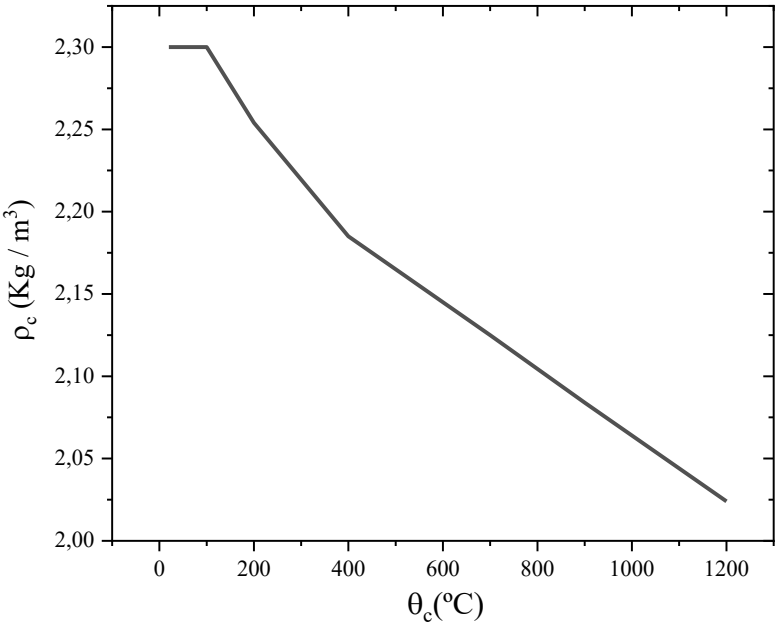

Figure 2.11: Density (ρ_c) of concrete with **moisture = 3%**

5. Fire Protection Materials

Fire protection materials must be tested and evaluated following relevant procedures in EN 13381 for consistency and suitability in design.

2.5.3. Air

The analysis of the air-gap effect, which involves a thin layer of air forming between the concrete and the steel deck during heating, must be incorporated into the study of composite slab behaviour under fire conditions. This phenomenon arises due to the thermal expansion during fire exposure, significantly impacting heat transfer in composite slabs [75].

The thermal properties of air were adopted from the work of Y. A. Çengel and A. J. Ghajar [67], who demonstrated that specific heat, thermal conductivity, and density vary with temperature. Consequently, these air properties are essential to accurately simulate the interaction between the steel deck and the "air gap."

Figure 2.12 illustrates the variation of air's thermal properties with temperature at

a pressure of 1 atm.

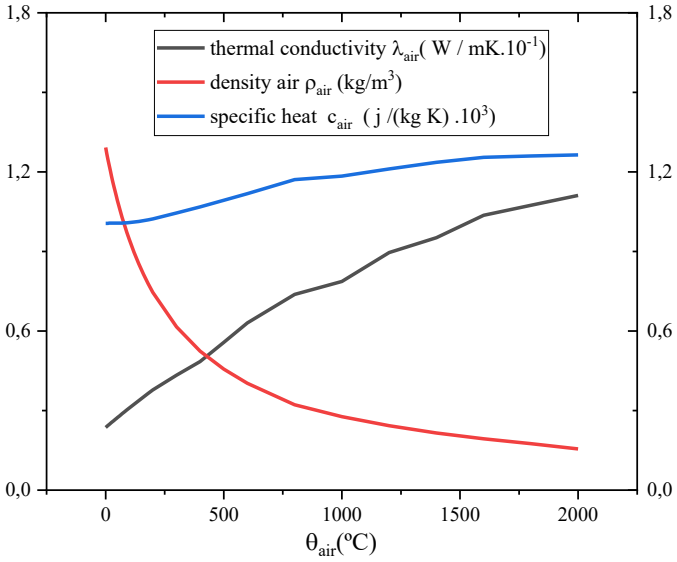

Figure 2.12: Variation of thermal material properties at elevated temperatures for air

2.5.4. Mineral wool

Based on prEN 1995-1-2 [70], the thermal properties of mineral wool manufactured by Rocterm® [76], PN 70, with a density of 70 kg/m³, presents the thermal properties depicted in Figure 2.13. The thermal properties depended on the density of mineral wool. In steel and concrete, as indicated in the preceding sections, thermal conductivity decreases with increasing temperature; however, in mineral wool, this thermal property exhibits an increase with elevated temperature.

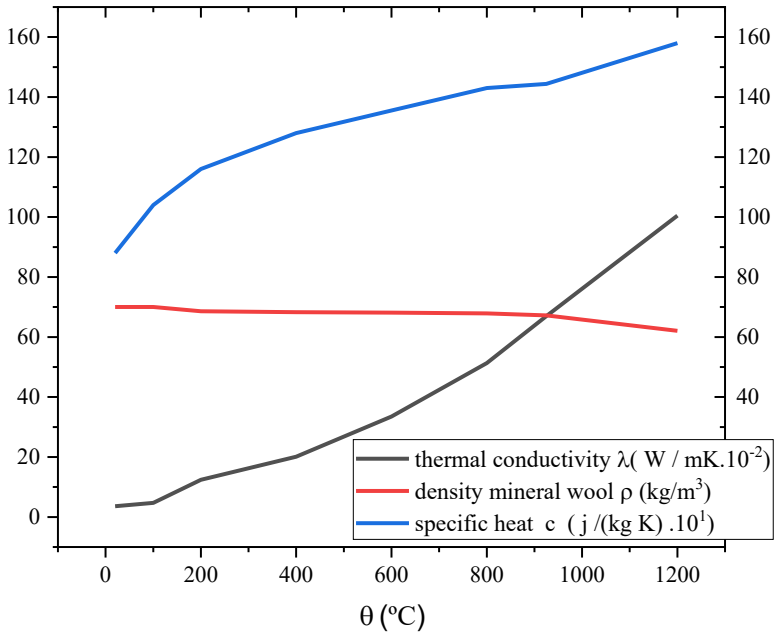

Figure 2.13: Variation of thermal material properties at elevated temperatures for mineral wool ($\rho = 70 \frac{kg}{m^3}$)

2.6. Fire Curves

Fire curves are critical tools in structural fire safety engineering, providing systematic frameworks to evaluate how buildings and materials respond to thermal exposure. These temperature-time relationships simulate fire development under controlled conditions, enabling engineers to quantify fire severity, predict structural behavior, and ensure compliance with safety regulations.

This section introduces the theoretical and practical foundations of fire curves, distinguishing between natural fire dynamics and standardised models. Subsection 2.7.1 examines *natural fire curves*, which describe the organic evolution of real fires through ignition, growth, decay, and cooling phases. Subsection 2.7.2 addresses nominal fire curves and simplified regulatory models that prioritise consistency over realism for comparative fire resistance assessments. Finally, subsection 2.7.3 focuses on the *ISO 834 standard fire curve*, a cornerstone of prescriptive fire safety codes that defines temperature progression for testing structural components.

Together, these subsections highlight the balance between capturing real-world fire complexity and employing standardized benchmarks to achieve reliable, code-compliant fire resistance design.

2.6.1. Natural Fire curves

Fire is the result of a highly exothermic thermochemical oxidation process. For combustion to occur, three elements are essential:

1. A combustible organic compound (fuel),
2. An oxidising agent (typically oxygen),
3. Sufficient activation energy to initiate the reaction.

Once combustion begins, the heat released sustains the reaction in a self-perpetuating cycle. As described by Paulo Vila Real [77], a natural fire develops through four distinct phases, illustrated in Figure 2.14:

- Ignition phase: Initial low-temperature stage with negligible structural impact.
- Propagation phase: Rapid fire spread and fuel consumption, marked by a sharp temperature rise known as flashover. This critical transition typically occurs when ceiling temperatures reach 450–600°C or when floor-level heat flux exceeds 20 kW/m².
- Fully developed phase: Sustained high-temperature burning with relatively stable thermal conditions.
- Cooling phase: Gradual temperature decline due to fuel depletion, firefighting efforts, or other interventions.

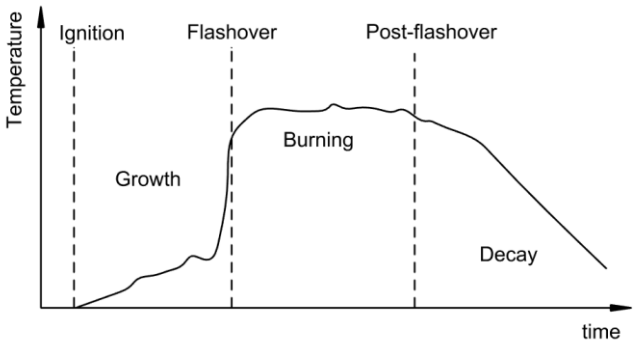

Figure 2.14: Fire curve for the complete process of fire development.

Regulatory frameworks like Eurocode define two primary fire curve types for evaluating structural fire resistance: the ISO 834 standard fire curve and **p**arametric fire curves. These models specify maximum temperature thresholds and simulate fire

exposure conditions, as discussed in subsequent sections.

2.6.2. Nominal standard fire curves

A standard fire curve represents a hypothetical worst-case scenario with continuously rising temperatures, omitting the cooling phase inherent to real fires. While criticised for their unrealistic monotonic temperature increase, these curves remain conservative benchmarks for comparing fire severity across structural elements.

EN 1991-1-2 [64] and other international standards outline the three most important nominal fire curves (Figure 2.15):

1. Hydrocarbon fire curve: Simulates high-temperature fires involving flammable liquids or gases, characterized by rapid temperature escalation.
2. ASTM E119 fire curve [22]: A U.S.-based standard curve used to evaluate fire resistance of building components.
3. External element fire curve: Models fires affecting external structural elements, considering factors like wind and exposure.

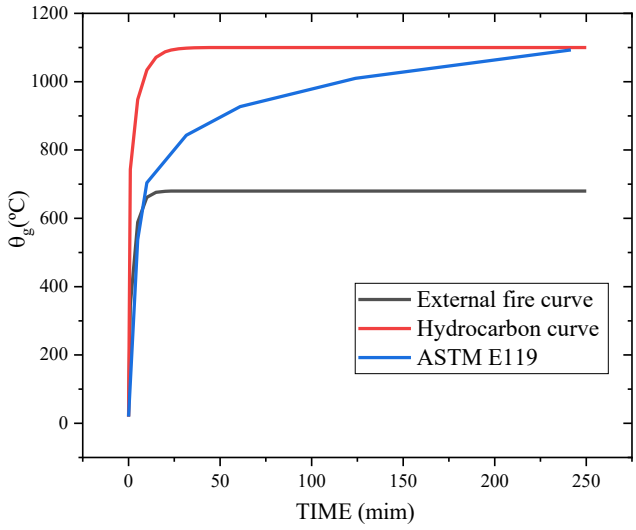

Figure 2.15: Nominal time-temperature fire curves.

These curves disregard building-specific factors like fire load and ventilation, making them poor predictors of real-world temperature evolution. However, they serve as standardised tools for assessing relative fire resistance. Crucially, resistance values derived from nominal curves do not replicate natural fire behaviour.

2.6.3. Standard Fire curve ISO-834

Modern fire safety building codes typically adopt either a prescriptive approach or a performance-based approach. While performance-based methods are widely recognized to offer substantial advantages over prescriptive ones—as they enable designers to assess structural fire safety through advanced fire engineering principles—most current fire regulations still rely on a combination of both approaches. This hybrid adoption stems from the inherent complexity of evaluating the holistic performance of entire structural systems under fire conditions [78].

According to ISO 834 [1], the fire resistance of a building component is defined as the duration, measured in completed minutes, that the element can withstand exposure to a standardized fire test before failing to meet one or more predefined failure criteria (e.g., load-bearing capacity, integrity, or insulation). The relationship between fire exposure time and temperature in such tests is described by the following empirical equation and presented by Figure 2.16:

$$\theta_g = 345 \cdot log_{10} \cdot (8t + 1) + 20 \tag{2.30}$$

where θ_g is the temperature in [°C], and t is the time elapsed in minutes.

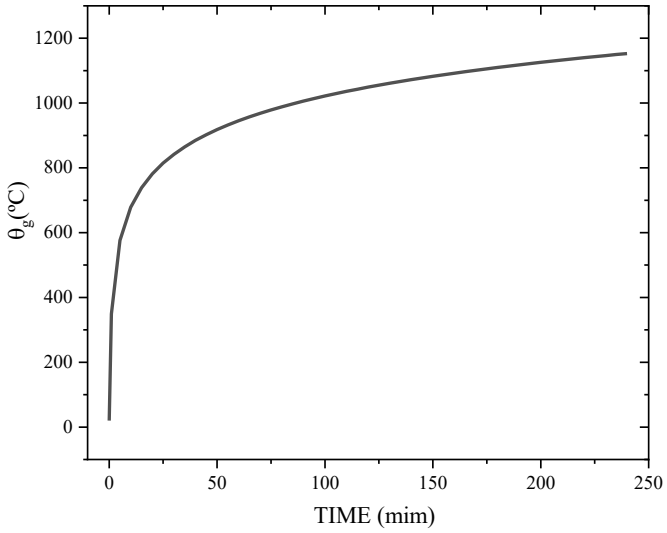

Figure 2.16: ISO 834 fire curve.

3. METHODOLOGY FOR THERMAL ANALYSIS

3.1. Thermal analysis using the Weighted Residual Method

The weighted residual method (WRM) is a fundamental approach for solving differential equations that govern heat transfer processes. This method systematically approximates the temperature field within a domain, ensuring that the discrepancy, or residual, between the actual and approximate solutions is minimized in an integral sense [79].

3.1.1. Governing Equations for Heat Transfer

The transient heat conduction equation is derived from energy conservation principles. For a differential element in 2D Cartesian coordinates, the net heat flux in the x and *y* directions is governed by Fourier's law (see Figure 3.1):

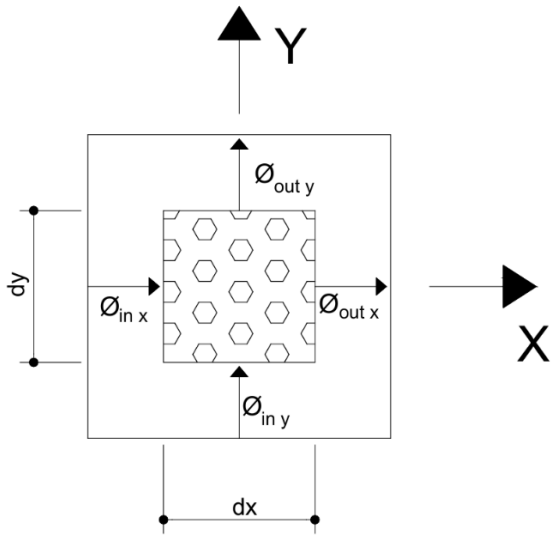

Figure 3.1: Heat Flux in the x and *y* directions.

$$\emptyset_{in\,x} = -\frac{\lambda \partial T}{\partial_x} \left[\frac{w}{m^2}\right] \tag{3.1}$$

$$\emptyset_{out\,x} = -\frac{\lambda \partial T}{\partial_x}\Big|_{X+\Delta x} \left[\frac{w}{m^2}\right] \tag{3.2}$$

where λ is the thermal conductivity. The net heat flow in the x*x*-direction for a control volume ($dx \times dy \times 1$) is:

$$\Delta h_x = \frac{\partial}{\partial_x}\left(\frac{\lambda \partial T}{\partial_x}\Big|_X\right) dx * (dy * 1)[w] \tag{3.3}$$

Similarly, for the y-direction:

$$\Delta h_y = \frac{\partial}{\partial_y}\left(\frac{\lambda \partial T}{\partial_y}\Big|_y\right) dy * (dx * 1)[w] \tag{3.4}$$

The energy balance equation, incorporating transient effects, becomes:

$$\frac{\partial}{\partial_x}\left(\frac{\lambda \partial T}{\partial_x}\right) + \frac{\partial}{\partial_y}\left(\frac{\lambda \partial T}{\partial_y}\right) = \rho * C_p * \frac{\partial T}{\partial_t} \tag{3.5}$$

Where ρ is the density and C_p is the specific heat capacity.

3.1.2. Numerical Solution via the Weighted Residuals Method (WRM)

The WRM approximates the temperature field $T(x)$ by minimizing the residual $R(x)$, defined as the deviation from the exact solution.

The heat conduction equation for two-dimensional steady-state heat transfer, including internal heat generation, is expressed as:

$$\frac{\partial}{\partial_x}\left(\frac{\lambda \partial T}{\partial_x}\right) + \frac{\partial}{\partial_y}\left(\frac{\lambda \partial T}{\partial_y}\right) - \rho * C_p * \frac{\partial T}{\partial_t} = 0 \tag{3.6}$$

To solve this equation numerically, the temperature distribution $T(x)$ is approximated by a trial function $\dot{T}(x, y)$, and the weighting function represented by Galerkin approximation [80]:

$$\dot{T}(\xi, \eta) = \sum_{i=1}^{4} N_i(\xi, \eta) T_i \tag{3.7}$$

where:

- $N_i(\xi, \eta)$: shape functions associated with each node (e.g., linear, quadratic),
- T_i: Nodal temperature values.

Substituting $\dot{T}\ (x)$ into the governing equation leads to the residual:

$$R(x,y) = \frac{\partial}{\partial_x}\left(\frac{\lambda\partial\dot{T}}{\partial_x}\right) + \frac{\partial}{\partial_y}\left(\frac{\lambda\partial\dot{T}}{\partial_y}\right) - \rho * C_p * \frac{\partial\dot{T}}{\partial_t} \tag{3.8}$$

The residual $R(x)$ quantifies the deviation of $\dot{T}(x)$ from satisfying the heat equation.

The WRM enforces the weighted integral of the residual to vanish:

$$\int \Psi * R(x,y) * dv = 0 \tag{3.9}$$

3.1.3. Matrix Formulation and Time Discretization

The discretized equations form a system:

$$[k][T] + \{F\} = [C]\{\dot{T}\} \tag{3.10}$$

where:

- $[K]$: Conductivity matrix by Eq.xx,
- $[C]$: Capacity matrix (Cp),
- {F}: Load vector (heat sources Q and boundary fluxes).

For transient analysis, the backward Euler scheme approximates the time derivative:

$$\{\dot{T}\} = \frac{\{T\}^{t+1} - \{T\}^{t}}{\Delta t} \tag{3.11}$$

3.1.4. Implementation in ANSYS: Iterative Solver

ANSYS employs the Finite Element Method (FEM), rooted in the WRM, to solve nonlinear thermal problems. The solution is incremental and iterative. The ky steps are detailed below.

- For radiation (T^4) or temperature-dependent λ, the Newton-Raphson method linearizes equations at each iteration.

- Solve $[K]\{\Delta T\}=\{F\}-[K]\{T^k\}$.

- Update $T^{k+1}=T^{k}+\Delta T$.

The iterative process requires a convergence method. Here on is going to control the solution by the heat flow

- Iterations halt when $\|h_{flow}{}^{k+1} - h_{flow}{}^{k}\|$<tolerance x minimum reference value.

The boundary conditions include time and space. The initial temperature is either equal to the experimental tests or 20ºC. The space boundary conditions apply to the exposed and unexposed composite slab. Additional boundary conditions are included in cavity region (radiation and convection), using appropriate finite elements.

- Convective ($\dot{h}_{net,c} = \alpha_c(\theta_s - \theta_\infty)$) and radiative ($\dot{h}_{net,r} = \emptyset\varepsilon_f \cdot \varepsilon_m \cdot \sigma[(\theta_r + 273)^4 - (\theta_m + 273)^4]$) heat fluxes are applied as Neumann conditions. The initial condition is used by the Dirichlet condition.

3.2. Finite element model (FEM)

This study employs the PLANE55 [81,82] element for two-dimensional thermal conduction analysis, featuring four nodes with a single temperature degree of freedom per node, supporting both steady-state and transient regimes while incorporating convective and radiative effects. Radiation heat exchange is modeled via the LINK31 [81,82] element in the cavity regions, which applies the Stefan-Boltzmann Law with parameters such as emissivity (constant or temperature-dependent) and geometric form factors, resolving nonlinearities iteratively through the Newton-Raphson method. Convective heat transfer is simulated using LINK34 [81,82] in the cavity regions, which incorporates a temperature- or time-dependent nonlinear film coefficient, with heat rates calculated based on convection area and film coefficient, excluding empirical terms. Together, these elements enable a coupled analysis of conduction, radiation, and convection within the thermal system.

3.2.1. PLANE 55

In this study, the PLANE55 element is utilized for thermal analysis to evaluate heat conduction in a 2D plane. PLANE55, a four-node element with a single degree of freedom (temperature) per node, supports both steady-state and transient analyses in plane or axisymmetric applications. The element facilitates detailed heat transfer studies by allowing input of convection, heat flux, and radiative surface loads. Additionally, body heat generation can be applied at each node, allowing the study of localized thermal effects. However, in the current configuration, mass transport and fluid flow options are not activated, aligning with standard restrictions of Ansys Mechanical Pro and Premium versions.

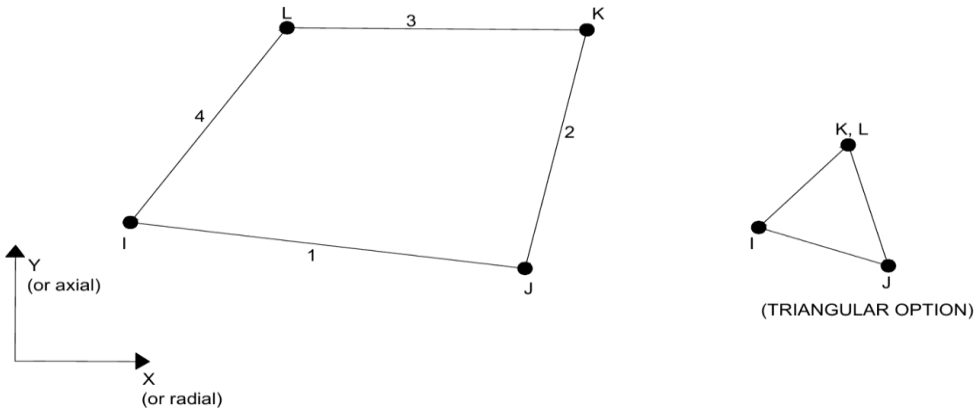

Figure 3.2: Nodal configuration of PLANE 55.

The mesh density of PLANE55 is optimised to ensure accurate heat flux distribution. Key settings, such as KEYOPT parameters, ensure the model conforms to a plane thermal simulation with prescribed boundary conditions. Adjustments to element geometry and mesh refinement further ensure the model's sensitivity and accuracy, which is critical for studying fine thermal gradients and transient behaviors within the material. The interpolating functions are linear, see Equation (3.12), written in natural coordinates, and the integration scheme uses full Gauss method (2x2).

$$T(\xi,\eta) = \frac{1}{4}[T_i(1-\xi)(1-\eta) + T_j(1+\xi)(1-\eta) + T_k(1+\xi)(1+\eta) + T_l(1-\xi)(1+\eta)] \tag{3.12}$$

3.2.2. LINK 31

The LINK31 element in ANSYS is designed for simulating radiative heat transfer between two nodes within a thermal system. This element is characterized by its two-node configuration, radiating surface area, geometric form factor, emissivity, and the Stefan-Boltzmann constant (SBC.), which is essential in calculating radiative heat flow. In axisymmetric analyses, the radiation area should be specified for the full 360° surface to accurately model radiative effects across the entire geometry.

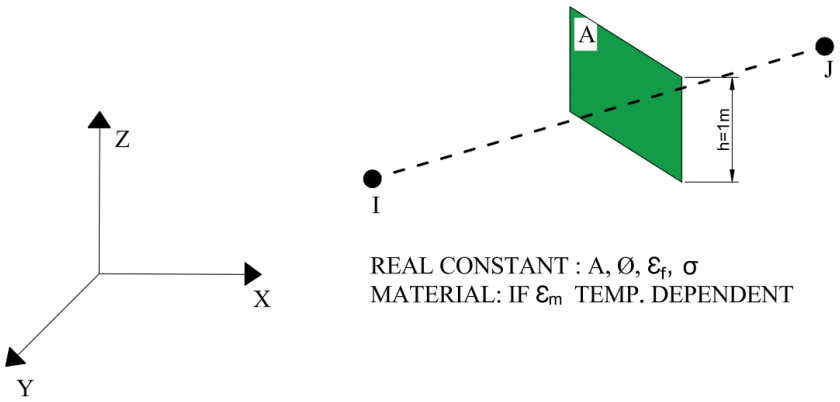

Figure 3.3: Nodal configuration of LINK 31.

For the emissivity ϵ, the LINK31 element provides flexibility to assign either a constant or temperature-dependent emissivity value. If emissivity is constant, it is directly entered as a real constant. However, for temperature-dependent emissivity, the values are defined through the material property EMIS, while the real constant is used to identify the relevant material property number. By default, EMIS is set to 1.0 if not specified, assuming a fully emissive surface.

The radiative heat transfer rate q in LINK31 is governed by the Stefan-Boltzmann Law, specifically:

$$q = \sigma * \epsilon * \phi * A \left(\theta_I^4 - \theta_J^4\right) \tag{3.13}$$

where:

- σ is the Stefan-Boltzmann constant (SBC), defaulting to $0.119 * 10^{-10} \frac{BTU}{hr} * in^2 * R^4$or equivalent in SI units, $\sigma = 5.67 \cdot 10^{-8}$ [W/$m^2 \cdot K^4$],
- ϵ represents the emissivity of the surface,

- ϕ is the geometric form factor, accounting for the shape and orientation between the radiative surfaces,
- A is the effective radiating area (in units of length squared),
- θ_I and θ_J are the absolute temperatures at nodes I and J.

To handle the nonlinear temperature dependency, the temperature equation is solved iteratively via the Newton-Raphson method, formulated as:

$$[(\theta_I^2 + \theta_J^2)(\theta_I + \theta_j)]_p(\theta_I - \theta_j) \tag{3.14}$$

Here, the bracketed term $[\,]_p$is evaluated based on the temperature from the previous substep to maintain solution stability. Importantly, the initial temperature should be close to the expected result and cannot be zero, ensuring convergence. For initialization, TUNIF and TOFFST should both not be set to zero.

Alternatively, an empirical radiation model can be activated using KEYOPT (3), which introduces arbitrary constants ϕ and A into the equation, such as:

$$q = \sigma * \epsilon * \left(\phi\theta_I^4 - A\,\theta_J^4\right) \tag{3.15}$$

This flexibility allows for customised radiative transfer simulations where F and A are input constants, suitable for scenarios where experimental data or specific conditions require non-standard radiation factors.

For more details on inputs and specific configurations, refer to "LINK31 Input Summary" and the general "Element Input" section. These configurations allow LINK31 to accommodate complex radiative heat transfer problems with precision, especially in systems with varying geometries and temperature gradients.

3.2.3. LINK 34

The LINK34 element is uniaxial and allows heat convection transfer between two nodes in a thermal analysis. Each node has one degree of freedom, temperature, and the element is applicable to 2D (plane or axisymmetric) and 3D analyses, both in steady-state and transient conditions.

When a model containing LINK34 is also structurally analyzed, the element

should be replaced by an equivalent (or null) structural element. This element can have a nonlinear film coefficient, which can depend on temperature or time.

LINK34 is defined h_f by two nodes, a convection area, two empirical terms (EN and CC), and a film coefficient. The convection area should be expressed on a full 360° basis for axisymmetric analyses.

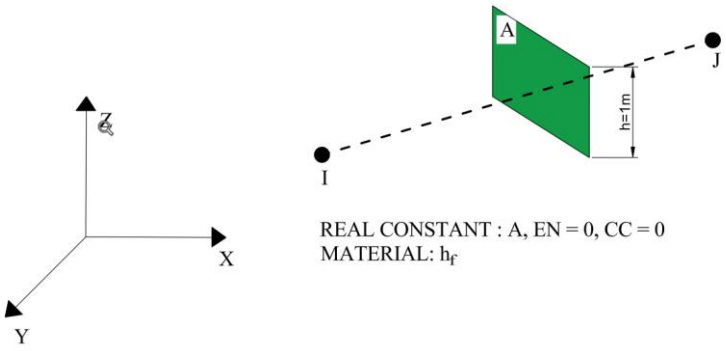

Figure 3.4: Nodal configuration of LINK 34.

The heat transfer rate q is given by:

$$q = h_f * A * E * (\theta_I - \theta_j) \tag{3.16}$$

where E is an empirical term, adjustable through KEYOPT (3) and EN and CC values.

$$E = F\left[\theta_i^p - \theta_j^p\right]^n + \frac{CC}{h_f} \tag{3.17}$$

Assuming n=EN=0, and CC=0, this means that E=F=1.

4. DEVELOPMENT OF THE NUMERICAL MODEL

4.1. Geometry and thermal affected regions of the composite slab

Figure 4.1 presents the geometry and temperature-affected regions of the composite steel and concrete slab made by Voidcon®, used by Claasen et al. [83]. This study presents a transient and non-linear thermal analysis of three protection types of composite slabs using two different insulation solutions. The composite slab insulation, protected by a steel shield, creates an air cavity in the UPPER 2 and WEB 2 regions, preventing these areas from being directly exposed to fire [15]. The second insulation was also assumed to be made using mineral wool in the cavity region formed by the steel shield.

In the present geometry, as shown in Figure 4.1, there are two distinct regions: a general trapezoidal region (T), composed of the lower region, WEB 2, and UPPER 2; and a reentrant region (R), formed by WEB 1 and UPPER 1.

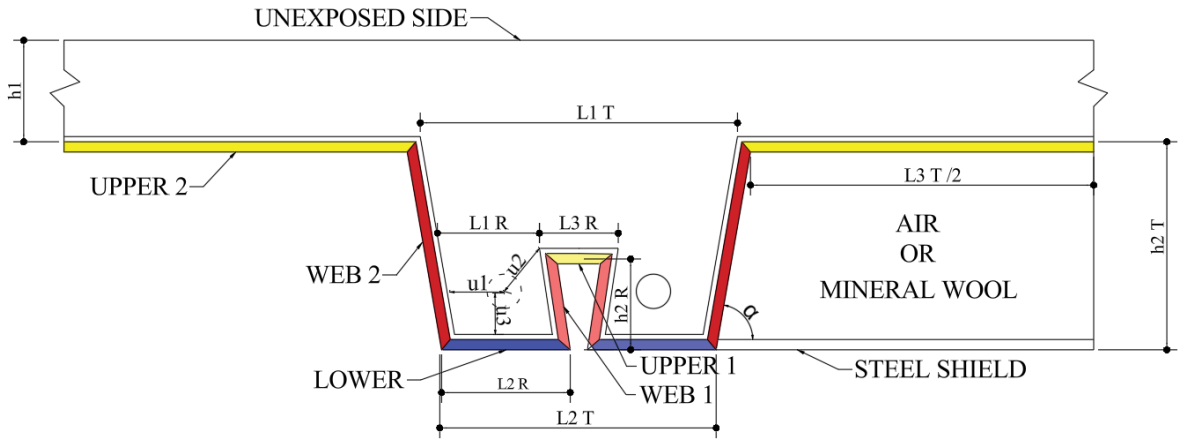

Figure 4.1. Indicated dimensions and zones of the slab by Voidcon®.

Table 4.1 presents the different types of steel decks and the geometry used for this investigation. The concrete cover has been considered constant and equal to 65 mm. Each region has unique dimensions, which are critical for calculating the average temperature within its respective elements using the simplified method [17]. This approach relies on accurately determining the view factors and boundary conditions, as they directly influence the resulting temperature field. The plate has a thickness of 0.8mm.

Table 4.1. Dimensions of the slab by Voidcon®.

	VP 50	VP115	VP 200
L1 R (mm)	30	50	85
L2 R (mm)	55	75	110
L3 R (mm)	25	25	25
L1 T (mm)	165	200	300
L2 T (mm)	115	150	230
L3 T (mm)	250	400	460
h1 (mm)	65	65	65
h2 T (mm)	50	115	200
h2 R (mm)	50	50	50
ϕ_{reb} (mm)	10	10	10
u1 (mm)	24	37	47
u2 (mm)	32	32	47
u3 (mm)	25	25	25
α (º)	63.40	77.73	80.07

In addition to the configurations employed above, numerical simulations were also conducted using a setup similar to the steel shield, albeit with the incorporation of a mineral wool board exhibiting variable insulation height (hi), as illustrated in Figure 4.2.

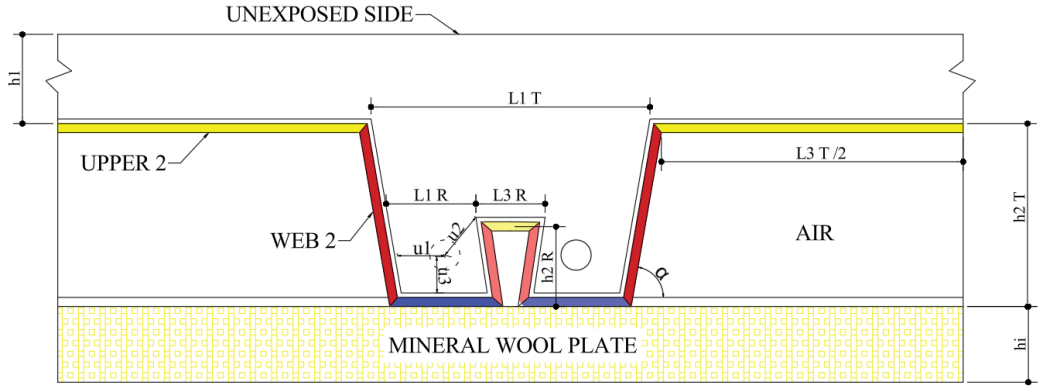

Figure 4.2. Indicated dimensions and zones of the slab by Voidcon®.

4.2. Parameters for the Simulation

Parametric simulations were developed using nonlinear thermal analyses involving composite slabs with commercial steel sheet profiles. The parametric study addresses the influence of various parameters on the temperatures of the steel profile components, as per the regions defined in Section 4.1, as well as the temperatures of the rebars. Additionally, attention is given to the impact of the slab's steel components on the thermal insulation criterion (*I*) and the load-bearing capacity criterion (*R*). The parametric studies

were developed based on the results of twenty-one thermal simulations, all of which were conducted using a two-dimensional approach via the ANSYS Mechanical APDL [84].

Regarding the concrete type, Normal Weight Concrete (NWC) of class C25/30 was considered for the composite slabs, with a moisture content of 3.00%, with h1=65mm for all. The steel grade for the deck is ISQ 230 galvanised steel grade 275. The reinforcing bars exhibit a characteristic tensile strength of 450 MPa.

All composite slabs were subjected to numerical simulations of fire exposure for 10,800 seconds (180 minutes), aiming to verify compliance with the fire resistance criteria related to thermal insulation and a new proposal based on new coefficients ai, bi and ci to determine the time of insulation for (I) criteria and the temperature of the regions for the (R) criteria. The following table summarises the range of the investigated parameters.

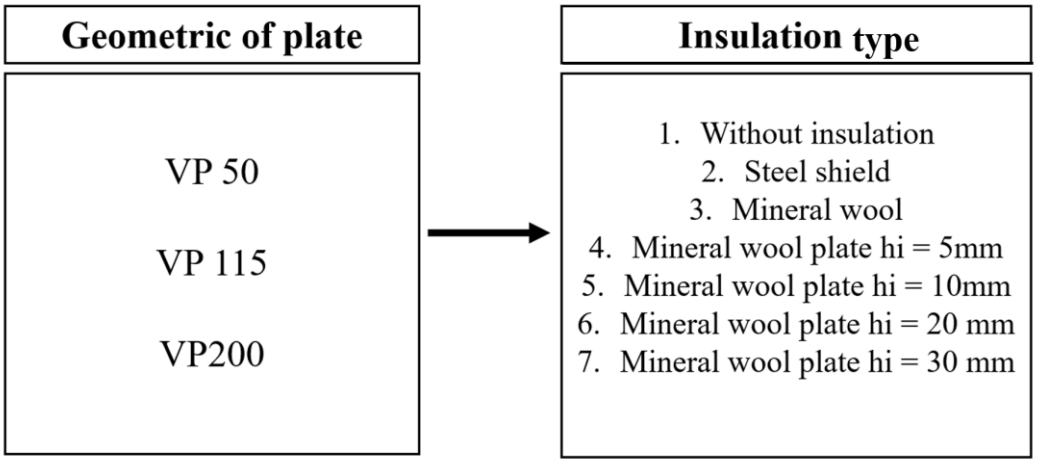

Figure 4.3. Parameters studies diagram.

Table 4.2 presents the view factors calculated according to Eqs. 2.12 and 2.13, for each steel deck profile. As discussed before, the view factor of the lower flange is always assumed as 1.

Table 4.2. View factors used for the composite slabs by Voidcon® [85].

	VP 50	VP115	VP 200
$\emptyset_{LOWER}$	1	1	1
$\emptyset_{WEB\ 2}$	0.697	0.480	0.480
$\emptyset_{\ UPPER\ 2}$	0.930	0.780	0.712
$\emptyset_{WEB\ 1}$	0.058	0.058	0.058
$\emptyset_{\ UPPER\ 1}$	0.064	0.064	0.064

4.3. Boundary conditions

Heat flux by convection and radiation is applied as primary thermal boundary conditions in accordance with EN1991-1-2 [64]. The convection coefficient of 25 W/m²K is assigned to the fire-exposed side. The flame emissivity factor of 1.0 is applied with a Stefan-Boltzmann constant of 5.67×10^{-8} W/m²K⁴, consistent with previous studies [86,87,88]. The room temperature on the exposed side was defined using the ISO834 standard fire time-temperature curve, while the non-exposed side was assumed to maintain a constant temperature of 20°C. Figures 4.4 to 4.7 illustrate the thermal boundary conditions applied to the steel deck with the steel shield insulation model.

Equation (2.5) represents the heat flux reaching the exposed line (surface) via radiation and convection, based on the temperature of the surrounding gas, which is subsequently transferred through the slab by convection and radiation. A uniform initial temperature (20°C) is applied to all nodes.

In accordance with the provisions of Eurocode EN 1991-1-2 [64], the upper surface of the slab (unexposed side) is subjected to a convective heat transfer coefficient of 9 W/m²K to account for radiative effects. The unexposed surface of the composite slab is also critical for determining the temperature evolution, as it governs the heat transfer from the compartment below the slab to the compartment above. The heat flux of the unexposed side is represented by the Equation (2.8).

The thermal analysis is conducted as an incremental and iterative non-linear analysis, configured with full option settings, using a regular time step size of 60 s, with minimum and maximum time steps of 1 s and 60 s, respectively. The convergence of the solution is based on heat flow criteria, with a tolerance value of 10^{-3} and a reference value of 10^{-6} W.

In Figures 4.4 and 4.5, within the cavity, heat transfer occurs via convection and radiation. At the midpoint of the cavity, the convective heat transfer coefficient is assumed to be 17 W/m²K, while the view factors are as specified in Table 4.2.

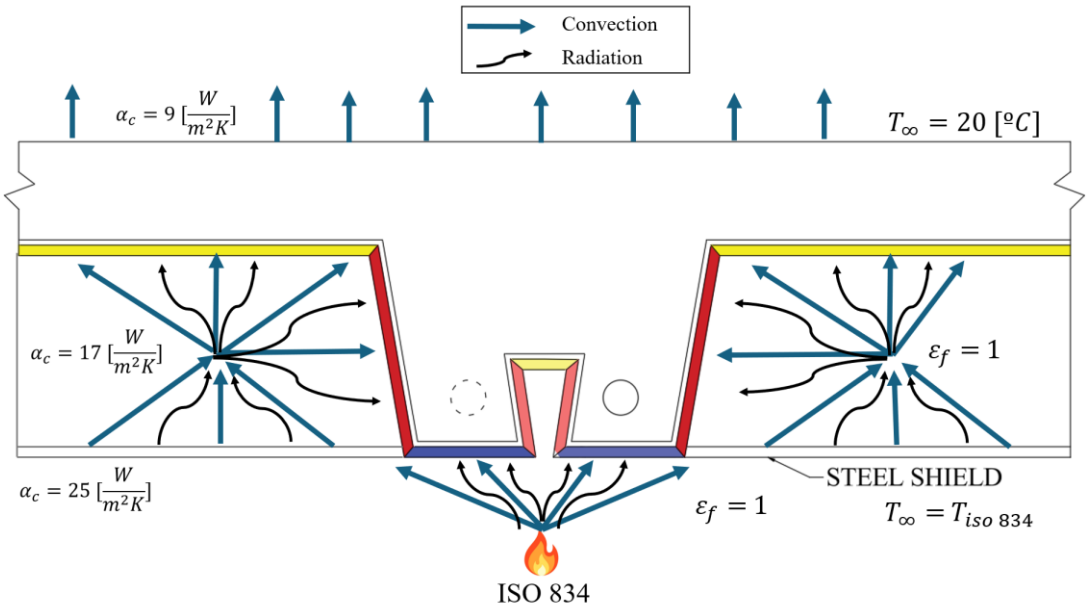

Figure 4.4. Thermal boundary condition of slab with steel shield insulation.

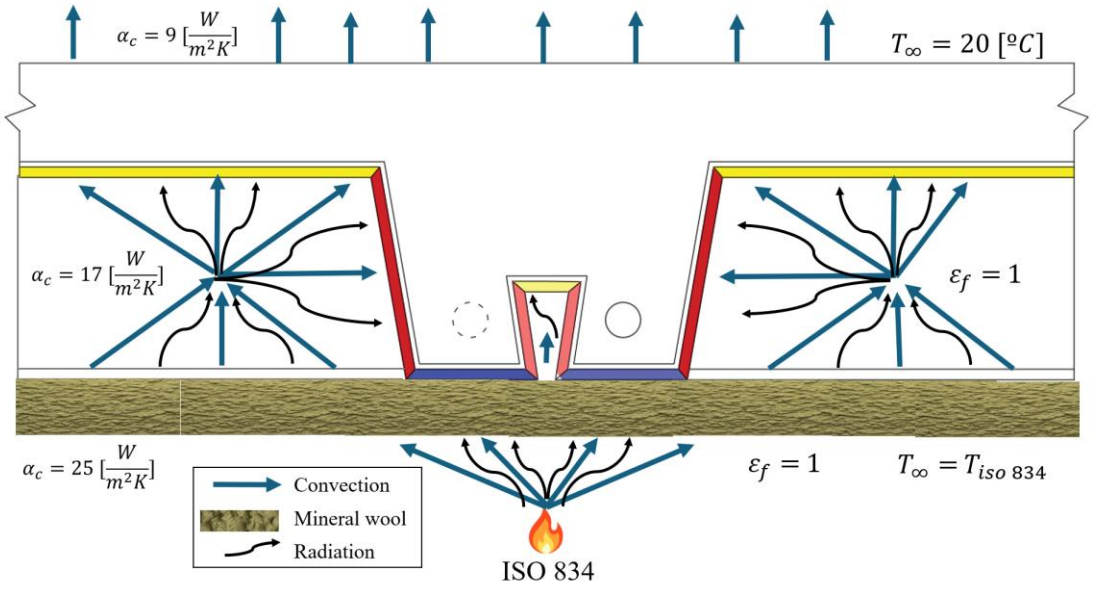

Figure 4.5. Thermal boundary condition of slab with mineral wool plate insulation.

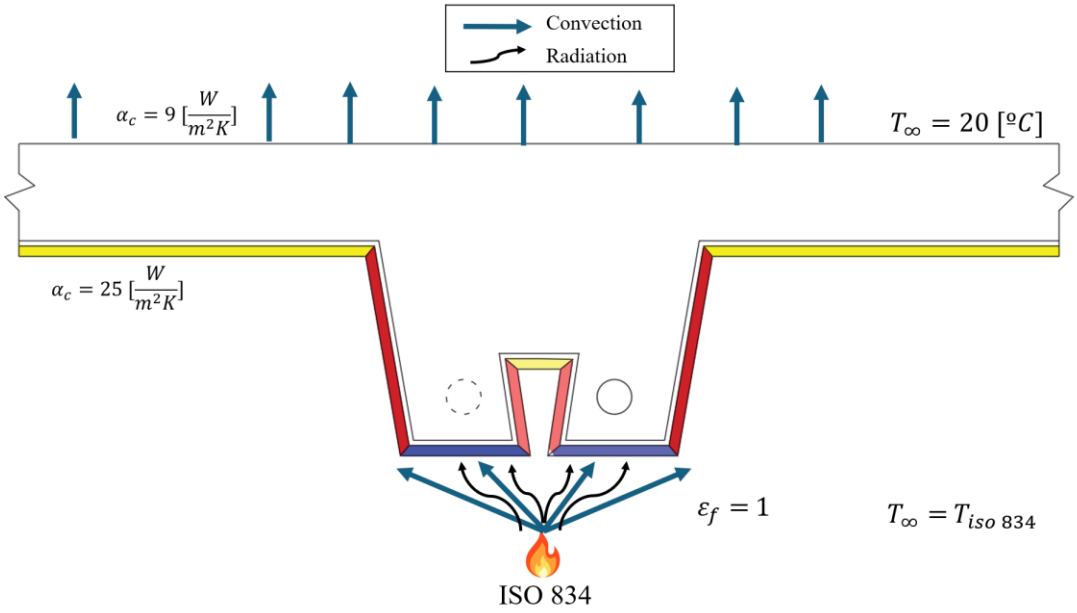

Figure 4.6. Thermal boundary condition of slab without insulation.

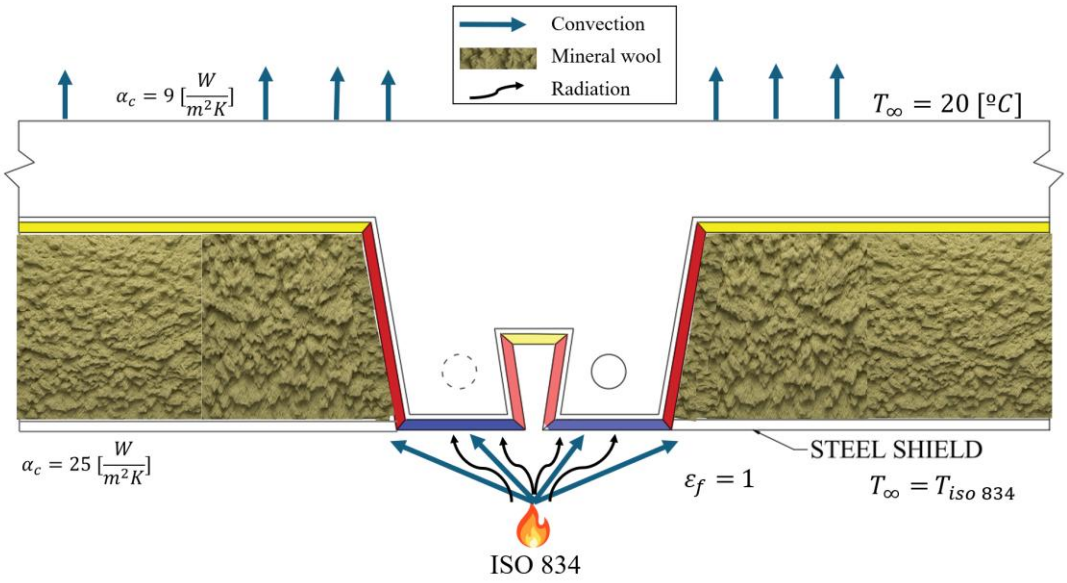

Figure 4.7. Thermal boundary condition of slab with mineral wool insulation.

4.4.FEM Mesh Density

The finite-element modelling was carried out in ANSYS using PLANE 55 elements for two-dimensional thermal conduction, LINK 31 elements for radiation and LINK 34 elements for convection, in accordance with the discretisation to be shown and convergence criteria already presented. The mesh density was chosen to balance accuracy

and computational efficiency and was subsequently validated against the experimental results presented in Section 6.1, where the results showed satisfactory agreement. Four simulation configurations were analysed, corresponding to different thermal-insulation strategies, differing only in the plate geometry.

Mesh for Case 1 (No Insulation): Heat transfer occurred solely by conduction through the steel, concrete and the air layer introduced to represent the debonding between steel and concrete, modelled entirely with PLANE55 elements. In this case, only direct contact between materials was assumed, with no additional cavities. Figure 4.8 illustrates the mesh for this scenario, showing structured elements in the straight regions and refinement adjacent to the critical interfaces.

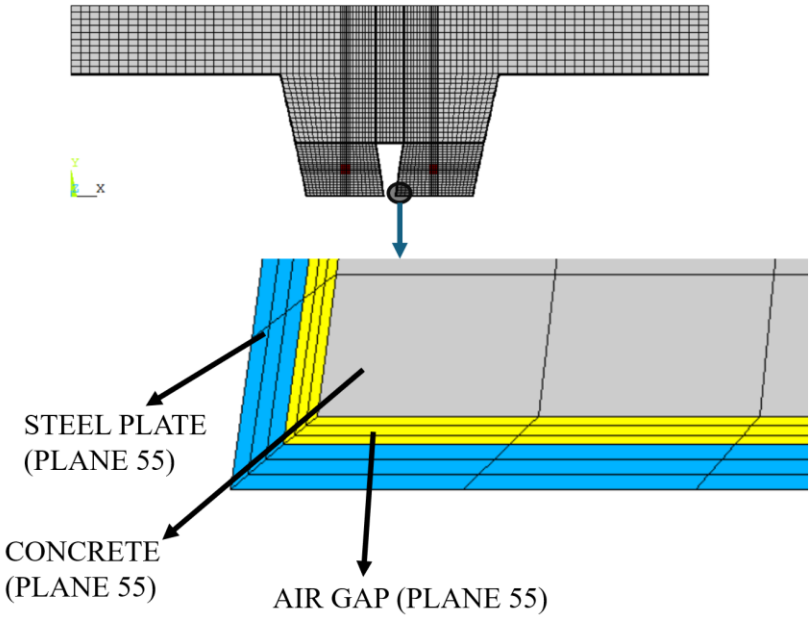

Figure 4.8. Mesh size for VP 115 without insulation.

Mesh for Case 2 (Steel Shield): This model accounted for the cavity formed between the steel shield and the UPPER 2 region, requiring the inclusion of LINK34 (radiation) and LINK31 (convection) elements to simulate the heat-transfer mechanisms in the cavity. Radiation was modelled with unit emissivity and a convection coefficient of 17 W/m²·K, as specified in Section 4.3. Figure 4.9 depicts the mesh for this configuration, emphasising the connectivity between the PLANE55 elements (slab) and the LINK31/34 elements (cavity), with particular attention to the regions where radiation and convection occur.

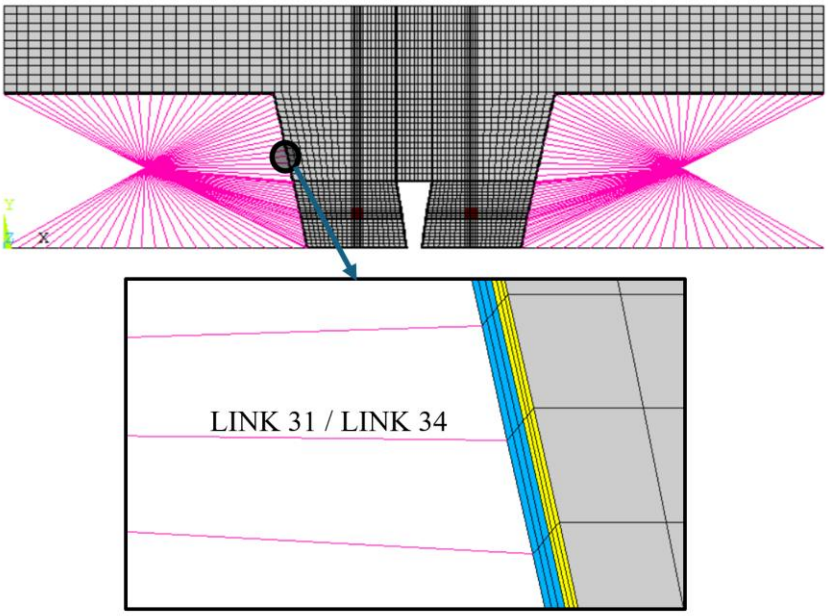

Figure 4.9. Mesh size for VP 115 with steel shield insulation.

Mesh for Case 3 (Rock Wool Insulation): The cavity was filled with mineral wool, replacing radiation and convection effects with pure conduction. PLANE55 elements were used to represent the insulating material, with equivalent thermal properties. Figure 4.10 shows the mesh for this configuration, with an adapted density to capture the heat flux accurately through the mineral wool, ensuring the precision of the thermal results.

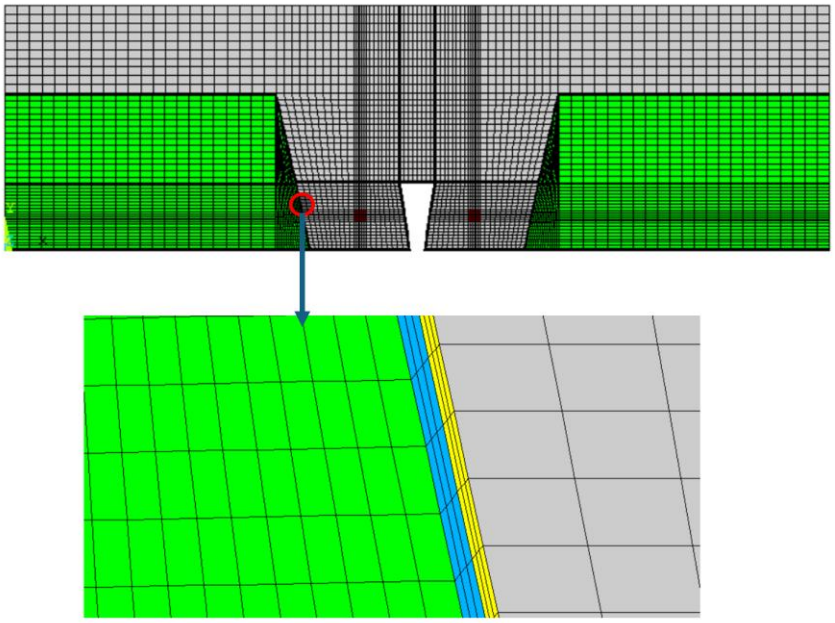

Figure 4.10. Mesh size for VP 115 with mineral wool insulation.

Mesh for Case 4 (Mineral Wool Plate): This configuration combined an external mineral wool plate (modelled with PLANE55) and a secondary cavity (with LINK31/34). The cavity region was treated according to the rules of Case 2, while the mineral wool acted as an additional thermal barrier. Nodal coupling guaranteed the interaction between elements, as illustrated in Figure 4.11, which details the boundary conditions for this configuration, including the temperature distribution and heat fluxes at the interfaces.

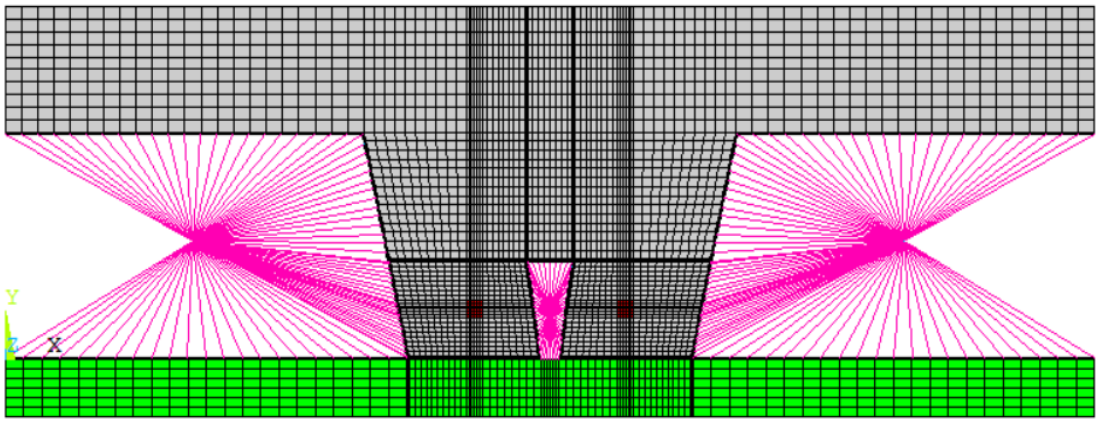

Figure 4.11. Mesh size for VP 115 with mineral wool plate insulation.

5. SIMPLIFIED CALCULATION METHODS

In Europe, the standardisation of these methods began with the European Convention for Steel Construction (ECCS), which in 1984 published pioneering guidelines for calculating the fire resistance of composite slabs with profiled steel sheeting [41]. Subsequent theoretical and numerical advances, such as those proposed by Hamerlink et al. [30] and Both [26], consolidated analytical approaches capable of predicting critical parameters, including thermal resistance (Criterion I) and load-bearing capacity under elevated temperatures (Criterion R).

Eurocode 4 Part 1-2 [17] incorporates these advances in its Annex B, providing simplified methodologies for determining the fire resistance of composite slabs with steel profiles. The method enables the calculation of metal component temperatures and verification of reduced flexural resistance due to heating, assuming conventional structural configurations. However, gaps persist: the standard does not address systems incorporating additional insulating layers, such as mineral wool. This section explores the theoretical foundations and limitations of these simplified methods, with emphasis on the application of Eurocode 4's Annex B.

5.1. Definition of steel decking by PR EN 1994-1-2

This subsection describes the processes required by the simplified temperature calculation method outlined in Annex B of PR EN 1994-1-2 [17]. When exposed to the ISO 834 standard fire [7], the simplified calculation approach for the load-bearing criterion (R) and thermal insulation criterion (I), as described in PR EN 1994-1-2, may be applied to supported composite slabs.

This simplified calculation model (PR EN 1994-1-2, 7.3) applies to unprotected slabs, and the bending resistance shall be determined using plastic theory. The following guidelines [17] cover only simply supported concrete slabs with steel deck (Figure 5.1), heated from below and subjected to the standard temperature-time curve.

The tables provided in Annex B of PR EN 1994-1-2 are used to determine the temperature of both materials. Direct actions caused by interactions with other structural elements are not considered (insulated member analysis).

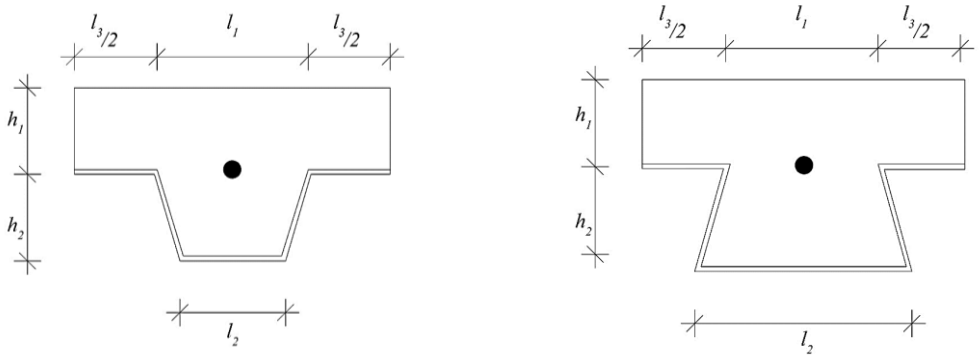

(a) (b)

Figure 5.1: Composite slabs parameters: (a) Trapezoidal, (b) Re-entrant [4].

Therefore, Table 5.1 outlines the geometric constraints for applying the simplified method specified in Annex B of PR EN 1994-1-2 to assess the fire-resistance performance with respect to Criterion I (insulation) and Criterion R (load-bearing capacity).

Table 5.1: Field of application for simplified calculation methods (PR EN 1994-1-2).

Trapezoidal steel decking profiles [mm]	**Re-entrant steel decking profiles [mm]**
$80 \leq l_1 \leq 155$	$77 \leq l_1 \leq 135$
$32 \leq l_2 \leq 132$	$110 \leq l_2 \leq 150$
$40 \leq l_3 \leq 115$	$38.5 \leq l_3 \leq 97.5$
$50 \leq h_1 \leq 125$	$50 \leq h_1 \leq 130$
$50 \leq h_2 \leq 100$	$30 \leq h_2 \leq 60$

5.2. Analysis of Insulation (I) criterion

Based on fire test results for flat concrete slabs, a rule has been established that correlates the minimum required slab thickness with the fire resistance rating. In principle, the thickness of the flat concrete slab is equivalent to the arithmetic mean thickness of the composite profiled slab, termed the effective thickness.

In addition to ensuring compliance with geometric limits, prEN 1994-1-2 provides two formulations to assess the Insulation criterion (I). The first employs Equation (5.1), which calculates the fire resistance time relative to insulation (t_i), expressed in [min]. The second method requires the calculation of the minimum effective slab thickness

(tabulated) to ensure the fire rating. Both methods adopt the insulation criteria when the unexposed slab face attains either:

- An average temperature rise of 140 °C, or
- A local maximum temperature rise of 180 °C,

relative to the initial average temperature.

$$t_i = a_0 + a_1 h_1 + a_2 \emptyset_{UPPER\,2} + a_3 \frac{A}{L_r} + a_4 \frac{1}{L_3} + a_5 \frac{A}{L_r} \frac{1}{L_3} \tag{5.1}$$

In the aforementioned equation, h_1 denotes the concrete thickness (mm);$\emptyset_{UPPER\,2}$ represents the top flange view factor [17], a dimensionless parameter derived from the spatial separation between the radiating and receiving surfaces, as well as their respective areas and orientations. The rib geometry factor *A*/*Lr*, expressed in [mm], is defined as the ratio of the concrete volume (mm³/m of rib length) to the exposed surface area A (mm²/m of rib length Lr) of the steel deck. This factor is calculated via the following formulation:

$$\frac{A}{L_r} = \frac{h_2 \left(\frac{L_1 + L_2}{2}\right)}{L_2 + 2\sqrt{h_2^2 + \left(\frac{L_1 - L_2}{2}\right)^2}} \tag{5.2}$$

The partial factors a_i are tabulated coefficients that are differentiated for normal-weight concrete (NWC) and lightweight concrete (LWC). These coefficients are shown in the following table.

Table 5.2: Coefficients for the determination of the fire resistance of composite slabs with NWC and LWC (adapted from EN 1994 -1-2[17]).

Concrete type	a_0 [min]	a_1 [min/mm]	a_2 [min]	a_3 [min/mm]	a_4 [min/mm]	a_5 [min]
NWC	-28.80	1.55	-12.6	0.33	-735	48.0
LWC	-79.2	2.18	-2.44	0.56	-542	52.3

The second method, as specified in prEN 1994-1-2, involves determining the effective thickness of a composite slab, denoted as h_{eff} [mm]. This parameter shall be calculated in accordance with Equations 5.3 and 5.4.

$$h_{eff} = h_1 + 0.5 \cdot h_2 \cdot \left(\frac{L_1 + L_2}{L_1 + L_3}\right) \qquad \text{for } {}^{h_2}/_{h_1} \leq 1.5 \text{ and } h_1 > 40 \text{ [mm]} \qquad (5.3)$$

$$h_{eff} = h_1 \cdot \left[1 + 0.75 \cdot \left(\frac{L_1 + L_2}{L_1 + L_3}\right)\right] \qquad \text{for } {}^{h_2}/_{h_1} > 1.5 \text{ and } h_1 > 40 \text{ [mm]} \qquad (5.4)$$

The relationship between the minimum effective slab thickness and the minimum fire resistance class (I) is presented in Table 5.3. The parameter $h3$ corresponds to the thickness of the screed layer, where present, applied atop the composite slab, as per Figure 5.2.

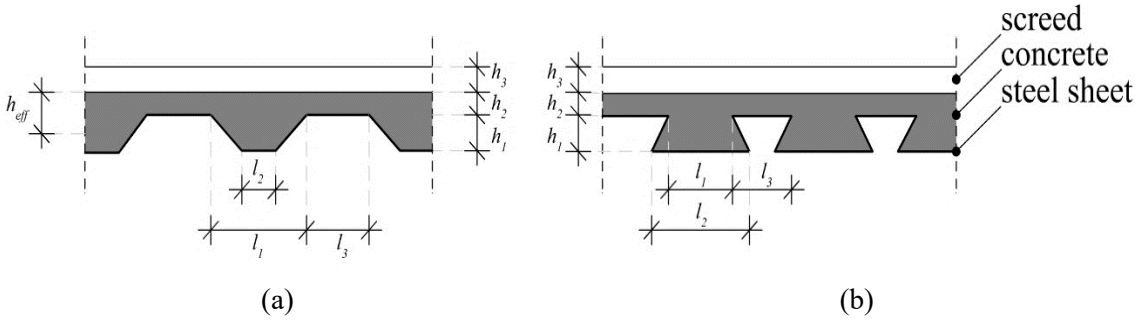

Figure 5.2: Symbols for (a) trapezoidal and (b) re-entrant sheeting (adapted [7]).

Table 5.3: Minimal effective thickness of the slab h_{eff} to satisfy the thermal insulation criteria.

Standard fire resistance	**Minimum effective thickness h_{eff} [mm]**
I 30	$60 - h_3$
I 60	$80 - h_3$
I 90	$100 - h_3$
I 120	$120 - h_3$
I 180	$150 - h_3$
I 240	$175 - h_3$

5.3.Analysis of load bearing (R) criterion

The simplified calculation method used for the (R) criterion presented by the prEN1994-1-2 [17] can be applied to simply supported composite slabs when exposed to standard fire ISO-834 [1]. To determine the bending moment capacity of the composite slab (sagging moment), this standard requires calculating the temperature for each component of the steel section (top flange, web, and bottom flange) for each required fire

rating, according to Eq. (5.5). The parameter ∅ is dimensionless and represents the view factor of the steel section component, as given by Eq. (2.12) and Eq. (2.13).

$$\theta_a = b_0 + b_1 \frac{1}{L_3} + b_2 \frac{A}{L_r} + b_3 \emptyset + b_4 \emptyset^2 \quad (5.5)$$

Where b_0, b_1, b_2, b_3, and b_4 are tabulated empirical coefficients only valid for the ISO 834 [7] and for fire ratings of 60, 90, and 120 minutes, see Table 5.4.

Table 5.4: Coefficients for the determination of the temperatures of the parts of the steel deck for slabs with NWC (adapted from EN 1994 – 1-2 [17]).

Standard fire resistance	Part of the steel deck	$\boldsymbol{b_0}$ [°C]	$\boldsymbol{b_1}$ [°C mm]	$\boldsymbol{b_2}$ [°C mm^{-1}]	$\boldsymbol{b_3}$ [°C]	$\boldsymbol{b_4}$ [°C]
R60	Lower flange	951	-1197	-2.32	86.4	-150.7
	Web	661	-833	-2.96	537.7	-351.9
	Upper flange	340	-3269	-2.62	1448.4	-679.8
R90	Lower flange	1018	-839	-1.55	65.1	-108.1
	Web	816	-959	-2.21	464.9	-340.2
	Upper flange	618	-2786	-1.79	767.9	-472.0
R120	Lower flange	1063	-679	-1.13	46.7	-82.8
	Web	925	-949	-1.82	344.2	-257.4
	Upper flange	770	-2460	-1.67	592.6	-379.0

Annex B of prEN 1994-1-2 [17] still defines the possibility to determine the rebar temperature, (θ_s) following Equation 5.6.

$$\theta_s = c_0 + c_1 \frac{u_3}{h_2} + c_2 z + c_3 \frac{A}{L_r} + c_4 \alpha + c_5 \frac{1}{L_3} \quad (5.6)$$

The z factor represents the position of the reinforcement relative to the slab rib, as shown in Eq. (5.7), given in mm$^{-0.5}$. The α represents the angle between the web component of the steel formwork and the horizontal direction in degrees (°), as shown in Figure 2. The ratio A/Lr is the rib geometry factor and represents the relationship between the concrete volume and the area exposed per meter of length of the steel formwork rib, given in mm, and its calculation is performed using Eq. (5.2). To facilitate the visualisation of these geometric factors, Figure 5.3 is presented.

$$\frac{1}{z} = \frac{1}{\sqrt{\frac{1}{u_1}}} + \frac{1}{\sqrt{\frac{1}{u_2}}} + \frac{1}{\sqrt{\frac{1}{u_3}}} \tag{5.7}$$

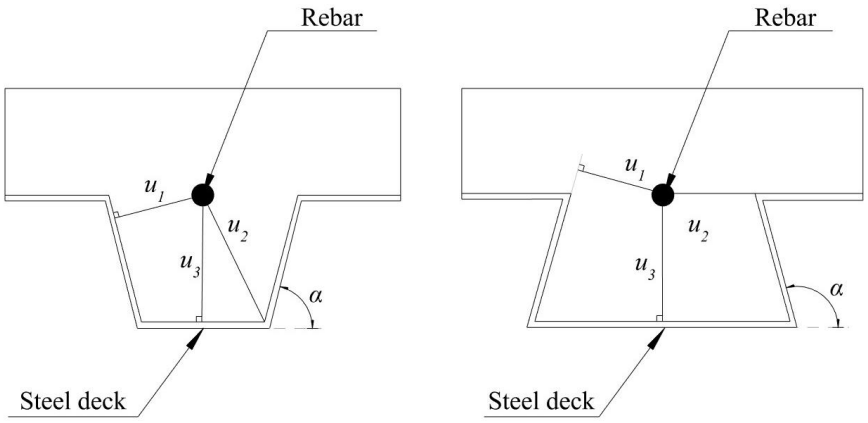

Figure 5.3: Parameters u_I for the z-factor calculation.

Table 5.5: Coefficients for the determination of the temperatures of the rebars for slabs with NWC (adapted from prEN 1994-1-2).

Standard fire resistance	c_0 **[°C]**	c_1 **[°C]**	c_2 **[°C** $mm^{-0.5}$**]**	c_3 **[°C mm^{-1}]**	c_4 **[°C/◦]**	c_5 **[°C mm]**
R60	1191	-250	-240	-5.01	1.04	-925
R90	1342	-256	-235	-5.30	1.39	-1267
R120	1387	-238	-227	-4.79	1.68	-1326

The method requires calculating the reduction factors (ky) with the defined temperatures according to prPREN 1994-1-2. The method neglects the effect of temperature on concrete. The first step is to define the neutral axis (z_i and z_j) using Eq. (5.8). Where "A_i" represents the effective area of the steel stress zone, adjusted by the factor (k_y); "A_j" is the effective area of concrete resisting to compression; and "α" is the coefficient weighting the contribution of the tension zone, taken as 0.85.

$$\sum_{i=1}^{m} A_i k_{y,i} \left(\frac{f_{y,i}}{\gamma_{M,y}}\right) + \alpha_{slab} \sum_{j=1}^{n} A_j k_{c,j} \left(\frac{f_{c,j}}{\gamma_{M,c}}\right) = 0 \tag{5.8}$$

Therefore, once the location of the plastic neutral axis (*Xpl*) has been established,

the design sagging moment resistance ($M_{Rd,fi,t}$) for composite slabs may be determined in accordance with Equation (5.9).

$$M_{Rd,fi,t} = \sum_{i=1}^{m} A_i z_i k_{y,i} (\frac{f_{y,i}}{\gamma_{M,y}}) + \alpha_{slab} \sum_{j=1}^{n} A_j z_j k_{c,j} (\frac{f_{c,j}}{\gamma_{M,c}}) \quad (5.9)$$

6. NUMERICAL AND SIMPLIFIED RESULTS

The results of the advanced thermal and simplified structural analyses encompass the behaviour of composite slabs under fire conditions, the performance of the proposed insulation systems, and the load-bearing capacity of the structures over time. The comparison between experimental results, figure 6.1, and numerical simulations demonstrates the validation of the models. The calibration of the empirical coefficients "ai", "bi" and "ci", are based on the numerical results obtained from the parametric study.

Figure 6.1. Specimen 2, by Fourie [15], after the test was completed.

6.1. Numerical validation

Figure 6.2(a) presents a comparison between the temperatures recorded in the unexposed region of the VP115 slab with steel shield, considering both the experimental test results obtained by Fourie [15] and by this study using ANSYS. Additionally, Figure 6.2 (b) compares Fourie's experimental results with the numerical results from this study for the upper 2 and web 2 zones. It can be noted that, for these regions, the experimental results show good agreement with the numerical results, as illustrated in Figure 7. The difference is highlighted in Figure 6.2, which displays Fourie's experimental temperature curves alongside the numerical curves from both Fourie and this study. According to Fourie [15], this difference is due to the formation of an air gap during the initial periods of the experiment, a phenomenon also noted by Piloto et al. (2020) [21].

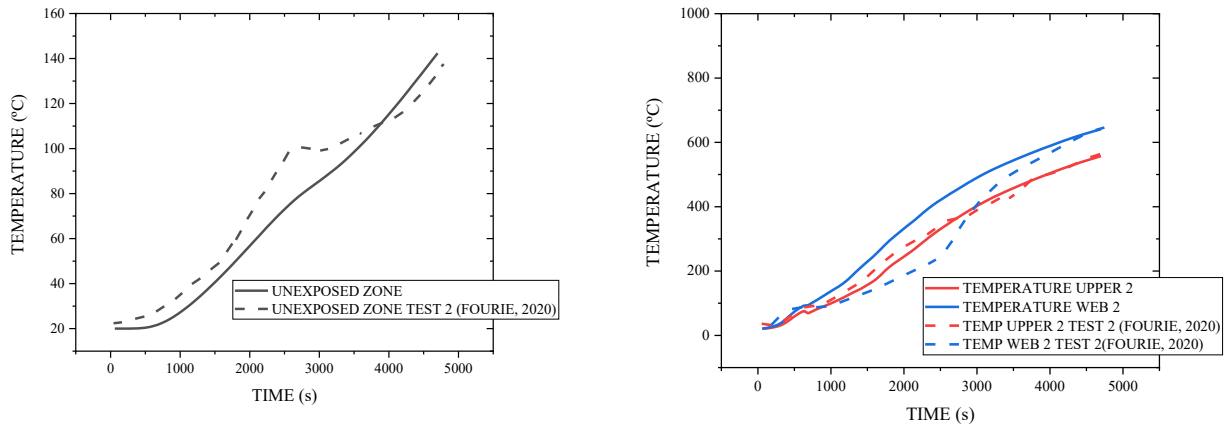

(a) (b)

Figure 6.2. Comparison of the experimental results by Fourie [15] with ANSYS model by this study. (a) Unexposed zone; (b) steel deck zones.

The air gap size is a constant average value, valid throughout the entire thermal simulation. The debonding effect results from the thermal expansion between steel and concrete. The actual air gap size in experiments is expected to increase depending on the fire event. The numerical results slightly underestimate the temperature of the unexposed concrete region and overestimate the steel temperature in the region UPPER 2.

The root mean square errors (RMS), calculated by Equation 6.1, are presented in Table 6.1. These values were determined between the numerical model and the experimental results throughout all the simulation, for the WEB 2, UPPER 2 and unexposed zones. This value reflects the accuracy of the computation model, considering that at any time after the first 10 minutes of any standard fire test, the temperature recorded by any thermocouple in the furnace should not differ from the corresponding temperature of the standard temperature/time curve by more than 100 °C [9].

$$\mathrm{RMSE} = \sqrt{\frac{1}{n}\sum_{i=1}^{n}(y_i - \mathcal{X}_i)^2}, \tag{6.1}$$

Where the temperature values obtained from the experimental test y_i for $i = 1,2,\ldots,80$ are compared with the numerical results $\mathcal{X}_i$ for $i = 1,2,\ldots,80$.

Table 6.1: Root mean square error (ºC) between experimental and numerical results.

REGION ZONE	RMS (ºC)
WEB 2	82.1
UPPER 2	18.1
UNEXPOSED	10.4

These results quantify the good agreement between the numerical model and the results determined by the experiment.

6.2. Fire resistance according to thermal insulation (I)

Regarding the first parametric study, the fire resistance (I) of composite slabs is predominantly governed by the average temperature rise criterion.

Figure 6.3 illustrates the fire insulation rating (I) for the VP115 profile, obtained through numerical modelling conducted in Ansys, on the unexposed surface during a 4 - hour simulation (ti = 240 minutes). The maximum temperature on the unexposed surface is expected to consistently correspond to the upper flange area of the steel profile in the absence of insulation. However, a distinct difference arises in the location of the maximum temperature point when any form of insulation is applied.

To calculate the average and maximum temperatures, 10 equally spaced nodes, from every simulation, were extracted. The node exhibiting the highest temperature was identified, and the arithmetic mean of all 10 points was determined to derive the average temperature curve.

The temperature rise on the unexposed surface of composite slabs is a significant concern from a thermal insulation perspective. It is crucial to control this temperature increase to prevent the ignition of materials on the unexposed face of the slab, thereby inhibiting fire spread.

This temperature is predicted by the model for a total simulation duration that ensures fire resistance predictions comply with regulatory standards. Weighted average and maximum temperatures are calculated on the unexposed side of the composite slab and compared against the criteria established for fire resistance (insulation).

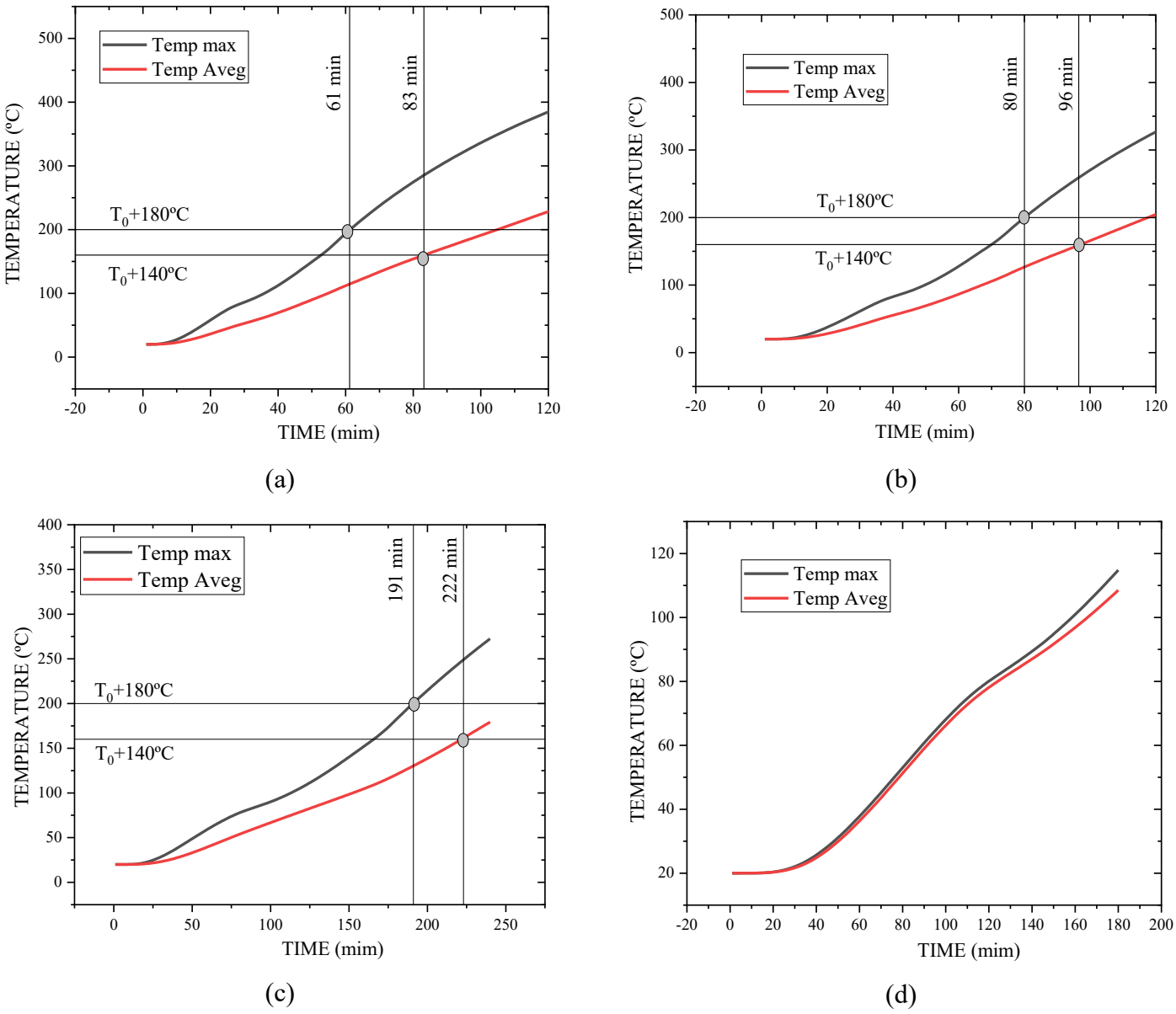

Figure 6.3: Unexposed temperature evolution for VP115: (a) without insulation; (b) steel shield insulation (c) Mineral Wool Plate with hi = 30mm; (d) mineral Wool insulation

Table 6.2 presents the results obtained for the fire resistance (criterion 'I') of the compoaite slab sections and their insulation types. The lowest value between the two limits determines fire resistance, according to EN1363-1 (2020) [9]. The prEN1994-1-2 [17] also defines the minimum effective thickness as a function of standard fire resistance.

After four hours of simulation using the ISO 834 curve [1], the results showed a time gain for the maximum and average temperatures on the unexposed surface compared to the composite slabs without insulation. The steel shield insulation in the three types of slabs resulted in a time gain of approximately 25% for the maximum temperature criterion in all slabs. The mineral wool in the VP50 slab section with h2 = 50 mm demonstrated a

total time gain of 43% compared to the slab without insulation.

The VP115 and VP200 with mineral wool slab sections, even after four hours, did not reach the temperature limit for the insulation criterion. The mineral wool plate insulation demonstrated significant improvements in fire resistance, with the fire insulation duration increasing proportionally to the insulation thickness (*hi*). On average, a *hi* of 30 mm exhibited a 65% enhancement in fire resistance compared to non-insulated slabs.

The fire resistance is presented in completed minutes, see table 6.1. The results in the table exemplify the values obtained for a steel platform thickness $t_s = 0.8$ [mm] and for rebar diameter $\emptyset_{rebar} = 10$ [mm].

Table 6.2: Time limit for the (I) criteria

Type of slabs	Insulation type		T_0+180 (min)	T_0+140 (min)
VP 50	without insulation		61	66
	steel shield		78	77
	mineral wool		109	113
	Mineral wool plate	hi = 5 mm	96	99
		hi = 10 mm	114	114
		hi = 20 mm	143	143
		hi = 30 mm	180	169
VP 115	without insulation		61	83
	steel shield		80	97
	mineral wool		333[a]	276[a]
	Mineral wool plate	hi = 5 mm	100	113
		hi = 10 mm	120	133
		hi = 20 mm	155	171
		hi = 30 mm	191	222
VP 200	without insulation		62	102
	steel shield		81	107
	mineral wool		449[a]	501[a]
	Mineral wool plate	hi = 5 mm	103	143
		hi = 10 mm	124	157
		hi = 20 mm	163	210
		hi = 30 mm	200	255 [a]

a) Exceeded the fire rating of 240 minutes for criterion (I) according to standard EN 13501-2 [59].

The temperatures at the unexposed surface and the fire resistance of composite slabs represent complex challenges in fire design, see Figure 6.4.

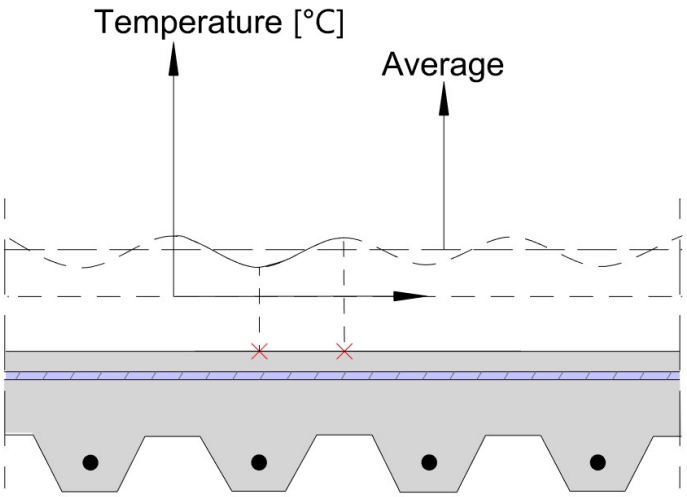

Figure 6.4: Theoretical temperature distribution at the unexposed surface of a fire exposed composite slab [4].

6.2.1. New proposal for Insulation Criterion for steel shield and mineral wool

Eurocode 4 Part 1-2 [17] provides generic guidelines for the design of composite steel-concrete structures under fire conditions. However, its provisions do not encompass composite slab systems incorporating insulating layers, as the simplified methods outlined in the standard assume conventional structural configurations, disregarding the influence of insulating materials on thermal redistribution and fire resistance. In the case of steel shield and mineral wool systems, adaptation of the coefficients, whether belonging to criterion (R) or criterion (I), is necessary to account for their thermal and structural behaviour during fire exposure.

The simplified method employs Eq. (5.1) to derive these coefficients for insulation time estimation. The calculation is performed using a non-linear evolutionary solver [89], implemented in Excel. Table 6.3 presents the newly established coefficients "a_i".

Table 6.3. New coefficients "a_i" proposed to determine the time of insulation in steel deck under fire curve ISO 834 for a Steel shield and mineral wool insulation

	a_0 (min)	a_1 (min/mm)	a_2 (min)	a_3 (min/mm)	a_4 (mm min)	a_5 (min)
Steel shield model	-28.79	1.72	-3.21	0	-734.5	7.9
Mineral wool model	-1207.42	19.71	-33.10	5.61	-26611.5	0.008

New empirical coefficients "a_i" were determined to calculate the fire resistance insulation time (in minutes) according to the standard prEN1994-1-2 [17].

6.2.2. New proposal for insulation criteria for Mineral Wool Plate

The proposed equation for determining the insulation time (*ti*) of mineral wool plates retains the fundamental structure of Eurocode 4 Part 1-2 [17], employing a linear combination of geometric and thermal parameters to estimate fire resistance. However, the formulation introduces two critical terms explicitly dependent on the insulation thickness (*hi*), addressing limitations in the Eurocode's methodology for systems incorporating mineral wool.

The general form of the equation aligns with Eurocode 4's framework:

$$t_i = a_0 + a_1 h_1 + a_2 \emptyset_{UPPER\,2} + a_3 \frac{A}{L_r} + a_4 \frac{1}{L_3} + a_5 \frac{A}{L_r}\frac{1}{L_3} + a_6 \log\left(\frac{hi}{1}\right) + a_7 * hi^{\frac{1}{h2^2}} \quad (6.1)$$

The coefficients a0 to a5 in Equation (6.1) are derived from the steel shield model (Section 6.2.1), ensuring continuity between insulation systems. This approach guarantees that when the thickness of the mineral wool insulation (*hi*) is zero, the equation simplifies to the steel shield configuration. Table 6.4 presents coefficients a6 and a7, which enable the calculation of thermal insulation for steel decking systems incorporating mineral wool plate.

Table 6.4. New coefficients "a_i" proposed to determine the time of insulation in steel deck under fire curve ISO 834 for mineral wool plate insulation

	a_6 (min)	a_7 (min)
Mineral wool plate model	112.6	-82.1

6.3. Temperature estimation according to Load-Bearing criteria (R)

Criterion (R) is verified by assuming a specific fire resistance rating for the structural element. Subsequently, it is necessary to confirm whether the load effect is less

than or equal to the bending resistance, determined by the reduction of the plastic moment due to temperature effects. The simulations were conducted for 180 minutes of fire exposure.

The current version of prEN 1994-1-2 provides a simplified method to determine temperatures for each fire resistance rating; however, as noted in previous sections, the standard does not encompass any type of insulation and offers no calculation methodology to assess criterion (R). Numerical results are averaged and compared for each temperature-affected component, in accordance with the geometries and regions outlined in Section 4.1.

A parametric analysis was developed, considering the temperature evolution and fire resistance. The critical temperatures of the steel components were determined based on fire resistance criteria.

Figures 6.5 to 6.6 show the temperature field in the composite slab after 7200 seconds of fire exposure, along with the time-averaged temperatures of the structural components for all insulation types analysed in this study. These include configurations with normal-weight concrete (NWC) thickness, concrete cover $h1$=65mm. The numerical results are identified by component names. The results presented in this subsection pertain to slabs with reinforcement diameter (Ørebar) of 10 [mm] and steel deck thickness (ts) of 0.8 [mm].

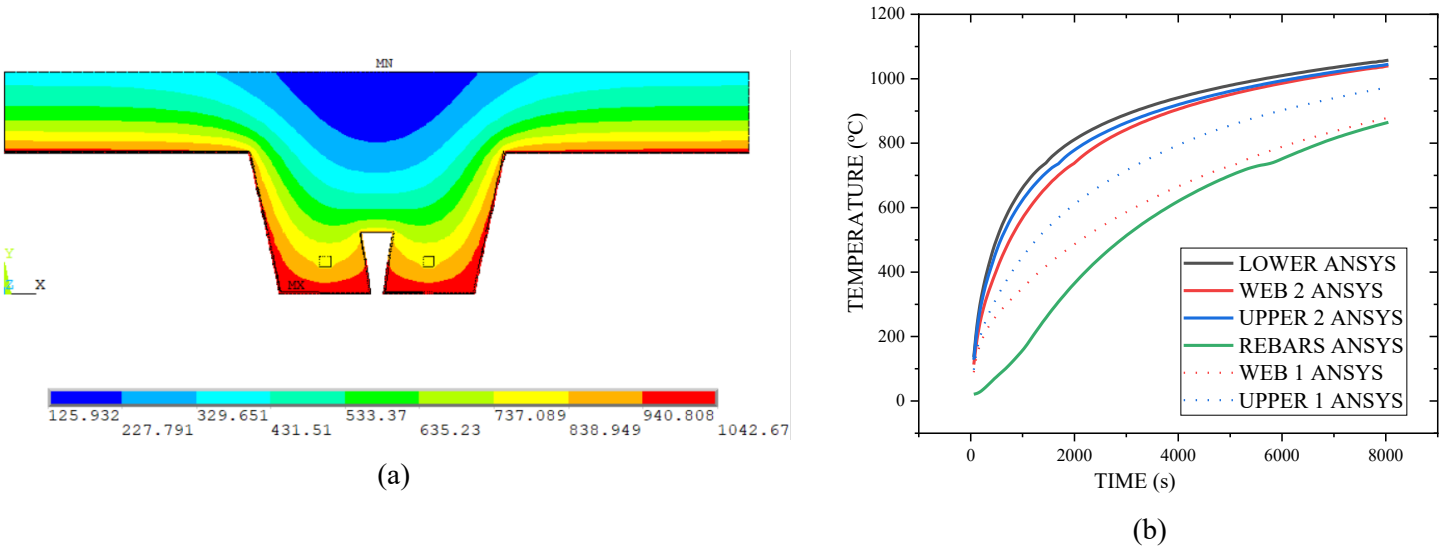

(a) (b)

Figure 6.5: Composite slab VP 115 without insulation under parametric of iso 834 curves for the same h_1=65mm. (a) Temperature field for a time equal to 7200 seconds. (b) temperature history of regions.

Figure 6.6 (a) presents the temperature field for the VP 115 steel deck with Steel

Shield insulation at the same time 7200 s, while Figure 6.6 (b) illustrates the temperature progression. A discernible temperature difference is observed across regions of the steel deck, with the most pronounced variations occurring in the WEB 2 and UPPER 2 zones. The remaining regions exhibited performance comparable to the without insulation configuration.

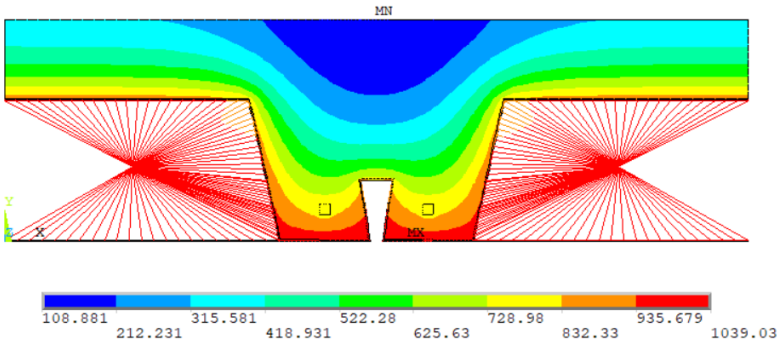

(a)

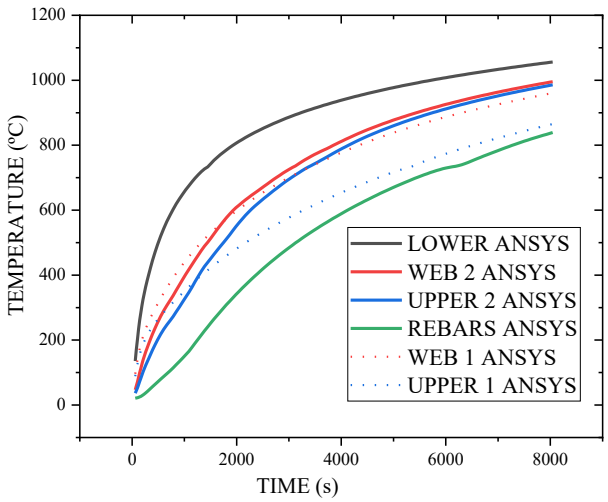

(b)

Figure 6.6: Composite slab VP 115 with steel shield insulation under parametric of iso 834 curves for the same h_l=65mm. (a) Temperature field for a time equal to 7200 seconds. (b) temperature history of regions.

Table 6.5 quantifies the differences between the two configurations.

Table 6.5. Comparison temperature between without insulation and steel shield insulation for VP115.

Time (min)	Region	Without insulation (ºC)	Steel shield (ºC)	Difference %
60	LOWER	923.2	920.6	0.27
	WEB 2	888.8	778.9	12.36
	UPPER 2	906.3	751.0	17.13
90	LOWER	994.4	990.6	0.40
	WEB 2	966.9	897.5	7.14
	UPPER 2	979.3	881.1	10.01
120	LOWER	1039.7	1038.1	0.09
	WEB 2	1018.7	969.7	4.81
	UPPER 2	1025.9	958.1	6.60

Figure 6.7 (a) displays the temperature field at 7200 seconds for the VP 115 deck configuration with mineral wool insulation filling the cavity. In this insulation format, the temperature differential in the WEB 2 and UPPER 2 regions is significantly higher

compared to the two previous configurations. However, the remaining regions exhibit thermal behaviour analogous to the earlier setups. Table 6.6 summarises the differences between the non-insulated configuration and the mineral wool insulation configuration.

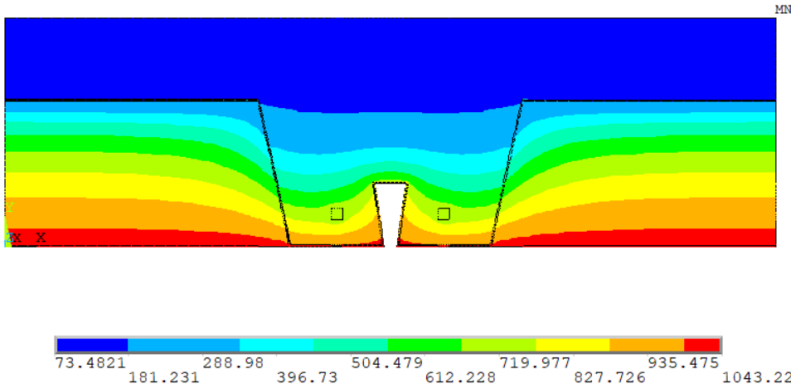

(a)

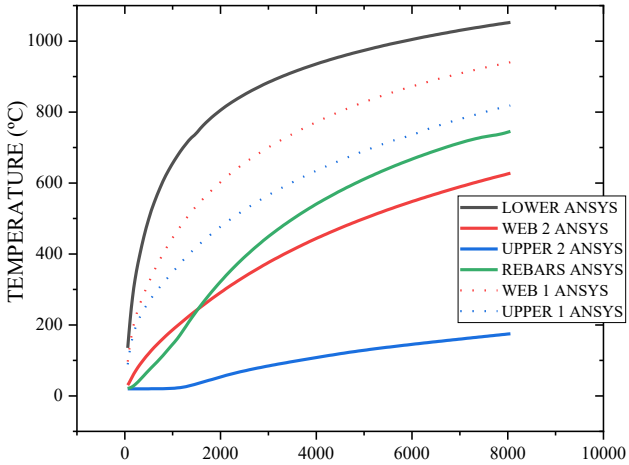

(b)

Figure 6.7: Composite slab VP 115 with mineral wool insulation under parametric of iso 834 curves for the same h_1=65mm. (a) Temperature field for a time equal to 7200 seconds. (b) temperature history of regions.

Table 6.6. Comparison temperature between without insulation and mineral wool insulation for VP115.

Time (min)	Region	Without insulation (ºC)	Mineral wool (ºC)	Difference %
60	LOWER	923.2	917.8	0.65
	WEB 2	888.8	391.3	44.00
	UPPER 2	906.3	99.3	89.07
90	LOWER	994.4	987.6	0.70
	WEB 2	966.9	491.2	49.14
	UPPER 2	979.3	135.9	86.21
120	LOWER	1039.7	1035.1	0.384
	WEB 2	1018.7	567.2	44.20
	UPPER 2	1025.9	163.2	84.07

Figure 6.8 (a) illustrates the temperature field at 7200 seconds for the VP 115 deck configuration insulated with a Mineral Wool Plate hi = 30mm. The insulation proved highly effective, as analysis of the temperature progression curves (Figure 6.8 (b)) reveals markedly greater temperature differentials across all regions compared to previous insulation systems.

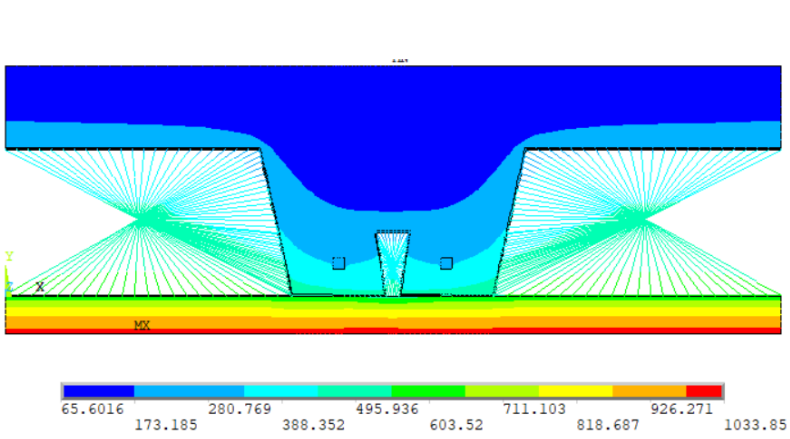

(a)

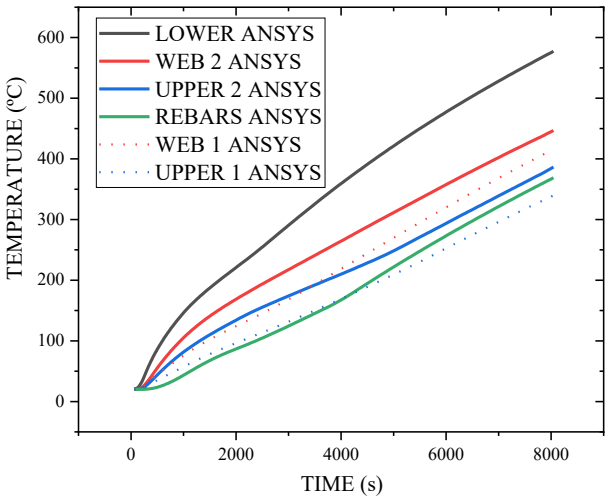

(b)

Figure 6.8: Composite slab VP 115 with mineral wool plate (hi=30mm) under parametric of iso 834 curves for the same h_l=65mm. (a) Temperature field for a time equal to 7200 seconds. (b) temperature history of regions.

Table 6.7 summarises the temperature differentials between the non-insulated configuration and the Mineral Wool Plate configuration.

Table 6.7. Comparison temperature between without insulation and mineral wool plate hi=30mm insulation for VP115.

Time (min)	Region	Without insulation (ºC)	Mineral wool plate hi = 30mm (ºC)	Difference %
60	LOWER	923.2	332.9	64.0
	WEB 2	888.8	254.8	71.0
	UPPER 2	906.3	195.8	78.0
90	LOWER	994.4	447.9	55.0
	WEB 2	966.9	332.9	66.0
	UPPER 2	979.3	269.5	72.0
120	LOWER	1039.7	538.0	48.0
	WEB 2	1018.7	411.0	60.0
	UPPER 2	1025.9	348.1	66.0

The observed differences in the previously presented configurations were analogous to those identified in comparison with the other configurations incorporating VP 50 and VP 200 plates. Moreover, the thermal insulation efficacy of the Mineral Wool Plate configuration, quantified via the thickness parameter (*hi*), demonstrates an intermediate performance between the Steel Shield insulation (baseline, *hi* = 0 mm) and the Mineral Wool Plate (*hi* = 30 mm). This is evidenced by comparative temperature gradient analysis across the two systems.

6.3.1. New temperature proposal for steel deck with steel shield and mineral wool

The numerical results obtained from ANSYS software are evaluated for each component of the composite slabs. The average temperatures are determined for the lower flange (LOWER zone), the web (WEB zone), and the upper flange (UPPER zone). Coefficients "b_i" and "c_i" are introduced for determining the average temperatures in the steel deck components insulated with Steel Shield and mineral wool, as well as in the reinforcing bars, considering the composite slabs under these fire conditions.

The proposed coefficients are obtained using Excel, which minimised the sum of the absolute differences between the numerical temperatures (obtained from the steel components in the parametric study) and the temperatures calculated by the model corresponding to Eq. (5.5) or Eq.(5.6). This minimisation is also performed using the non-linear evolutionary solver [89], available in the Excel SOLVER tool. The tool iteratively adjusted the values of "b_i" and "c_i" with the objective of achieving the lowest possible absolute error between the simplified method (with the new coefficients) and the numerical results.

Table 6.8 presents the proposed b_i coefficients for determining the temperature in steel deck components using the Steel Shield, maintaining their use in Eq. (5.5). It is noted that in the lower region, the "b_2" parameters are low, since in this insulation proposal the lower region is not protected, making the geometric parameters less relevant. This is due to the exposure in this region being practically the same.

Table 6.8. New coefficient "b_i" proposed to determine the temperature in steel deck under fire curve iso 834 for a steel shield insulation.

TIME (min)	STEEL DECK REGION	b_0 (ºC)	b_1 (ºC.mm)	b_2 (ºC.mm)	b_3 (ºC)	b_4 (ºC)
60	UPPER 2	655.63	-734.815	-0.32	193.9096	-52.90
	WEB 2	898.73	-18071.9	-1.57	276.0602	-210.84
	LOWER	953.79	-868.995	-0.13	17.31293	-40.132
90	UPPER 2	770.62	-17598.3	-1.14	511.3276	-186.22
	WEB 2	892.69	-12026.7	-1.09	491.0991	-404.97
	LOWER	1047.78	-473.694	-0.09	7.664627	-57.90
120	UPPER 2	897.64	-16998.5	-1.20	443.8899	-178.63
	WEB 2	973. 99	-5684.49	-0.61	228.0133	-188.25
	LOWER	980.55	-170.244	-0.05	75.57389	-14.705

Table 6.9 presents the proposed "b_i" coefficients for determining the temperature in steel deck components using the mineral wool, maintaining their use in Eq. (5.5).

Table 6.9. New coefficients "b_i" proposed to determine the temperature in steel deck under fire curve iso 834 for a mineral wool insulation.

TIME (min)	STEEL DECK REGION	b_0 (ºC)	b_1 (ºC.mm)	b_2 (ºC.mm)	b_3 (ºC)	b_4 (ºC)
60	UPPER 2	0	-80115.3	-5.54224	1182.233	-0.00016
	WEB 2	546.542	-5772.11	-4.82394	291.80	-0.00262
	LOWER	953.796	-868.995	-0.13103	17.31	-40.1328
90	UPPER 2	0	-131140	-8.22638	1844.938	-0.00041
	WEB 2	474.912	-0.3311	-4.53379	718.85	-378.888
	LOWER	1047.79	-473.694	-0.09809	7.66	-57.907
120	UPPER 2	0	-189471	-11.2556	2582.478	0
	WEB 2	802.465	-13254.1	-5.70221	325.1772	-0.00084
	LOWER	980.556	-170.244	-0.05367	75.57389	-14.7057

For the regions UPER 1 and WEB 1, which are areas without any insulation, the calculations can be performed using the coefficients presented in the new approach proposed by Carlos Balsa et al. [90].

Tables 6.10 and 6.11 present new coefficients to determine the average temperatures of the rebars with Steel Shield and Mineral Wool insulation, respectively, maintaining their use in Eq. (5.6).

Table 6.10. New coefficients "c_i" proposed to determine the temperature in steel deck under fire curve iso 834 for a steel shield insulation.

TIME (min)	c_0 (ºC)	c_1 (ºC)	c_2 (ºC.mm$^{0.5}$)	c_3 (ºC.mm)	c_4 (ºC/º)	c_5 (ºC.mm)
60	947.1	-201.6	-268.1	-3.25	4.17	-4585.2
90	1027.5	-198.8	-176.1	-3.98	3.63	-14491.4
120	1153.7	-271.6	-158.3	-3.92	2.94	-12363.0

Table 6.11. New coefficients "ci" proposed to determine the temperature in steel deck under fire curve iso 834 for a mineral wool insulation.

TIME (min)	c_0 (ºC)	c_1 (ºC)	c_2 (ºC.mm$^{0.5}$)	c_3 (ºC.mm)	c_4 (ºC/º)	c_5 (ºC.mm)
60	930.078	-292.355	-117.716	-3.74446	0.936562	-7273.17
90	963.447	-143.803	-177.807	-1.52391	1.434412	-10.1888
120	1007.2	-253.709	-198.434	-3.50322	4.105537	-8.06392

6.3.2. New steel temperature proposal for the steel deck with mineral wool plate

For the insulation proposal utilising mineral wool board with a density of 70 kg/m³,

the calculation of the temperature at the deck incorporates two additional factors dependent on the thickness of the insulating material. The governing equation 6.2 for this insulation approach employs the coefficients bi from Table 6.8, corresponding to Steel Shield insulation, and includes the parameters b5 and b6.

$$\theta_a = b_0 + b_1\frac{1}{L_3} + b_2\frac{A}{L_r} + b_3\emptyset + b_4\emptyset^2 + b_5 * hi^{\frac{1}{h2^2}} + b_6 \log\left(\frac{hi}{1}\right) \qquad (6.2)$$

Table 6.12 presents these coefficients b5 and b6, derived from the results of the parametric study in Section 4.2, which was also conducted utilising the non-linear evolutionary solver [89].

Table 6.12. New coefficient "b_i" proposed to determine the temperature in steel deck under fire curve iso 834 for a mineral wool plate insulation.

TIME (min)	STEEL DECK REGION	b5 (ºC)	b6 (ºC)
60	Upper 1-2	81,8	-437.8
	Web 1-2	205,1	-518,687
	Lower	270,8	-580,242
90	Upper 1-2	261,2041	-598,867
	Web 1-2	295,8592	-605,429
	Lower	336,9763	-596,251
120	Upper 1-2	337,2489	-646,264
	Web 1-2	357,831	-641,31
	Lower	353,4428	-572,978

Equation 6.3 provides the temperature estimate for the steel bars in the mineral wool board insulation proposal, where the coefficients c_0 to c_5 are obtained from Table 6.10 And the new coefficients c_6 are presented in table 6.13.

$$\theta_s = c_0 + c_1\frac{u_3}{h_2} + c_2 z + c_3\frac{A}{L_r} + c_4\,\alpha + c_5\frac{1}{L_3} + c_6 \log\left(\frac{hi}{1}\right) \qquad (6.3)$$

Table 6.13. New coefficient "c_6" proposed to determine the temperature in rebars under fire curve iso 834 for a mineral wool plate insulation.

TIME (min)	C_6 (ºC)
60	930.078
90	963.447
120	1007.2

7. THERMO-MECHANICAL PERFORMANCE

The assessment of the thermomechanical performance of composite slabs under fire conditions requires the integration of thermal and structural analyses, aiming to ensure safety and functionality during fire exposure. This section explores the degradation of the load-bearing capacity of the slabs as a function of increasing temperature, with emphasis on the interaction between heat transfer and the loss of material stiffness. The results presented provide critical insights for optimising passive protection strategies and mitigating the risk of premature failure.

7.1. Bending resistance under fire

The criterion for the load-bearing capacity of a structure under fire exposure, measured in minutes, is defined by its ability to withstand the design load demands. Accordingly, the maximum duration of mechanical resistance of the structure is verified in accordance with Inequation 7.1, which stipulates that the resisting bending moment $M^{+}_{Rd,fi,t}$ must always exceed the design-applied bending moment M_{sd}.

$$M_{Rd,fi,t}{}^{+} > M_{sd} \tag{7.1}$$

Using Equations 5.8 and 5.9 from Section 5.3 for calculating the resisting bending moment, computations were performed for the slabs in the parametric study (VP 50, VP 115, and VP 200), as presented in Figures 7.1 to 7.3. The loss of load bearing is represented In these figures. The left-hand axis denotes the actual load-bearing capacity in kN·m, while the right-hand axis represents the structure's load-bearing capacity percentage.

Table 7.1 presents the loss of load-bearing capacity percentage for different fire ratings, for configurations utilising the VP 115 deck. Analysis of the table reveals the varying degrees of fire resistance conferred by distinct insulation types on a VP 115 deck structure under fire conditions.

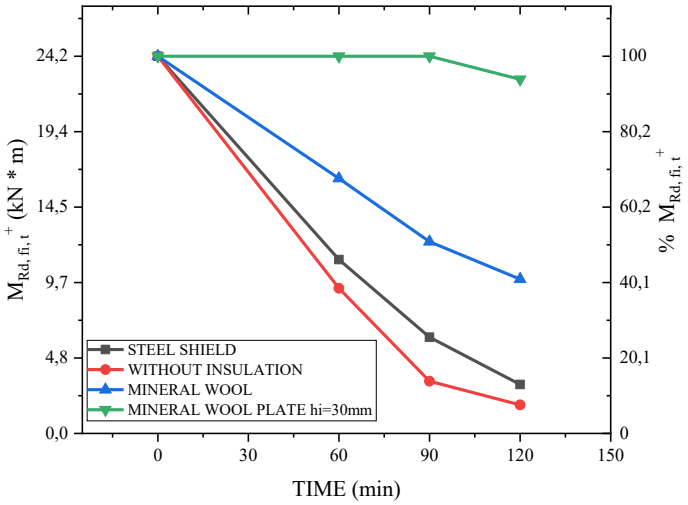

Figure 7.1. Evolution of the loss of load-bearing capacity of the slab ($M_{Rd,fi,t}$) over time under the ISO 834 fire curve for VP115.

At 60 minutes, for instance, the uninsulated structure retains only 38.5% of its load-bearing capacity. The incorporation of Steel Shield insulation yields a significant enhancement, achieving 46% greater resistance compared to the intact structure. Notably, the Mineral Wool Plate configuration with a thickness (hi) of 30 mm remains undamaged at the 60-minute mark. The operational range for Steel Shield configurations spans from hi = 0 mm to hi = 30 mm, thereby providing enhanced decision-making flexibility in selecting the optimal insulation type for fire protection.

Table 7.1. Loss of load bearing (% $M_{Rd,fi,t}$) capacity for VP115 in relation t = 0 min.

Time (min)	% $M_{Rd,fi,t}$			
	Without insulation	Steel Shield Insulation	Mineral wool Insulation	Mineral wool plate hi = 30mm
0	100	100	100	100
60	38.5	46.0	67.5	100
90	13.8	25.5	50.8	100
120	7.5	12.9	40.9	93.8

The figure 7.2 presents the loss of load-bearing capacity percentage for the steel deck VP 50.

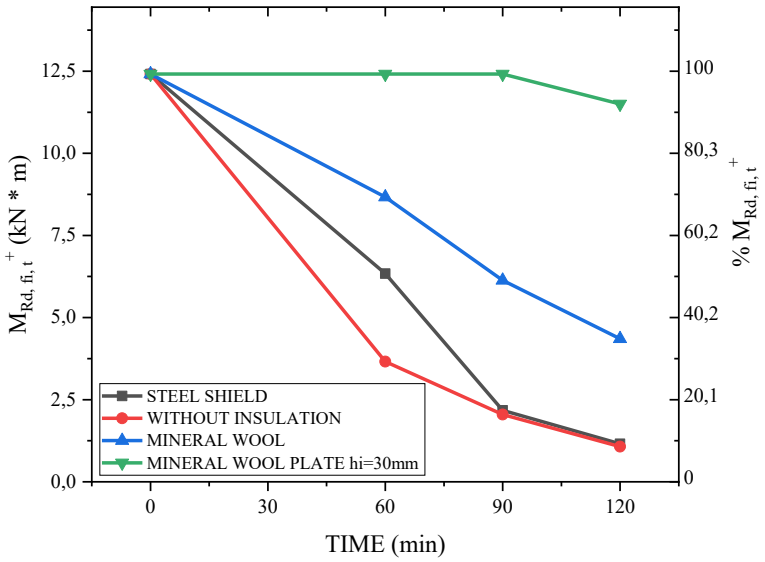

Figure 7.2. Evolution of the loss of load-bearing capacity of the slab ($M_{Rd,fi,t}$) over time under the ISO 834 fire curve for VP50.

Table 7.2 presents the loss of load-bearing capacity percentage as a function of the fire rating, for configurations utilising the VP 50 deck. The fire resistance enhancements are comparable to those observed in the VP 115 structure analysed above.

Table 7.2. Loss of load bearing (% $M_{Rd,fi,t}$) capacity for VP50 in relation t = 0 min.

Time (min)	% $M_{Rd,fi,t}$			
	Without insulation	Steel Shield Insulation	Mineral wool Insulation	Mineral wool plate hi = 30mm
0	100	100	100	100
60	29.4	51.0	69.8	100
90	16.5	17.5	49.4	100
120	8.6	9.3	35.1	92.6

The figure 7.3 presents the loss of load-bearing capacity percentage for the steel deck VP 200.

Table 7.3 presents the loss of load-bearing capacity percentage as a function of fire rating, for configurations utilising the VP 200 deck.

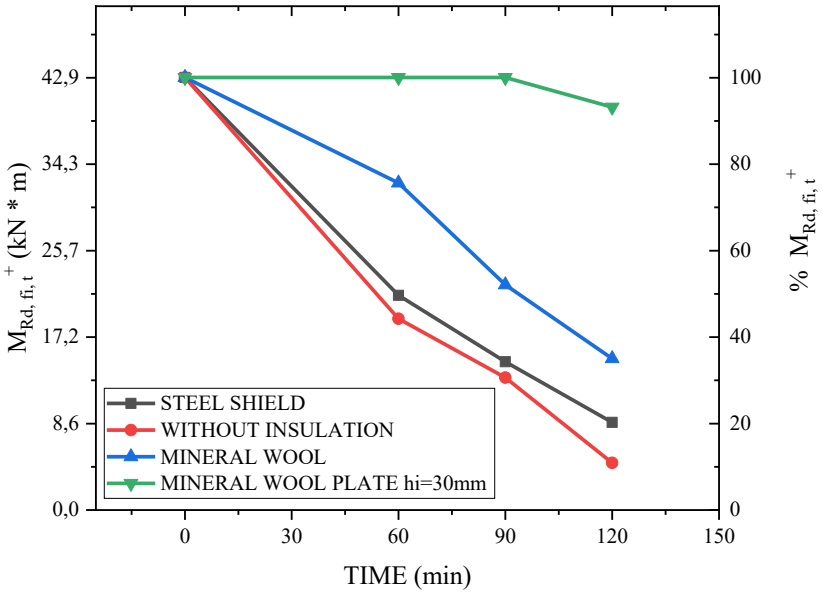

Figure 7.3. Evolution of the loss of load-bearing capacity of the slab ($M_{Rd,fi,t}$) over time under the ISO 834 fire curve for VP200.

Table 7.3. Loss of load bearing (% $M_{Rd,fi,t}$) capacity for VP200 in relation t = 0 min.

Time (min)	% $M_{Rd,fi,t}$			
	Without insulation	Steel Shield Insulation	Mineral wool Insulation	Mineral wool plate hi = 30mm
0	100	100	100	100
60	44.2	49.6	75.6	100
90	30.6	34.2	52.1	100
120	10.9	20.2	35.0	93.1

The analysis of the fire resistance enhancements provided by insulation systems for a given slab enables a broader range of fire scenario design decisions. In addition to extending the fire resistance duration of the slab, it is also feasible to substitute slabs with equivalent mechanical resistance capacities, as demonstrated in Section 7.1.

According to the results, the fire resistance increases with the increase of the steel deck size.

7.2. Carbon emissions regarding the load bearing under fire

Through a mechanical analysis of the differences in insulation systems and their mechanical behaviours, it is possible to leverage the gain in mechanical strength of structures under fire exposure to optimise and reduce concrete usage.

Conventional concrete emits approximately 430 kg of CO2 per cubic metre [91].

By replacing a slab constructed with VP 200 (without insulation), as outlined in the parametric studies in Section 4.2 of this work, with a VP 115 slab incorporating a 30 mm-thick mineral wool board insulation (hi = 30 mm) to ensure 60-minute fire resistance, a reduction in concrete volume is achieved.

Table 7.4 presents a comparison of carbon emissions and the mechanical strength enhancement for slabs with 30 mm mineral wool board insulation and uninsulated slabs. The carbon footprint per square metre of slab is calculated by summing the CO2 emissions from the concrete and mineral wool. The mineral wool insulation (hi = 30 mm) has a carbon emission of 3.09 kg of CO2 per square metre [92].

In the case of replacing VP 200 slabs with VP 115 slabs incorporating insulation, a reduction of approximately 20% in carbon emissions is achieved. This represents a significant figure, particularly in light of current demands for carbon reduction, given that cement is not only the most widely used material globally but also the largest contributor to CO2 emissions within the construction sector.

Table 7.4: Carbon emissions in comparison for Load Bearing of the steel deck slabs

STEEL DECK PLATE	Model Without insulation		Mineral Wool Plate hi = 30 mm	
	Emissions of CO_2 (Kg/m^2)	Load bearing after 60 min (KN * m)	Emissions of CO_2 (Kg/m^2)	Load bearing after 60 min (KN * m)
VP 50	34.76	3.65	37.85	12.41
VP 115	42.40	9.34	45.49	24.27
VP 200	58.21	21.31	61.30	42.93

8. CONCLUSIONS

In this thesis, the fire performance of composite steel-deck slabs has been rigorously investigated through a combination of two-dimensional numerical simulations, experimental validation and parametric sustainability analyses. The work has demonstrated that by integrating passive thermal insulation — either via a bespoke steel shield or mineral wool panel — substantial improvements can be achieved in both fire resistance and environmental impact, without compromising structural efficiency.

First, advanced numerical models were calibrated against Fourie's full-scale furnace tests to capture the critical "air-gap" debonding phenomenon arising from thermal expansion between steel and concrete. The validated thermal simulations revealed that the adoption of steel shields reduced peak temperatures in the unexposed concrete by up to 41 %, while mineral wool panels yielded comparable insulation performance. These findings confirm that passive insulation strategies effectively delay the thermal ingress into the primary load-bearing components of the slab.

Second, by extracting empirical coefficients (a_i, b_i, c_i) from the validated models, new simplified calculation rules have been proposed to extend Eurocode 4's prescriptive framework to insulated composite decks . In particular, the revised quadratic relationships between fire-resistance duration and effective slab thickness enable designers to predict insulation criterion (I) performance with higher accuracy than current Eurocode Annex B methods, which neglect air-gap effects and cooling-phase phenomena.

Third, a detailed mechanical-analysis study under fire loading showed that the combination of thermal insulation and optimised steel-mesh reinforcement substantially prolongs the load-bearing capacity (R) of the slab. Notably, sections insulated with 30 mm mineral wool achieved full 60-minute ratings at a reduced concrete thickness (VP 115), compared to uninsulated VP 200 slabs, thereby unlocking up to 20 % savings in concrete volume and associated CO_2 emissions. Such material optimisation aligns directly with global sustainability measures, reducing embodied carbon while maintaining or enhancing structural resilience.

Overall, the conclusions drawn are as follows:

1. Enhanced Fire Resistance through Passive Insulation.

   Both steel shields and mineral wool panels significantly delay temperature rise in critical slab regions, extending fire-resistance durations without reliance on conventional concrete cover or additional rebar.

2. Refined Simplified Design Rules

   Newly calibrated coefficients for insulated profiles offer a pragmatic extension to Eurocode 4, improving predictive accuracy for both insulation (I) and load-bearing (R) criteria by accounting for air-gap insulation and cooling-phase effects.

3. Sustainability Gains

   Insulation-driven reductions in required concrete thickness translate directly into lower CO_2 emissions—up to a 20 % decrease per square metre—thereby contributing to the construction sector's decarbonisation goals.

4. Practical Design Recommendations

   For buildings requiring 60–90 minute fire ratings, the use of VP 115 sections with 30 mm mineral wool insulation is recommended as a cost-effective and sustainable alternative to thicker uninsulated slabs.

5. Limitations and Future Work

   While two-dimensional modelling captured the principal thermal and structural behaviour, three-dimensional effects—such as edge radiation, slab–beam interface detailing and mechanical load redistribution—merit further investigation. Future research should also explore long-term durability of insulation under cyclic thermal exposure and full-scale validation of the proposed simplified rules in varied geometries also using different tipes of insulation, e.g gypsum plate. Also simulate the displacement of the steel shield and its connections for future experiments.

In conclusion, this study bridges critical gaps in composite slab fire design by integrating innovative insulation strategies with advanced numerical modelling and sustainability assessment. The proposed methodologies and design rules empower engineers to achieve robust fire safety, structural efficiency and carbon reduction in composite steel-deck construction.

REFERENCES

[1] ISO 834-1. Fire Resistance Tests—Elements of Building Construction—Part 1: General Requirements. International Organization for Standardization: Geneva, Switzerland, 1999.

[2] Buchanan, A. H. & Abu, A. K. (2017), Structural design for fire safety, John Wiley & Sons.

[3] Gillie, M.; Usmani, A.; Rotter, M.; O' Connor, M. Modelling of heated composite floor slabs with reference to the Cardington experiments. Fire Saf. J. 2001, 36, 745–767.

[4] Lima, Lídia da Rocha Souza. *Three-Dimensional Simulation of Composite Slabs Under Fire Conditions*. MS thesis. Instituto Politecnico de Braganca (Portugal), 2022.

[5] Mikulčić, Hrvoje, et al. "Reducing greenhouse gasses emissions by fostering the deployment of alternative raw materials and energy sources in the cleaner cement manufacturing process." *Journal of cleaner production* 136 (2016): 119-132.

[6] Reis, Daniel Costa, et al. "Potential CO2 reduction and uptake due to industrialization and efficient cement use in Brazil by 2050." Journal of Industrial Ecology 25.2 (2021): 344-358.

[7] Filho, Marcílio MA; Piloto, Paulo AG; Balsa, Carlos. Thermal behaviour of rebars and steel deck components of composite slabs under natural fire. *Journal of Composites Science*, 2022, 6.8: 232.

[8] Yu, X.; Huang, Z.; Burgess, I.; Plank, R. Non-linear analysis of orthotropic composite slabs in fire. Eng. Struct. 2008, 30, 67–80.

[9] EN 1363-1:2020. Fire resistance tests - Part 1: General requirements. European Committee for Standardization (CEN), 2020.

[10] Pantousa, D.; Mistakidis, E. Advanced modeling of composite slabs with thin-walled steel sheeting submitted to fire. Fire Technol. 2013, 49, 293–327.

[11] Crisinel, M., Recent Developments in Steel/Concrete Composite Slabs, Struct. Eng. Int., vol. 6, no. 1, pp. 4141, 1996, doi: 10.2749/101686696780495987.

[12] G. M. Cooke, G. M. E., LKawson, R. M., Newman, Fire resistance of composite deck slabs, Struct. Eng., vol. 66, 1988.

[13] Jiang, Jian, et al. "Improved calculation method for insulation-based fire resistance of composite slabs." Fire Safety Journal 105 (2019): 144-153.

[14] S. Lamont, A. S. Usmani, and M. Gillie, Behaviour of a small composite steel frame structure in a long-cool and a short-hot fire, Fire Saf. J., vol. 39, no. 5, pp. 327357, Jul. 2004, doi: 10.1016/j.firesaf.2004.01.002.

[15] Fourie, Stephen Junior. Design and construction of an intermediate-scale fire resistance furnace, with commissioning and validation on a novel composite floor system. Diss. Stellenbosch: Stellenbosch University, 2020.

[16] Jiang, J.; Cai, W.; Chen, W.; Ye, J.; Li, G.-Q. An insight into eurocode 4 design rules for thermal behaviour of composite slabs. Fire Saf. J. 2021, 120, 103084.

[17] PR EN 1994-1-2. Design of Composite Steel and Concrete StructuresPart 12: General rules Structural Fire Design. CEN European Committee for Standardization: Brussels, Belgium, 2024.

[18] Gernay, T.; Franssen, J.-M. A performance indicator for structures under natural fire. Eng. Struct. 2015, 100, 94103.

[19] Ramesh, S.; Ramesh, S.; Choe, L.; Seif, M.; Hoehler, M.; Grosshandler, W.; Sauca, A.; Bundy, M.; Luecke, W.E.; Bao, Y.; et al. Compartment Fire Experiments on Long-Span Composite-Beams with Simple Shear Connections Part 1; NIST Technical Note 2054; US Department of Commerce, National Institute of Standards and Technology: Gaithersburg, MD, USA, 2019.

[20] Choe, L.Y.; Ramesh, S.; Hoehler, M.S.; Seif, M.S.; Bundy, M.F.; Reilly, J.; Glisic, B. Compartment Fire Experiments on Long-Span Composite-Beams with Simple Shear Connections Part 2; NIST Technical Note 2054; US Department of Commerce, National Institute of Standards and Technology: Gaithersburg, MD, USA, 2019.

[21] Piloto, Paulo AG, et al. "Effect of the load level on the resistance of composite slabs with steel decking under fire conditions." Journal of Fire Sciences 38.2 (2020): 212-231.

[22] American Society for Testing and Materials, ASTM E119 - Standard test methods for fire test of building construction and materials., ASTM - Am. Soc. Test. Mater., vol. 552, no. 1, p. 36, 1992, [Online]. Available: www.aslm.org

[23] Publication 32. ECCS, ECCS, Calculation of the fire resistance of composite concrete slabs with profiled steel sheet exposed to the standard fire, Comm. T3-Fire Saf. steel Struct. Tech. note, p. 48, 1983.

[24] P. Piloto, L. Prates, C. Balsa, and R. Rigobello, Fire Resistance of Composite Slabs with Steel Deck: From Experiments to Numerical Simulation, Mecânica Exp., vol.

31, pp. 8594, 2019.

[25] British Steel. The Behaviour of Multi-Storey Steel Frame Buildings in Fire; British Steel: Rotherham, UK, 1999.

[26] Both, C. "The fire resistance of composite steel-concrete slabs [PhDs thesis], Delft University Press." (1998).

[27] D. C. O. Mohamed. A. H. Abdel-Halim, M. R. Hakmi, Fire resistance of composite floor slabs using a model fire test facility, Eng. Struct., vol. 21, no. 2, pp. 176182, 1999, doi: https://doi.org/10.1016/S0141-0296(97)00153-3.

[28] C. G. Bailey, T. Lennon, and D. B. Moore, The behaviour of full-scale steel-framed buildings subjected to compartment fires, Struct. Eng., vol. 77, no. 8, pp. 1521, 1999.

[29] F. Bolina, B. Tutikian, and J. P. C. Rodrigues, Thermal analysis of steel decking concrete slabs in case of fire, Fire Saf. J., vol. 121, p. 103295, May 2021, doi: 10.1016/j.firesaf.2021.103295.

[30] R. Hamerlinck and J. W. B. Stark, Scholars Mine A Numerical Model for Fire-exposed Composite Steel / concrete Slabs, 1990.

[31] European Convention for Constructional Steelwork, 1984.

[32] R. Hamerlinck, The Beahaviour of Fire-Exposed Composite Steel/Cconcrete Slabs. 1991. doi: 10.6100/IR348360.

[33] C. Both, Fire-exposed continuous span composite steel-concrete slabs, Heron, vol. 41, no. 3, pp. 187199, 1996.

[34] Both, C., J. H. H. Fellinger, and L. Twilt. "Shallow floor construction with deep composite deck: from fire tests to simple calculation rules." HERON-ENGLISH EDITION- 42 (1997): 145-158.

[35] Lamont, S., Asif Sohail Usmani, and D. D. Drysdale. "Heat transfer analysis of the composite slab in the Cardington frame fire tests." Fire Safety Journal 36.8 (2001): 815-839.

[36] J. Jiang, J. A. Main, F. Sadek, and J. M. Weigand, Numerical Modeling and Analysis of Heat Transfer in Composite Slabs with Profiled Steel Decking, Natl. Inst. Stand. Technol., no. April, pp. 156, 2017, [Online]. Available: https://doi.org/10.6028/NIST.TN.1958

[37] P. A. G. Piloto, L. M. S. Prates, C. Balsa, and R. Rigobello, Numerical simulation of the fire resistance of composite slabs with steel deck, Int. J. Eng. Technol., vol. 7, no. 2, pp. 8386, 2018, doi: 10.14419/ijet.v7i2.23.11889.

[38] P. A. G. Piloto, C. Balsa, F. Ribeiro, L. Santos, R. Rigobello, and É. Kimura, Three-Dimensional Numerical Modelling of Fire Exposed Composite Slabs With Steel Deck, MATTER Int. J. Sci. Technol., vol. 5, no. 2, pp. 4867, 2019, doi: 10.20319/mijst.2019.52.4867.

[39] P. Piloto, C. Balsa, F. Ribeiro, R. Rigobello, L. Santos, and E. Kimura, Validation models on the fire resistance of composite slab with steel deck, Congr. Numer. Methods Eng. C. 2019, no. ISBN: 978-989-54496-0-6, pp. 625642, 2019.

[40] C. M. B. M. V. Piloto, Paulo A. G.; Balsa, Computational Modeling of the Thermal Effects on Composite Slabs Under Fire Conditions, Commun. Comput. Inf. Sci., pp. 497511, 2021, doi: 10.1007/978-3-030-90241-4.38.

[41] EuropeanConvention for Constructional Steelwork. Technical Committee 3, F. S. o. S. S. Calculation of the Fire Resistance of Composite Concrete Slabs with Profiled Steel Sheet Exposed to the Standard Fire Calculation of the Fire Resistance of Composite Concrete Slabs with Profiled Steel Sheet Exposed to the Standard Fire Nº 32-37 (European Convention for Constructional Steelwork, 1984).

[42] C.K. Chau, W.K. Hui, W.Y. Ng, G. Powell, Assessment of CO2 emissions reduction in high-rise concrete office buildings using different material use options, Resour. Conserv. Recycl. 61 (2012) 2234, https://doi.org/10.1016/j. Resconrec.2012.01.001.

[43] Azarbayjani, Mona, and David Jacob Thaddeus. "Environmental Dimensions of Climate Change: Endurance and Change in Material Culture." Towards Net Zero Carbon Emissions in the Building Industry. Cham: Springer International Publishing, 2022. 293-371.

[44] Control CfD, Prevention. Deaths resulting from residential fires and the prevalence of smoke alarms--United States, 1991-1995. MMWR: Morbidity and Mortality Weekly Report. 1998;47(38):803-6.

[45] Cowlard A, Bittern A, Abecassis-Empis C, Torero J. Fire safety design for tall buildings. Procedia Engineering. 2013;62:169-81.

[46] Ma J, Song WG, Tian W, Lo SM, Liao G. Experimental study on an ultra high-rise building evacuation in China. Safety Science. 2012;50(8):1665 74.

[47] Holborn PG, Nolan PF, Golt J. An analysis of fatal unintentional dwelling fires investigated by London Fire Brigade between 1996 and 2000. Fire Safety Journal. 2003;38(1):1-42.

[48] Kobes M, Helsloot I, de Vries B, Post JG. Building safety and human behaviour in

fire: a literature review. Fire Safety Journal. 2010;45(1):1-11.

[49] Zhang X. Study on rapid evacuation in high-rise buildings. Engineering Science and Technology, an International Journal. 2017;20(3):1203-10.

[50] Istre GR, McCoy MA, Osborn L, Barnard JJ, Bolton A. Deaths and injuries from house fires. N Engl J Med. 2001 Jun 21;344(25):1911-6.

[51] Xin J, Huang C. Fire risk analysis of residential buildings based on scenario clusters and its application in fire risk management. Fire Safety Journal. 2013;62:72-8.

[52] Chen H, Qi H, Long R, Zhang M. Research on 10-year tendency of China coal mine accidents and the characteristics of human factors. Safety Sci ence. 2012;50(4):745-50.

[53] Yau RK, Marshall SW. Association between fire-safe cigarette legislation and residential fire deaths in the United States. Injury Epidemiology. 2014;1(1):10.

[54] Ginnelly L, Sculpher M, Bojke C, Roberts I, Wade A, Diguiseppi C. Determining the cost effectiveness of a smoke alarm give-away program using data from a randomized controlled trial. The European Journal of Public Health. Eur J Public Health. 2005 Oct;15(5):448-53.

[55] Shokouhi, Mohammadreza, et al. "Preventive measures for fire-related injuries and their risk factors in residential buildings: a systematic review." Journal of injury and violence research 11.1 (2019): 1.

[56] Warda L, Tenenbein M, Moffatt ME. House fire injury prevention update. Part I. A review of risk factors for fatal and non-fatal house fire injury. Injury Prev. 1999;5(2):145-50.

[57] Hossain, K. M. A., et al. "High performance composite slabs with profiled steel deck and Engineered Cementitious CompositeStrength and shear bond characteristics." Construction and building materials 125 (2016): 227-240.

[58] De Silva, S. Sandun, and David P. Thambiratnam. "Dynamic characteristics of steeldeck composite floors under human-induced loads." Computers & Structures 87.17-18 (2009): 1067-1076.

[59] EN 13501-2:2009: Fire Classification of Construction Products and Building Elements Part 2: Classification Using Data from Fire Resistance Tests, Excluding Ventilation Services. European Committee for Standardization (CEN), 2009.

[60] Buchanan, Andrew H., and Anthony Kwabena Abu. Structural design for fire safety. John Wiley & Sons, 2017.

[61] Hidalgo, Juan P., Stephen Welch, and José L. Torero. "Performance criteria for the

fire safe use of thermal insulation in buildings." Construction and Building Materials 100 (2015): 285-297.

[62] Thi, V. D., et al. "Finite element analysis of heat transfer through timber elements exposed to fire." Engineering Structures 143 (2017): 11-21

[63] Liu, Jin-Cheng, Kang Hai Tan, and Yao Yao. "A new perspective on nature of fire-induced spalling in concrete." Construction and Building Materials 184 (2018): 581-590.

[64] EN-1991-1-2, Eurocode 1: Actions on structuresPart 1-2: General actionsActions on structures exposed to fire [Authority: The European Union Per Regulation 305/2011, Directive 98/34/EC, Directive 2004/18/EC]. British Standards (2002), 58.

[65] J. Jiang, J. A. Main, J. M. Weigand, and F. H. Sadek, Thermal performance of composite slabs with profiled steel decking exposed to fire effects, Fire Saf. J., vol. 95, no. May 2017, pp. 2541, 2018, doi: 10.1016/j.firesaf.2017.10.003.

[66] J. Jiang, A. Pintar, J. M. Weigand, J. A. Main, and F. Sadek, Improved calculation method for insulation-based fire resistance of composite slabs, Fire Saf. J., vol. 105,no., pp. 144153, 2018

[67] Çengel, Yunus A., and Afshin J. Ghajar. Heat and Mass Transfer: Fundamentals and Applications. 6th ed., McGraw-Hill Education, 2020.

[68] CEN - European Committee for Standardization, EN 1992-1-2: Design of concrete structures - Part 1-2: General rules - Structural fire design. Brussels, 2004.

[69] FprEN 1993-1-2, Eurocode 3: Design of steel structures - Part 1-2: General rules - Structural fire design [Authority: The European Union Per Regulation 305/2011, Directive 98/34/EC, Directive 2004/18/EC]. Final Draft (2023).

[70] Comité Européen de Normalisation. Eurocode 5: Design of Timber Structures - Part 1-2: Structural Fire Design. prEN 1995-1-2, CEN, 2023.

[71] International Organization for Standardization. EN ISO 1461: Hot Dip Galvanized Coatings on Fabricated Iron and Steel Articles Specifications and Test Methods. ISO, 2009.

[72] International Organization for Standardization. EN ISO 14713-2:2020: Zinc Coatings Guidelines and Recommendations for the Protection Against Corrosion of Iron and Steel in Structures Part 2: Hot Dip Galvanizing. ISO, 2020.

[73] Prado, Taís Cristina, et al. "Caracterização do carbono em amostras de aço." Instituto de Pesquisas Energéticas e Nucleares IPEN/CNEN-SP, Paulo (2000).

[74] Choi, In-Rak, Kyung-Soo Chung, and Hyerin Lee. "Thermal and mechanical properties of structural steel SN400 at elevated temperatures." International Journal of Steel Structures 17 (2017): 999-1007.

[75] Dos Santos, Lucas Manoel Cunha. Efeito do Nível de Carga no Comportamento ao Fogo de Lajes Mistas com Chapa de aço Colaborante. MS thesis. Instituto Politecnico de Braganca (Portugal), 2019

[76] ROCTERM+. Rocterm PN 70: Painel de Lã de Rocha Não Revestido. Obras360, 2020.

[77] P. Vila Real, Incêndio em estruturas metálicas: cálculo estrutural, 1a ed. Alfragide, 2003.

[78] E. Fonseca and P. V. Real, Análise não-linear do comportamento termo-mecânico de componentes em aço sujeitas ao fogo. 1999.

[79] Sobamowo, M. G. "Thermal analysis of longitudinal fin with temperature-dependent properties and internal heat generation using Galerkin's method of weighted residual." Applied Thermal Engineering 99 (2016): 1316-1330.

[80] Ghattassi, Mohamed, et al. "Galerkin method for solving combined radiative and conductive heat transfer." International Journal of Thermal Sciences 102 (2016): 122-136.

[81] ANSYS Mechanical APDL Element Reference. ANSYS, Inc., n.d. Web. 16 Feb. 2025.

[82] Thompson, Mary Kathryn, and John Martin Thompson. ANSYS mechanical APDL for finite element analysis. Butterworth-Heinemann, 2017.

[83] Claasen, J., Cicione, A., Streicher, D. et al. Behavior of a Composite Steel Decking and Boarding System in Fire Based on Large-Scale Experimental Testing and Numerical Modelling. Fire Technol 59, 23892414 (2023).

[84] ANSYS®, Academic Research Mechanical, Release R2, 2024.

[85] Voidcon Group. Voidcon Innovative Permanent Formwork, Scribd, 2025.

[86] Khetata, S. M., Piloto, P. A., and Gavilán, A. B., Fire resistance of composite non-

load bearing light steel framing walls. Journal of Fire Sciences, 38, (2020), 136-155. https://doi.org/10.1177/0734904119900931

[87] Torres, L., Couto, C., Real, P. V., and Piloto, P., Numerical study of the fire behaviour of external walls in light steel framing. Fire safety journal, 141, (2023), 103946. https://doi.org/10.1016/j.firesaf.2023.103946

[88] Piloto, P. A., Khetata, M. S., and Ramos-Gavilán, A. B., Analysis of the critical temperature on load bearing LSF walls under fire. Engineering Structures, 270, (2022).

[89] Barati, Reza. "Application of excel solver for parameter estimation of the non-linear Muskingum models." KSCE Journal of Civil Engineering 17 (2013): 1139-1148.

[90] Carlos Balsa, Fernando Ribeiro, Paulo A.G. Piloto, Ronaldo Rigobello "A new calculation method for the temperature of the components of composite slabs under fire." Journal of Computational Applied Mechanics 52.2 (2021).

[91] Zhao, Yu, Tingwei Wang, and Wen Yi. "Emergy-accounting-based comparison of carbon emissions of solid waste recycled concrete." Construction and Building Materials 387 (2023): 131674.

[92] Huang, Meng Chi, and Yan Jiao Zhang. "Carbon emissions analysis of rock wool board products." Materials Science Forum. Vol. 993. Trans Tech Publications Ltd, 2020.

[93] Wald, F.; Da Silva, L.S.; Moore, D.B.; Lennon, T.; Chladna, M.; Santiago, A.; Bene, M.; Borges, L. Experimental behaviour of a steel structure under natural fire. Fire Saf. J. 2006, 41, 509522.

[94] Concrete, F. Fire design of concrete structures in accordance with CEB FIP model code 90 isbn: 9782883940130 (CEB, 1991).

APPENDIX A

Data Sheet for the simulations performed for the thermal simulations performed in the parametric study of 4.2 section.

DATA SHEET			
Model 1: Slab 1 – VP115 – h1 = 65 mm			
Model 1 - Basic Data (1/2)			
Experimental type	Title: VP115 – h1 = 65 mm		
Parametric study	Author: Otávio G. N. Ribeiro		Year: 2024
Detailing			
Steel Deck	Concrete	Steel Bars	Insulation type
Geometry: VP-115 Thickness: 0.8mm Grade: ISQ 230 Steel galvanized 275	Density: Normal Weight Class: 25/30 Moisture: 3.0%	Description: 2Ø10 Grade: S450	steel shield
Cross – Section			

L1 R (mm)	50
L2 R (mm)	75
L3 R (mm)	25
L1 T (mm)	200
L2 T (mm)	150
L3 T (mm)	400
h1 (mm)	65
h2 T (mm)	115
h2 R (mm)	50

Mesh size

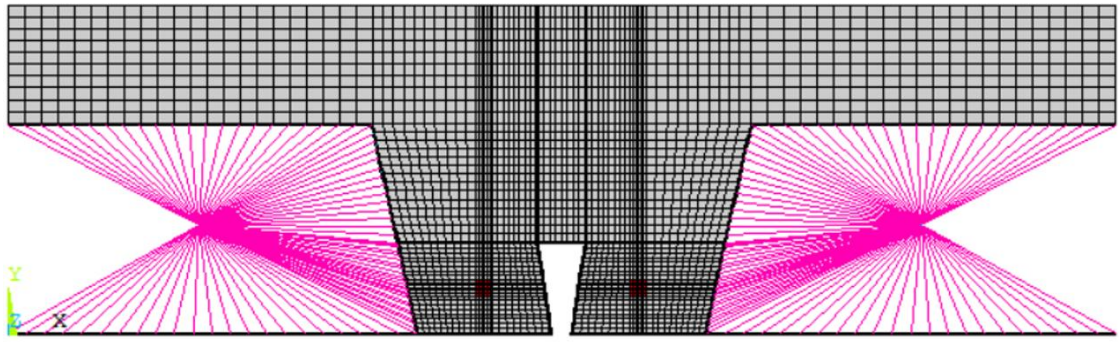

Model 1 - Basic Data (2/2)				
Ansys element	Convection Coef. (αc)	View Factor (Ø)		Temperature Curve
Plane 55: Steel, concrete and air convection. Link 31: radiation. Link 34: convection.	Exposed Surface: 25 W/(m² K) Unexposed Surface: 9 W/(m² K)	$Ø_{LOWER}$	1	Exposed Surface: ISO-834 Unexposed Surface: 20ºC
		$Ø_{WEB\ 2}$	0.48	
		$Ø_{UPPER\ 2}$	0.78	
		$Ø_{WEB\ 1}$	0.058	
		$Ø_{UPPER\ 1}$	0.064	

Temperature field

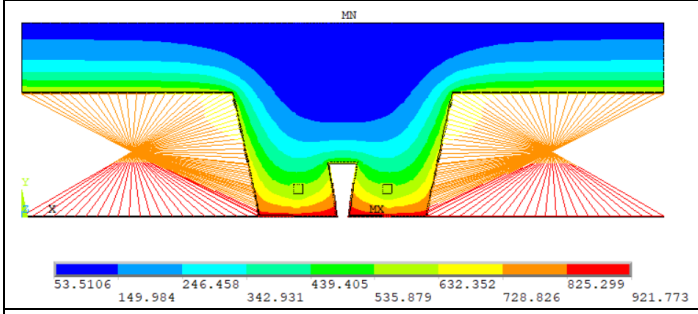

60 (min)

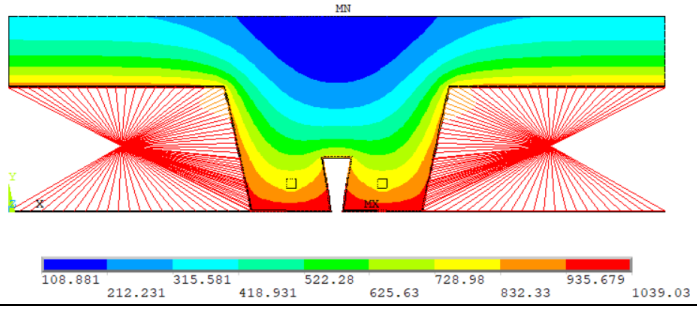

120 (min)

Temperature Graph - R

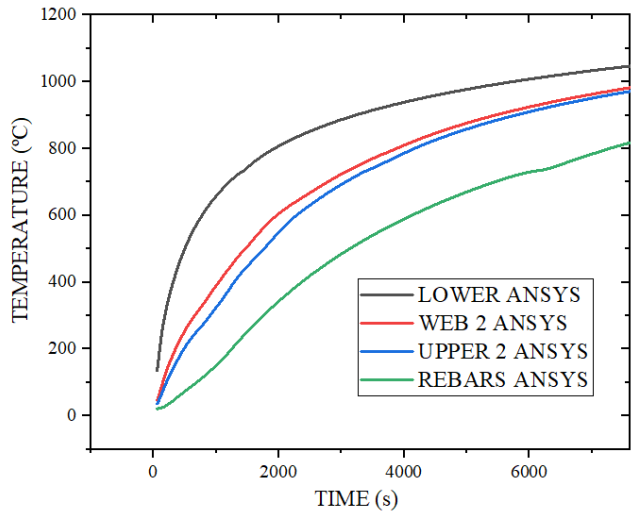

Temperature Graph - I

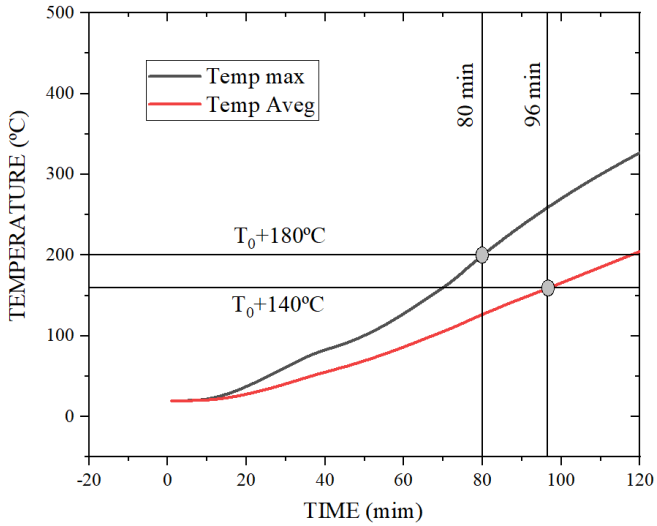

DATA SHEET			
Model 2: Slab 1 – VP115 – h1 = 65 mm			
Model 2 - Basic Data (1/2)			
Experimental type	Title: VP115 – h1 = 65 mm		
Parametric study	Author: Otávio G. N. Ribeiro		Year: 2024
Detailing			
Steel Deck	Concrete	Steel Bars	Insulation type
Geometry: VP-115 Thickness: 0.8mm Grade: ISQ 230 Steel galvanized 275	Density: Normal Weight Class: 25/30 Moisture: 3.0%	Description: 2Ø10 Grade: S450	Without insulation
Cross – Section			

L1 R (mm)	50
L2 R (mm)	75
L3 R (mm)	25
L1 T (mm)	200
L2 T (mm)	150
L3 T (mm)	400
h1 (mm)	65
h2 T (mm)	115
h2 R (mm)	50

Mesh size

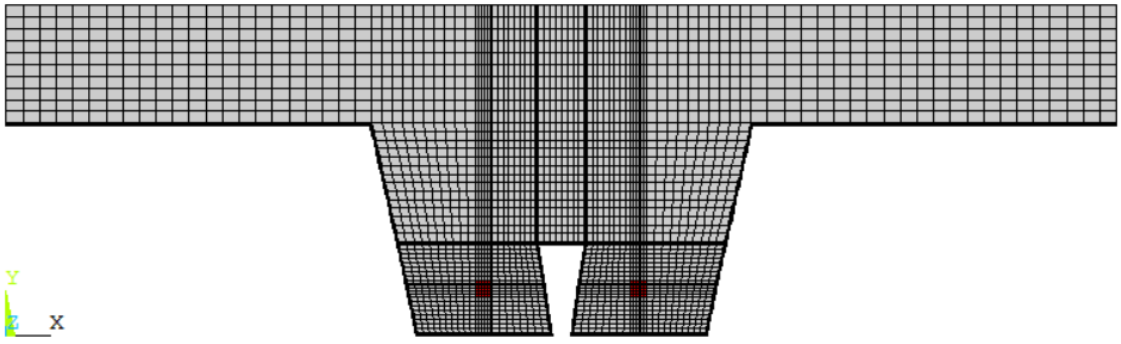

<table>
<tr><td colspan="4">Model 2 - Basic Data (2/2)</td></tr>
<tr><td>Ansys element</td><td>Convection Coef. (αc)</td><td colspan="2">View Factor (Ø)</td><td>Temperature Curve</td></tr>
<tr><td rowspan="6">Plane 55: Steel, concrete and air convection.</td><td rowspan="6">Exposed Surface:
25 W/(m^2 K)
Unexposed Surface:
9 W/(m^2 K)</td><td>$Ø_{LOWER}$</td><td>1</td><td rowspan="6">Exposed Surface:
ISO-834
Unexposed Surface: 20ºC</td></tr>
<tr><td>$Ø_{WEB\ 2}$</td><td>0.48</td></tr>
<tr><td>$Ø_{UPPER\ 2}$</td><td>0.78</td></tr>
<tr><td>$Ø_{WEB\ 1}$</td><td>0.058</td></tr>
<tr><td>$Ø_{UPPER\ 1}$</td><td>0.064</td></tr>
<tr><td colspan="2"></td></tr>
<tr><td colspan="5">Temperature field</td></tr>
<tr><td colspan="3"> 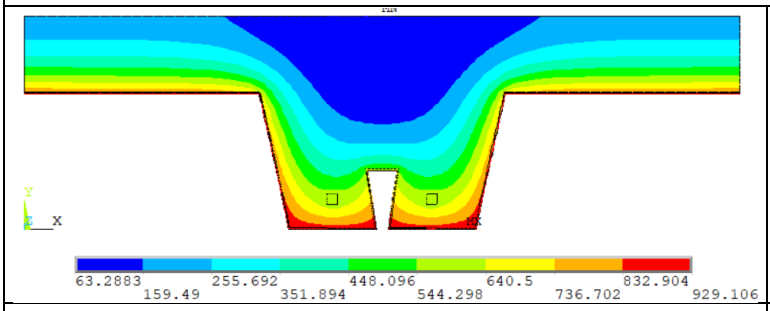
</td><td colspan="2"> 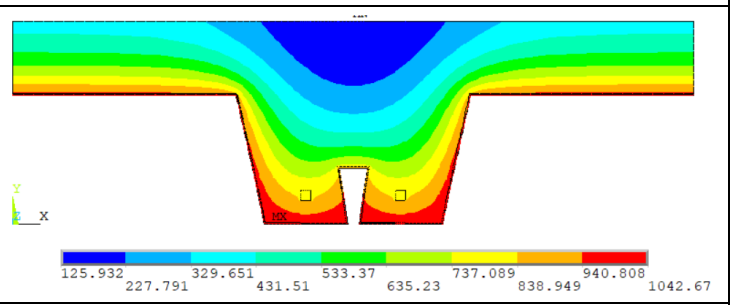
</td></tr>
<tr><td colspan="3">60 (min)</td><td colspan="2">120 (min)</td></tr>
<tr><td colspan="3">Temperature Graph - R</td><td colspan="2">Temperature Graph - I</td></tr>
<tr><td colspan="3"> 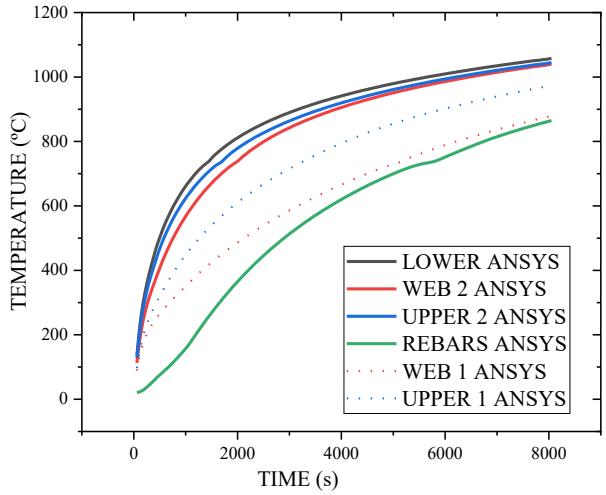
</td><td colspan="2"> 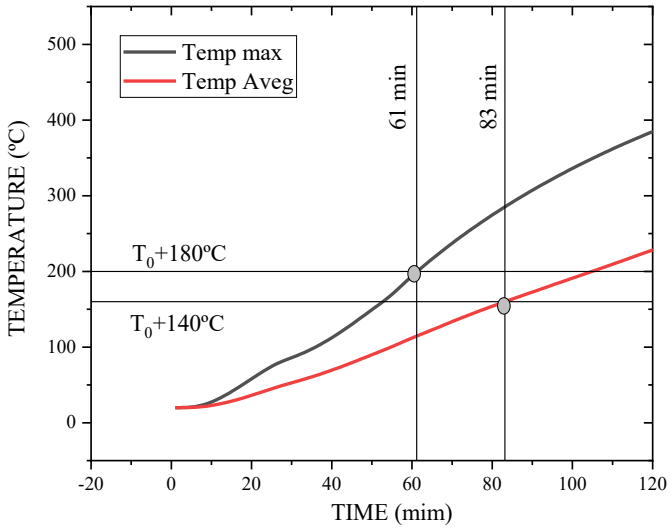
</td></tr>
</table>

DATA SHEET			
Model 3: Slab 1 – VP115 – h1 = 65 mm			
Model 3 - Basic Data (1/2)			
Experimental type	Title: VP115 – h1 = 65 mm		
Parametric study	Author: Otávio G. N. Ribeiro		Year: 2024
Detailing			
Steel Deck	Concrete	Steel Bars	Insulation type
Geometry: VP-115 Thickness: 0.8mm Grade: ISQ 230 Steel galvanized 275	Density: Normal Weight Class: 25/30 Moisture: 3.0%	Description: 2Ø10 Grade: S450	Mineral wool $\rho = 70 \frac{kg}{m^3}$
Cross – Section			

	L1 R (mm)	50
	L2 R (mm)	75
	L3 R (mm)	25
	L1 T (mm)	200
	L2 T (mm)	150
	L3 T (mm)	400
	h1 (mm)	65
	h2 T (mm)	115
	h2 R (mm)	50

Mesh size

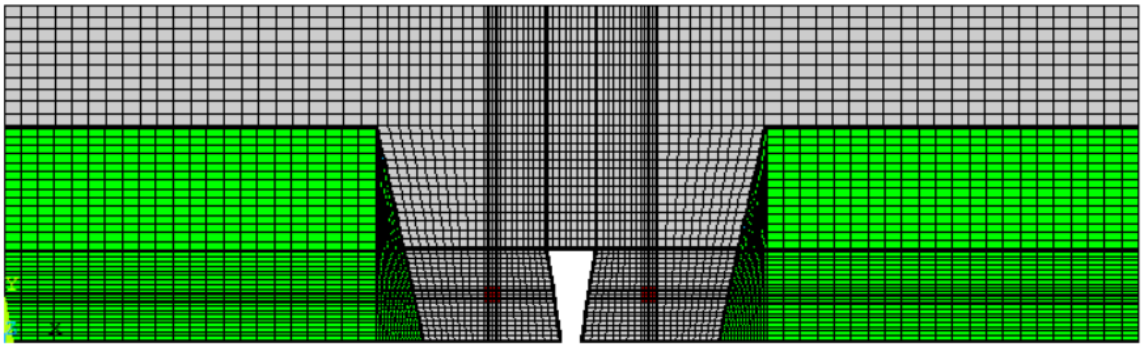

Model 3 - Basic Data (2/2)				
Ansys element	Convection Coef. (αc)	View Factor (Ø)		Temperature Curve
Plane 55: Steel, concrete, mineral wool and air convection.	Exposed Surface: 25 W/(m^2 K) Unexposed Surface: 9 W/(m^2 K)	$Ø_{LOWER}$	1	Exposed Surface: ISO-834 Unexposed Surface: 20ºC
		$Ø_{WEB\ 2}$	0.48	
		$Ø_{UPPER\ 2}$	0.78	
		$Ø_{WEB\ 1}$	0.058	
		$Ø_{UPPER\ 1}$	0.064	

Temperature field

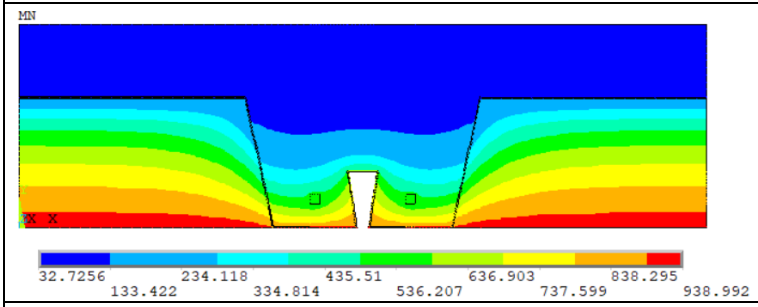

60 (min)

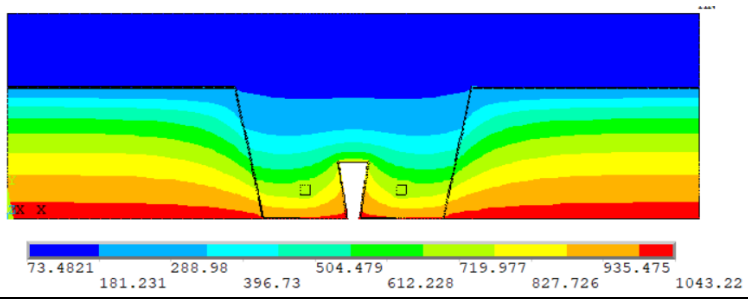

120 (min)

Temperature Graph - R

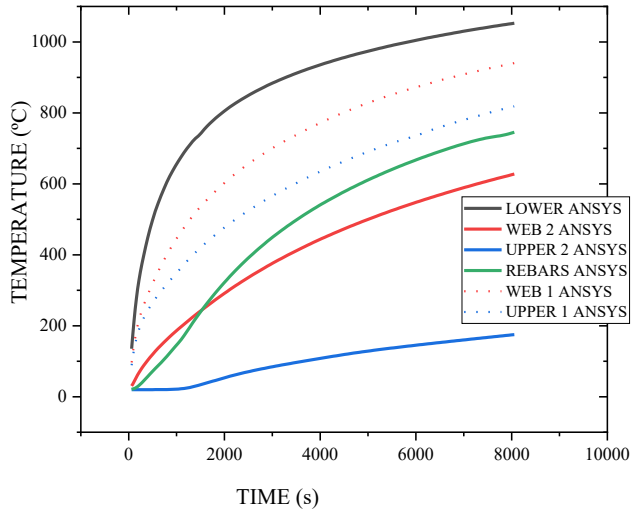

Temperature Graph - I

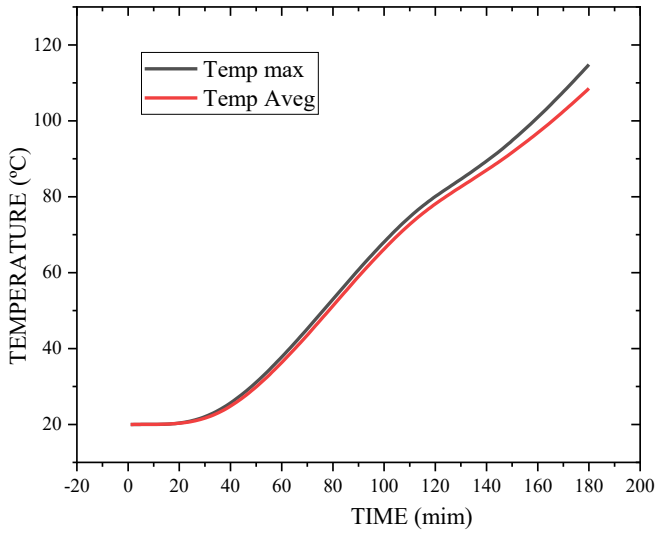

DATA SHEET			
Model 4: Slab 1 – VP115 – h1 = 65 mm			
Model 4 - Basic Data (1/2)			
Experimental type	Title: VP115 – h1 = 65 mm		
Parametric study	Author: Otávio G. N. Ribeiro		Year: 2024
Detailing			
Steel Deck	Concrete	Steel Bars	Insulation type
Geometry: VP-115 Thickness: 0.8mm Grade: ISQ 230 Steel galvanized 275	Density: Normal Weight Class: 25/30 Moisture: 3.0%	Description: 2Ø10 Grade: S450	Mineral wool plate hi = 5 mm $\rho = 70 \frac{kg}{m^3}$
Cross – Section			

L1 R (mm)	50
L2 R (mm)	75
L3 R (mm)	25
L1 T (mm)	200
L2 T (mm)	150
L3 T (mm)	400
h1 (mm)	65
h2 T (mm)	115
h2 R (mm)	50

Mesh size

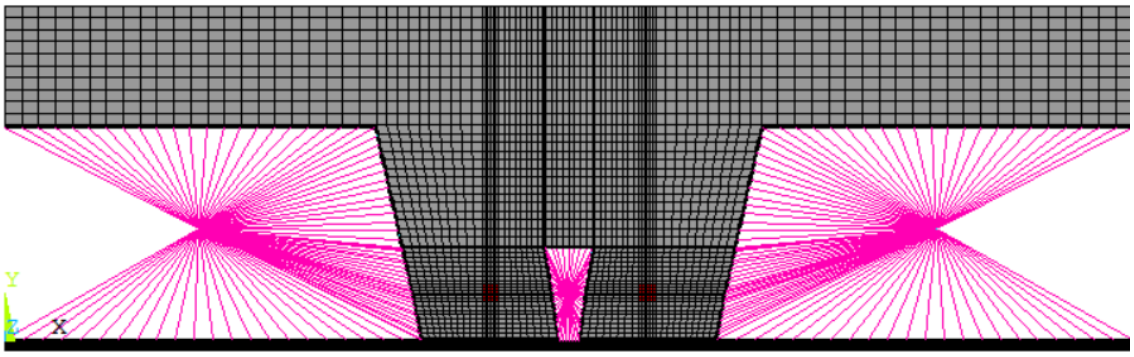

Model 4 - Basic Data (2/2)				
Ansys element	Convection Coef. (αc)	View Factor (Ø)		Temperature Curve
Plane 55: Steel, concrete, mineral wool and air convection. Link 31: radiation. Link 34: convection.	Exposed Surface: 25 W/(m^2 K) Unexposed Surface: 9 W/(m^2 K)	$Ø_{LOWER}$	1	Exposed Surface: ISO-834 Unexposed Surface: 20ºC
		$Ø_{WEB\ 2}$	0.48	
		$Ø_{UPPER\ 2}$	0.78	
		$Ø_{WEB\ 1}$	0.058	
		$Ø_{UPPER\ 1}$	0.064	

Temperature field

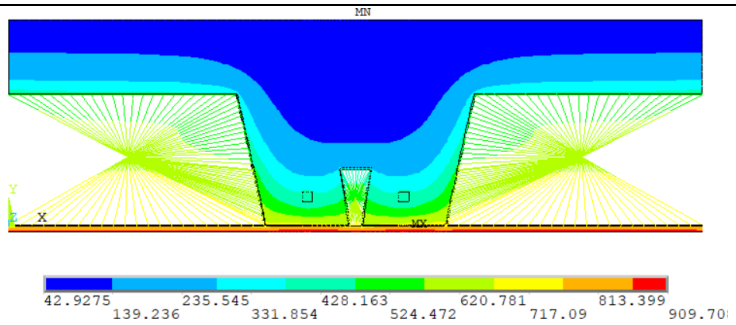

60 (min)

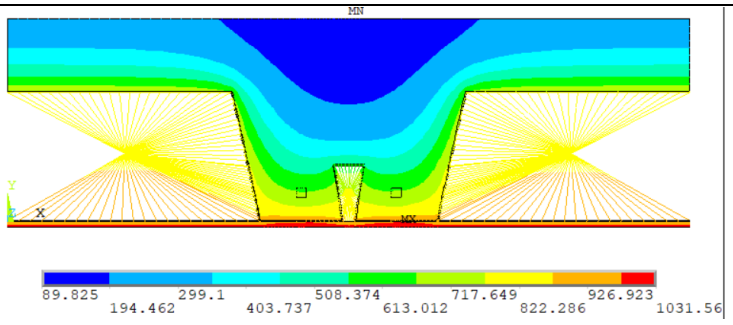

120 (min)

Temperature Graph - R

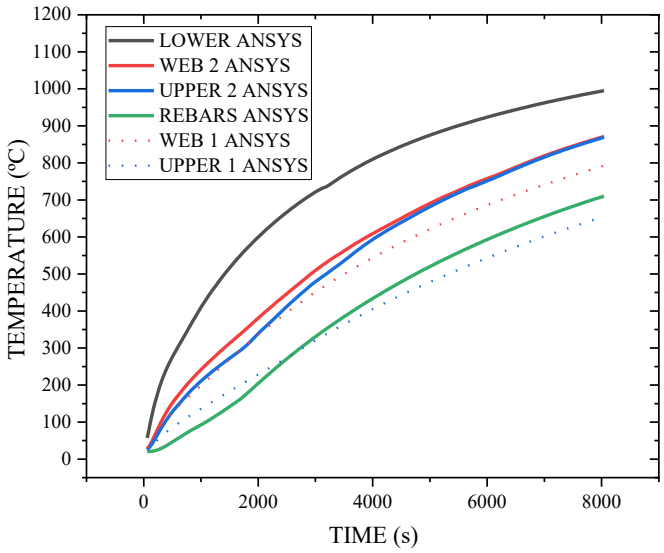

Temperature Graph - I

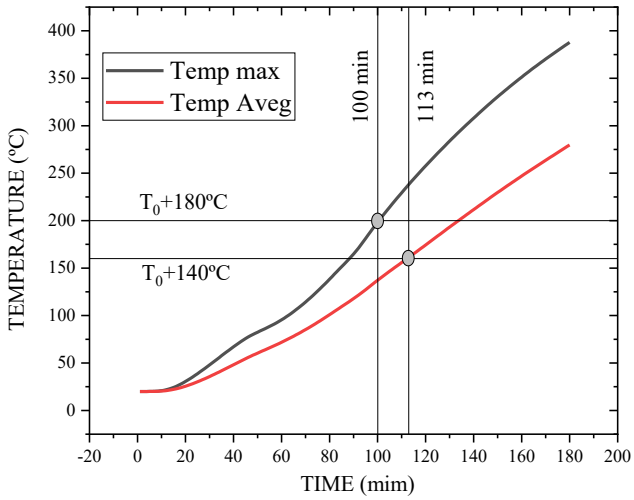

DATA SHEET			
Model 5: Slab 1 – VP115 – h1 = 65 mm			
Model 5 - Basic Data (1/2)			
Experimental type	Title: VP115 – h1 = 65 mm		
Parametric study	Author: Otávio G. N. Ribeiro		Year: 2024
Detailing			
Steel Deck	Concrete	Steel Bars	Insulation type
Geometry: VP-115 Thickness: 0.8mm Grade: ISQ 230 Steel galvanized 275	Density: Normal Weight Class: 25/30 Moisture: 3.0%	Description: 2Ø10 Grade: S450	Mineral wool plate hi = 10 mm $\rho = 70 \frac{kg}{m^3}$
Cross – Section			

L1 R (mm)	50
L2 R (mm)	75
L3 R (mm)	25
L1 T (mm)	200
L2 T (mm)	150
L3 T (mm)	400
h1 (mm)	65
h2 T (mm)	115
h2 R (mm)	50

Mesh size

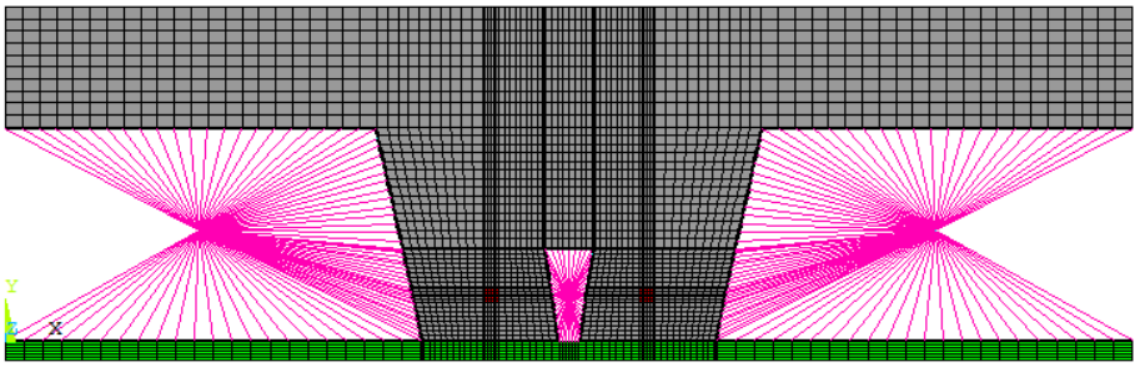

Model 5 - Basic Data (2/2)

Ansys element	Convection Coef. (αc)	View Factor (Ø)		Temperature Curve
Plane 55: Steel, concrete, mineral wool and air convection. Link 31: radiation. Link 34: convection.	Exposed Surface: 25 W/(m^2 K) Unexposed Surface: 9 W/(m^2 K)	$Ø_{LOWER}$	1	Exposed Surface: ISO-834 Unexposed Surface: 20ºC
		$Ø_{WEB\ 2}$	0.48	
		$Ø_{UPPER\ 2}$	0.78	
		$Ø_{WEB\ 1}$	0.058	
		$Ø_{UPPER\ 1}$	0.064	

Temperature field

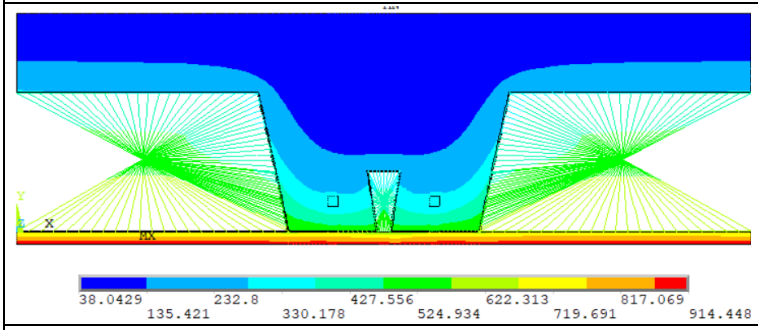

60 (min)

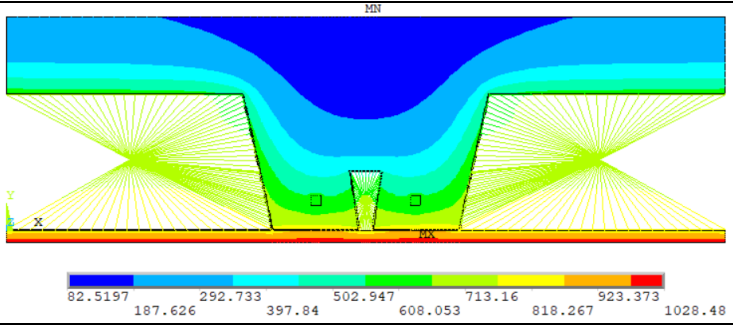

120 (min)

Temperature Graph - R

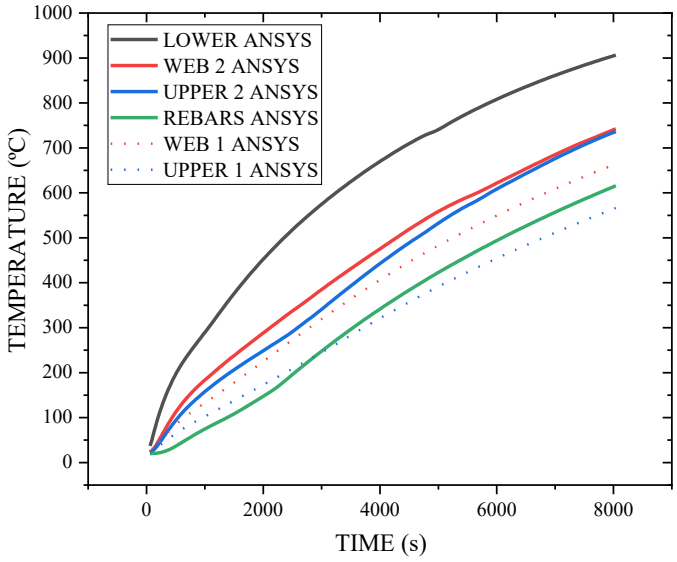

Temperature Graph - I

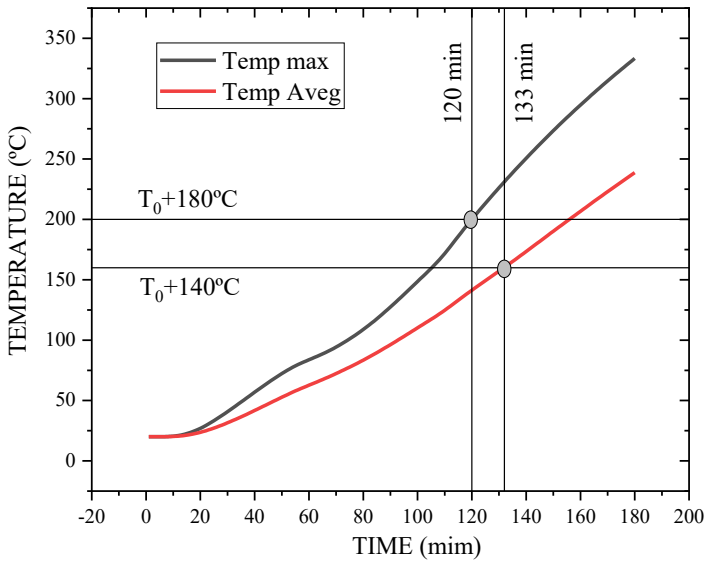

DATA SHEET			
Model 6: Slab 1 – VP115 – h1 = 65 mm			
Model 6 - Basic Data (1/2)			
Experimental type	Title: VP115 – h1 = 65 mm		
Parametric study	Author: Otávio G. N. Ribeiro		Year: 2024
Detailing			
Steel Deck	Concrete	Steel Bars	Insulation type
Geometry: VP-115 Thickness: 0.8mm Grade: ISQ 230 Steel galvanized 275	Density: Normal Weight Class: 25/30 Moisture: 3.0%	Description: 2Ø10 Grade: S450	Mineral wool plate hi = 20 mm $\rho = 70 \frac{kg}{m^3}$
Cross – Section			

	L1 R (mm)	50
	L2 R (mm)	75
	L3 R (mm)	25
	L1 T (mm)	200
	L2 T (mm)	150
	L3 T (mm)	400
	h1 (mm)	65
	h2 T (mm)	115
	h2 R (mm)	50

Mesh size

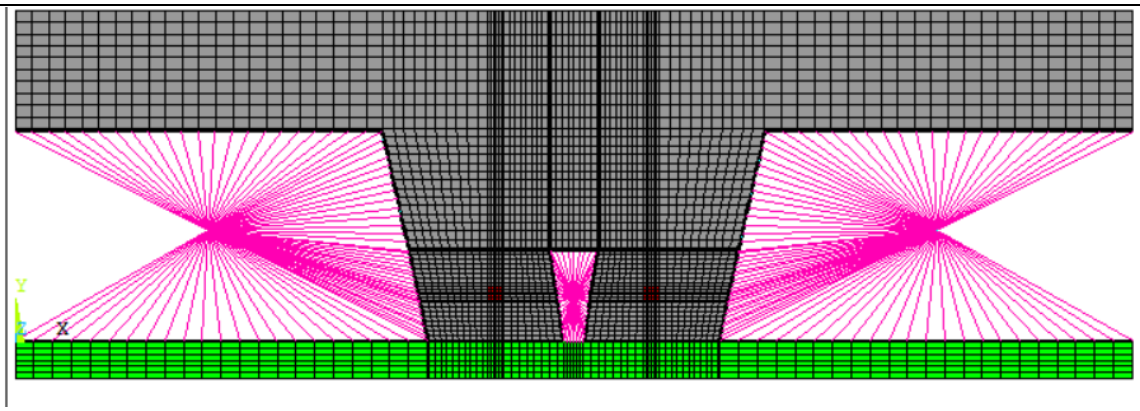

Model 6 - Basic Data (2/2)				
Ansys element	Convection Coef. (αc)	View Factor (Ø)		Temperature Curve
Plane 55: Steel, concrete, mineral wool and air convection. Link 31: radiation. Link 34: convection.	Exposed Surface: 25 W/(m^2 K) Unexposed Surface: 9 W/(m^2 K)	$Ø_{LOWER}$	1	Exposed Surface: ISO-834 Unexposed Surface: 20ºC
		$Ø_{WEB\ 2}$	0.48	
		$Ø_{UPPER\ 2}$	0.78	
		$Ø_{WEB\ 1}$	0.058	
		$Ø_{UPPER\ 1}$	0.064	

Temperature field

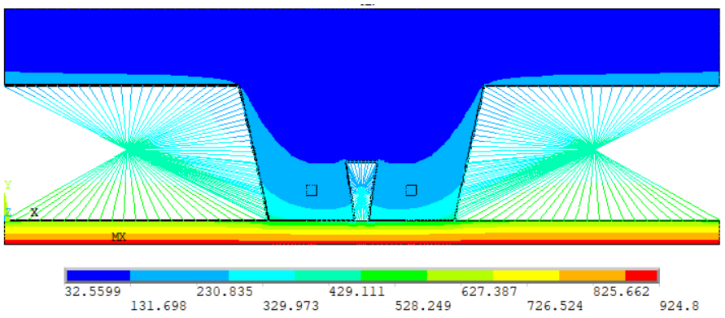

60 (min)

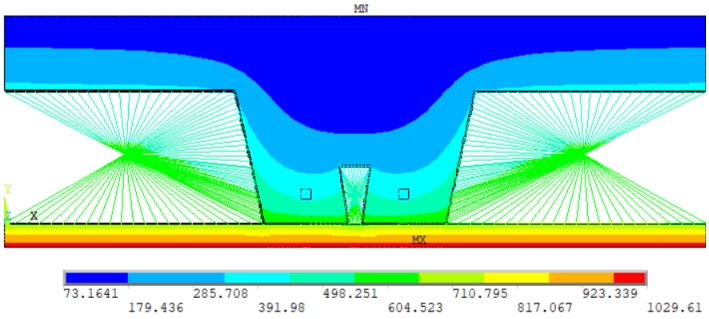

120 (min)

Temperature Graph - R

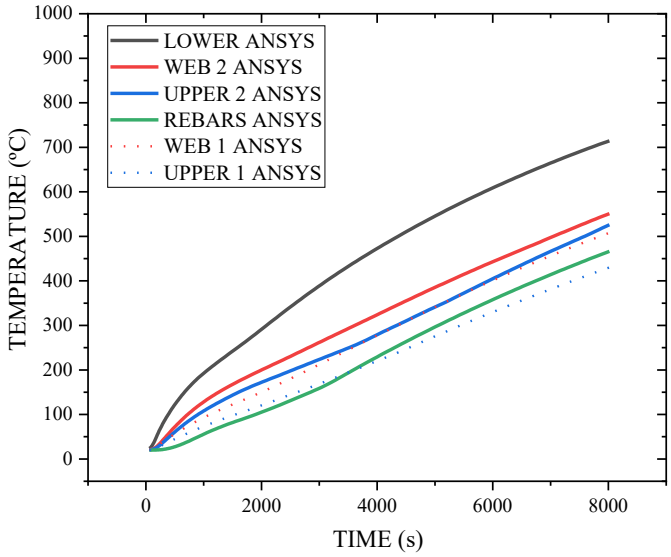

Temperature Graph - I

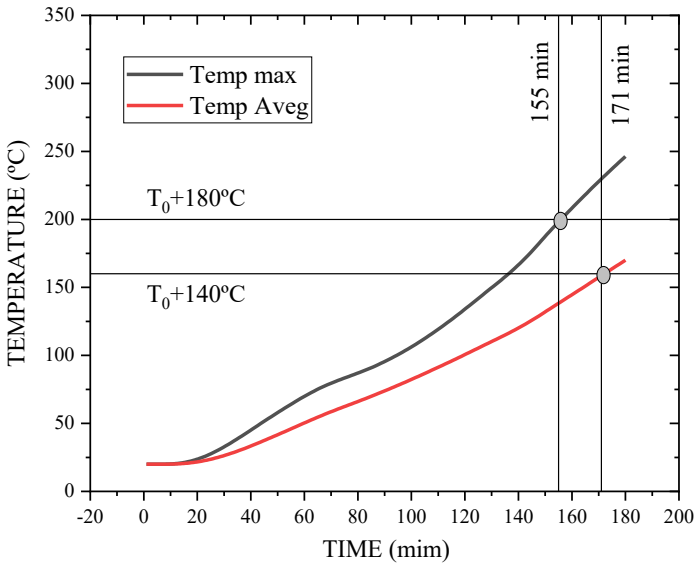

DATA SHEET			
Model 7: Slab 1 – VP115 – h1 = 65 mm			
Model 7 - Basic Data (1/2)			
Experimental type	Title: VP115 – h1 = 65 mm		
Parametric study	Author: Otávio G. N. Ribeiro		Year: 2024
Detailing			
Steel Deck	Concrete	Steel Bars	Insulation type
Geometry: VP-115 Thickness: 0.8mm Grade: ISQ 230 Steel galvanized 275	Density: Normal Weight Class: 25/30 Moisture: 3.0%	Description: 2Ø10 Grade: S450	Mineral wool plate hi = 30 mm $\rho = 70 \frac{kg}{m^3}$
Cross – Section			

	L1 R (mm)	50
	L2 R (mm)	75
	L3 R (mm)	25
	L1 T (mm)	200
	L2 T (mm)	150
	L3 T (mm)	400
	h1 (mm)	65
	h2 T (mm)	115
	h2 R (mm)	50

Mesh size

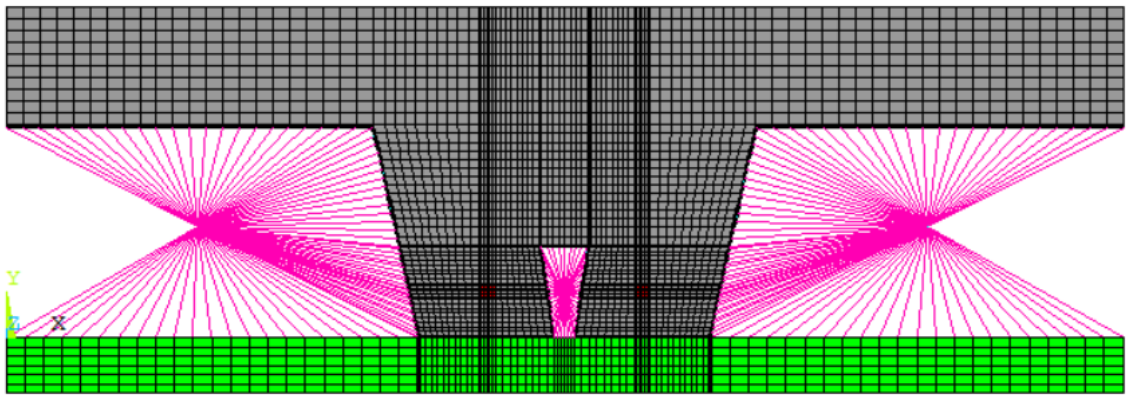

Model 7 - Basic Data (2/2)				
Ansys element	Convection Coef. (αc)	View Factor (Ø)		Temperature Curve
Plane 55: Steel, concrete, mineral wool and air convection. Link 31: radiation. Link 34: convection.	Exposed Surface: 25 W/(m² K) Unexposed Surface: 9 W/(m² K)	$Ø_{LOWER}$	1	Exposed Surface: ISO-834 Unexposed Surface: 20ºC
		$Ø_{WEB\ 2}$	0.48	
		$Ø_{UPPER\ 2}$	0.78	
		$Ø_{WEB\ 1}$	0.058	
		$Ø_{UPPER\ 1}$	0.064	

Temperature field

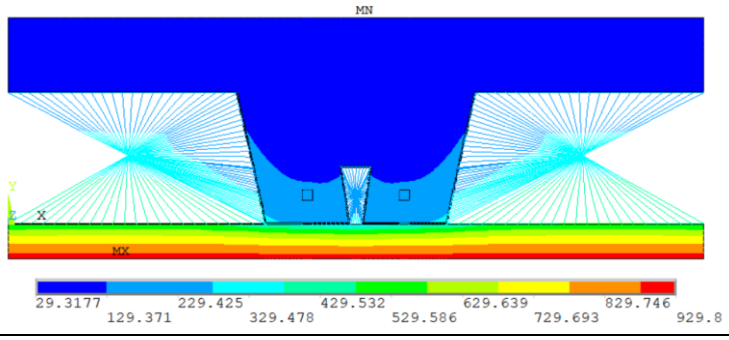

60 (min)

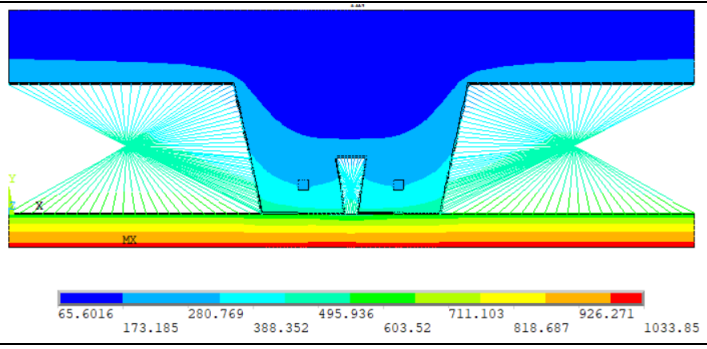

120 (min)

Temperature Graph - R

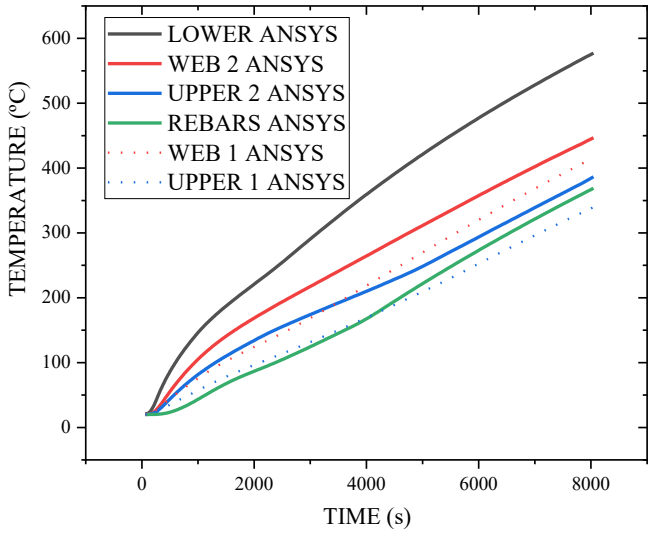

Temperature Graph - I

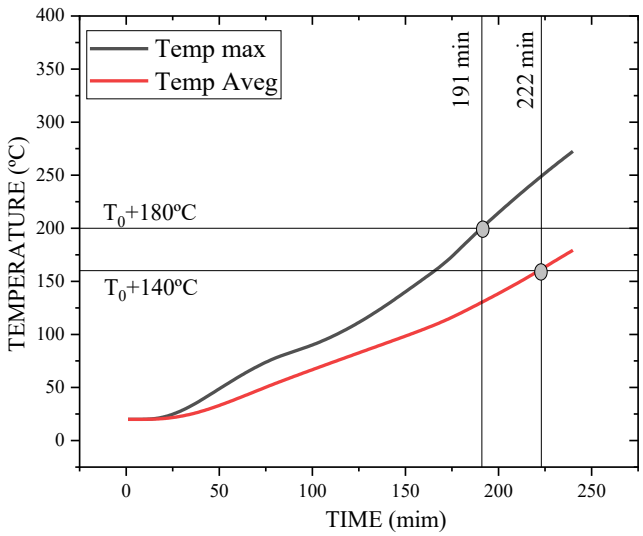

DATA SHEET			
Model 8: Slab 2 – VP50 – h1 = 65 mm			
Model 8 - Basic Data (1/2)			
Experimental type	Title: VP50 – h1 = 65 mm		
Parametric study	Author: Otávio G. N. Ribeiro		Year: 2024
Detailing			
Steel Deck	Concrete	Steel Bars	Insulation type
Geometry: VP-50 Thickness: 0.8mm Grade: ISQ 230 Steel galvanized 275	Density: Normal Weight Class: 25/30 Moisture: 3.0%	Description: 2Ø10 Grade: S450	steel shield
Cross – Section			

L1 R (mm)	30
L2 R (mm)	55
L3 R (mm)	25
L1 T (mm)	165
L2 T (mm)	115
L3 T (mm)	250
h1 (mm)	65
h2 T (mm)	50
h2 R (mm)	50

Mesh size

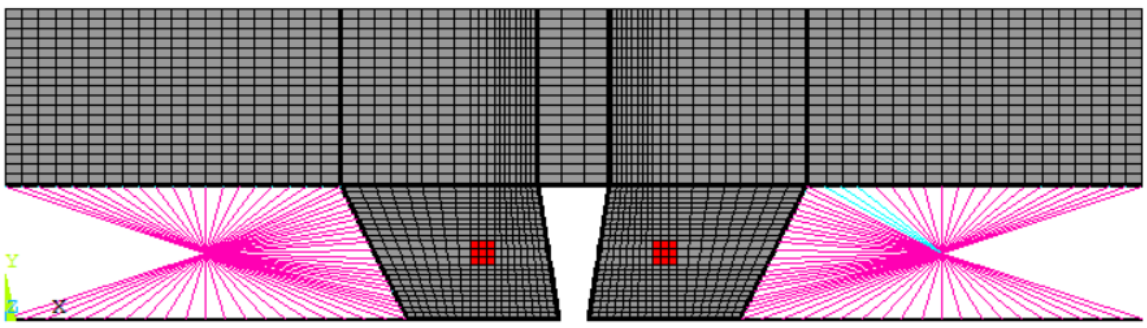

Model 8 - Basic Data (2/2)				
Ansys element	Convection Coef. (αc)	View Factor (Ø)		Temperature Curve
Plane 55: Steel, concrete and air convection. Link 31: radiation. Link 34: convection.	Exposed Surface: 25 W/(m² K) Unexposed Surface: 9 W/(m² K)	$Ø_{LOWER}$	1	Exposed Surface: ISO-834 Unexposed Surface: 20ºC
		$Ø_{WEB\ 2}$	0.6974	
		$Ø_{\ UPPER\ 2}$	0.9301	
		$Ø_{WEB\ 1}$	0.058	
		$Ø_{\ UPPER\ 1}$	0.064	

Temperature field

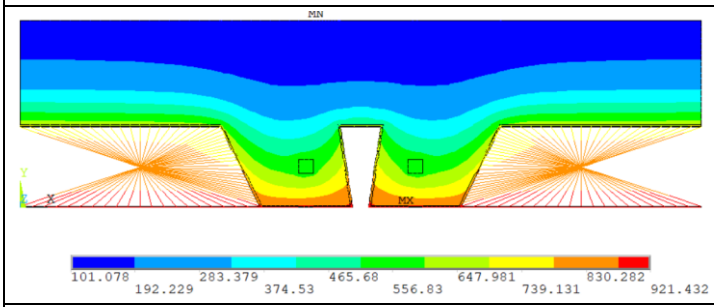

60 (min)

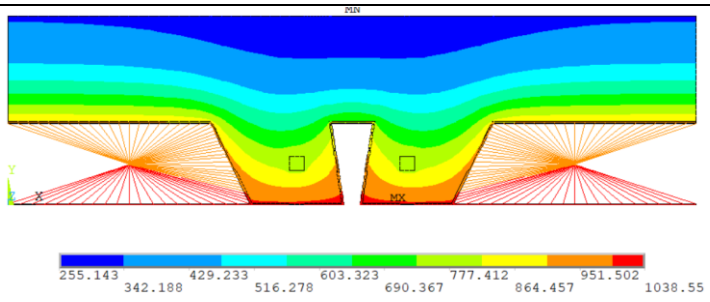

120 (min)

Temperature Graph - R

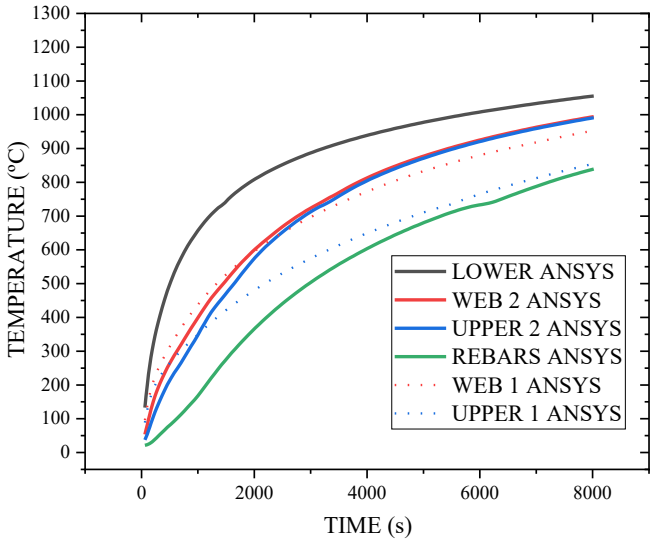

Temperature Graph - I

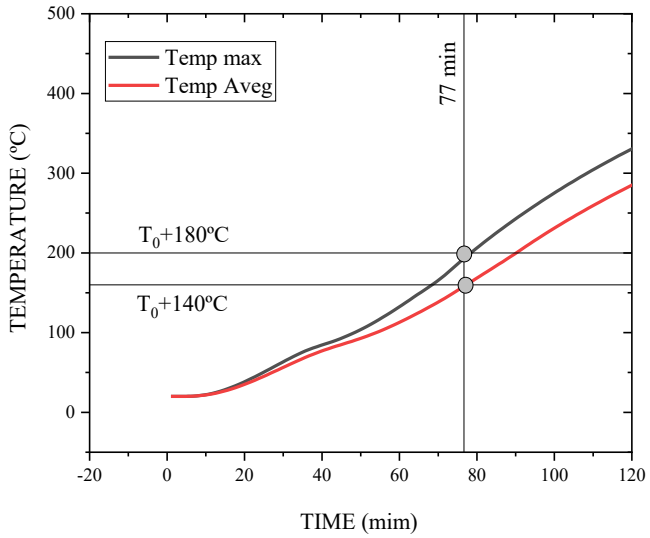

DATA SHEET			
Model 9: Slab 2 – VP50 – h1 = 65 mm			
Model 9 - Basic Data (1/2)			
Experimental type	Title: VP50 – h1 = 65 mm		
Parametric study	Author: Otávio G. N. Ribeiro		Year: 2024
Detailing			
Steel Deck	Concrete	Steel Bars	Insulation type
Geometry: VP-50 Thickness: 0.8mm Grade: ISQ 230 Steel galvanized 275	Density: Normal Weight Class: 25/30 Moisture: 3.0%	Description: 2Ø10 Grade: S450	Without insulation
Cross – Section			

L1 R (mm)	30
L2 R (mm)	55
L3 R (mm)	25
L1 T (mm)	165
L2 T (mm)	115
L3 T (mm)	250
h1 (mm)	65
h2 T (mm)	50
h2 R (mm)	50

Mesh size

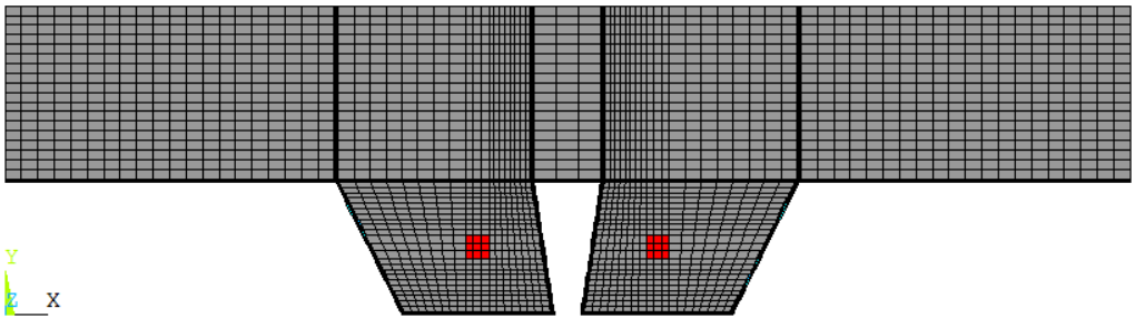

Model 9 - Basic Data (2/2)				
Ansys element	Convection Coef. (αc)	View Factor (Ø)		Temperature Curve
Plane 55: Steel, concrete and air convection.	Exposed Surface: 25 W/(m² K) Unexposed Surface: 9 W/(m² K)	$Ø_{LOWER}$	1	Exposed Surface: ISO-834 Unexposed Surface: 20ºC
		$Ø_{WEB\ 2}$	0.6974	
		$Ø_{UPPER\ 2}$	0.9301	
		$Ø_{WEB\ 1}$	0.058	
		$Ø_{UPPER\ 1}$	0.064	

Temperature field

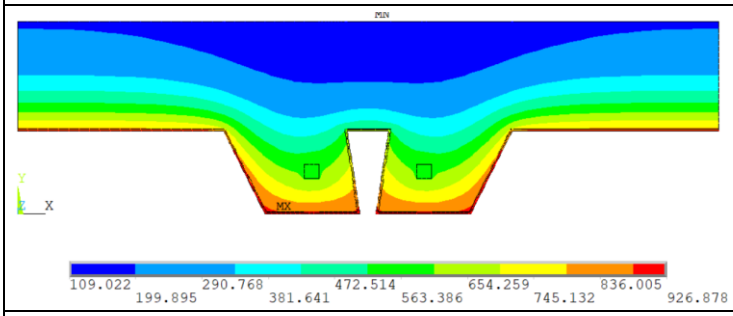

60 (min)

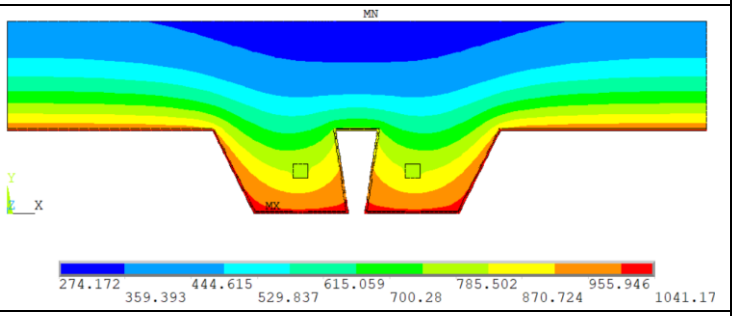

120 (min)

Temperature Graph - R

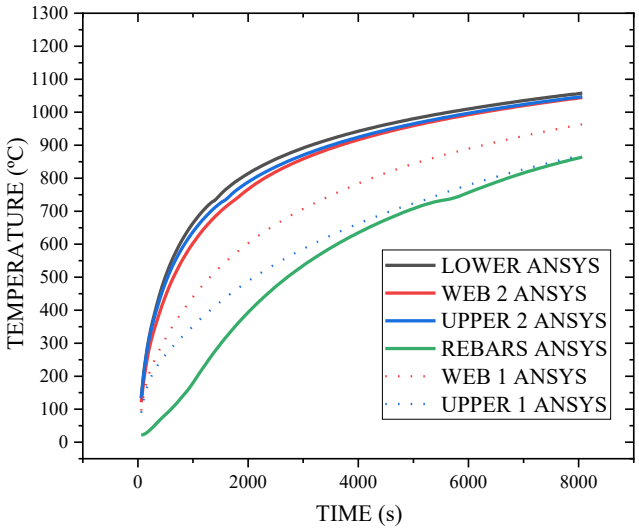

Temperature Graph - I

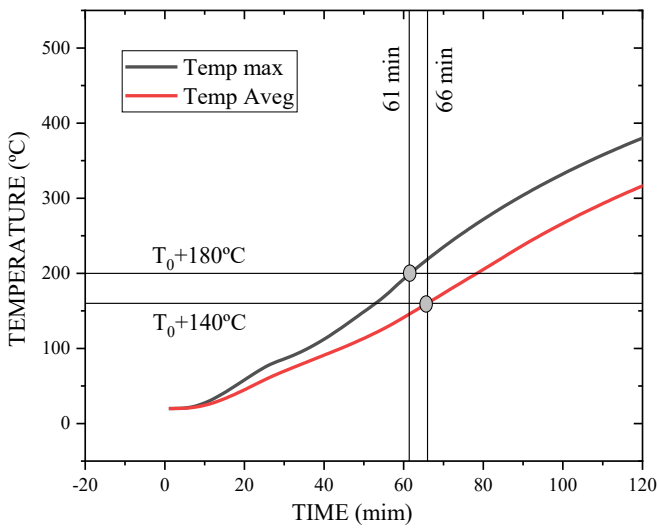

DATA SHEET			
Model 10: Slab 2 – VP50 – h1 = 65 mm			
Model 10 - Basic Data (1/2)			
Experimental type	Title: VP50 – h1 = 65 mm		
Parametric study	Author: Otávio G. N. Ribeiro		Year: 2024
Detailing			
Steel Deck	Concrete	Steel Bars	Insulation type
Geometry: VP-50 Thickness: 0.8mm Grade: ISQ 230 Steel galvanized 275	Density: Normal Weight Class: 25/30 Moisture: 3.0%	Description: 2Ø10 Grade: S450	Mineral wool $\rho = 70 \frac{kg}{m^3}$
Cross – Section			

L1 R (mm)	30
L2 R (mm)	55
L3 R (mm)	25
L1 T (mm)	165
L2 T (mm)	115
L3 T (mm)	250
h1 (mm)	65
h2 T (mm)	50
h2 R (mm)	50

Mesh size

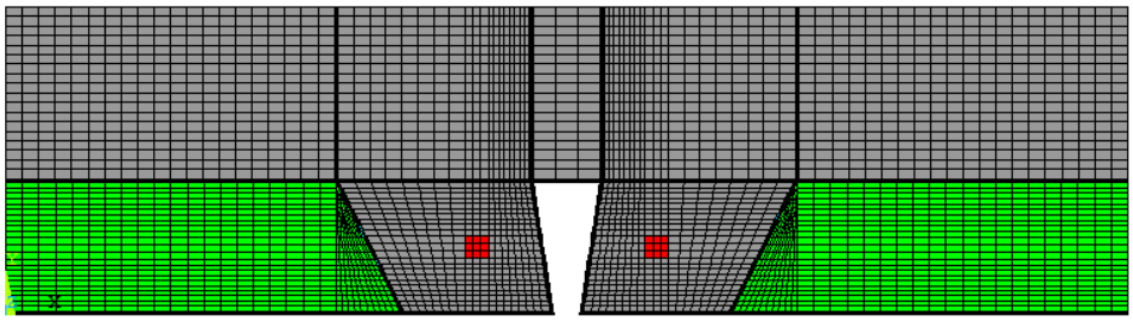

Model 10 - Basic Data (2/2)				
Ansys element	Convection Coef. (αc)	View Factor (Ø)		Temperature Curve
Plane 55: Steel, concrete, mineral wool and air convection.	Exposed Surface: 25 W/(m² K) Unexposed Surface: 9 W/(m² K)	$Ø_{LOWER}$	1	Exposed Surface: ISO-834 Unexposed Surface: 20ºC
		$Ø_{WEB\ 2}$	0.6974	
		$Ø_{UPPER\ 2}$	0.9301	
		$Ø_{WEB\ 1}$	0.058	
		$Ø_{UPPER\ 1}$	0.064	

Temperature field

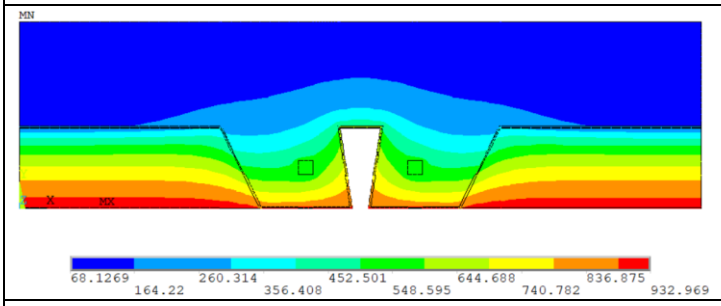

60 (min)

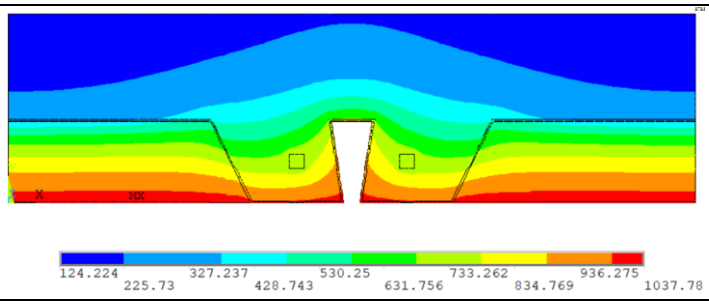

120 (min)

Temperature Graph - R

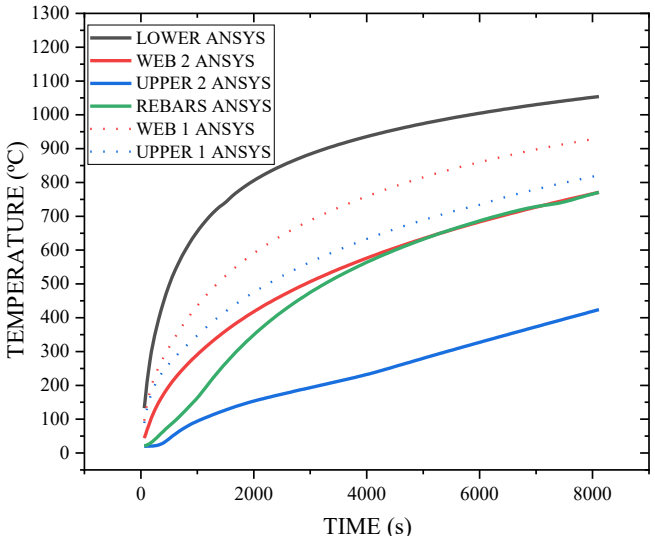

Temperature Graph - I

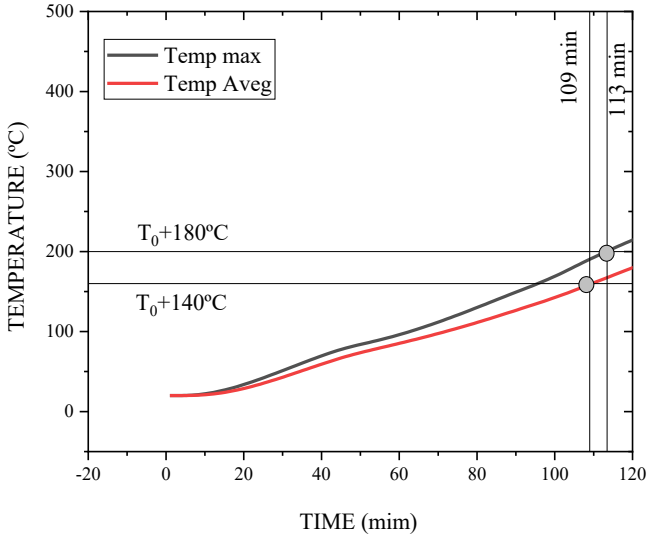

DATA SHEET			
Model 11: Slab 2 – VP50 – h1 = 65 mm			
Model 11 - Basic Data (1/2)			
Experimental type	Title: VP50 – h1 = 65 mm		
Parametric study	Author: Otávio G. N. Ribeiro		Year: 2024
Detailing			
Steel Deck	Concrete	Steel Bars	Insulation type
Geometry: VP-50 Thickness: 0.8mm Grade: ISQ 230 Steel galvanized 275	Density: Normal Weight Class: 25/30 Moisture: 3.0%	Description: 2Ø10 Grade: S450	Mineral wool plate hi = 5 mm $\rho = 70 \frac{kg}{m^3}$
Cross – Section			
L1 R (mm)	30		
L2 R (mm)	55		
L3 R (mm)	25		
L1 T (mm)	165		
L2 T (mm)	115		
L3 T (mm)	250		
h1 (mm)	65		
h2 T (mm)	50		
h2 R (mm)	50		
Mesh size			

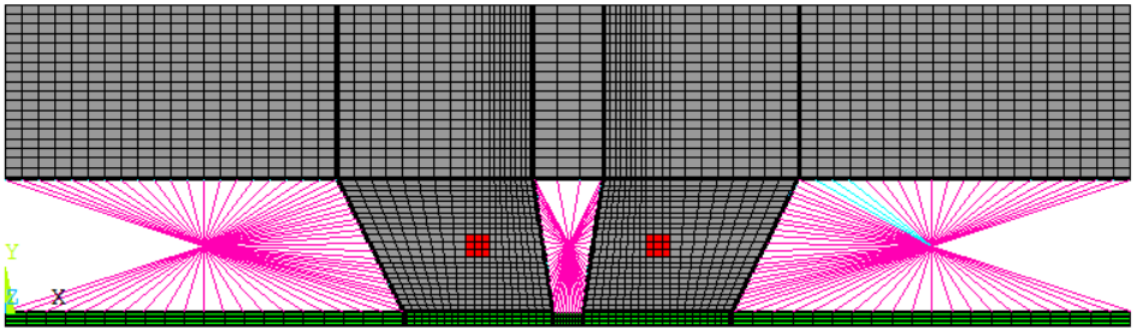

Model 11 - Basic Data (2/2)				
Ansys element	Convection Coef. (αc)	View Factor (Ø)		Temperature Curve
Plane 55: Steel, concrete, mineral wool and air convection. Link 31: radiation. Link 34: convection.	Exposed Surface: 25 W/(m² K) Unexposed Surface: 9 W/(m² K)	$Ø_{LOWER}$	1	Exposed Surface: ISO-834 Unexposed Surface: 20ºC
		$Ø_{WEB\ 2}$	0.6974	
		$Ø_{UPPER\ 2}$	0.9301	
		$Ø_{WEB\ 1}$	0.058	
		$Ø_{UPPER\ 1}$	0.064	

Temperature field

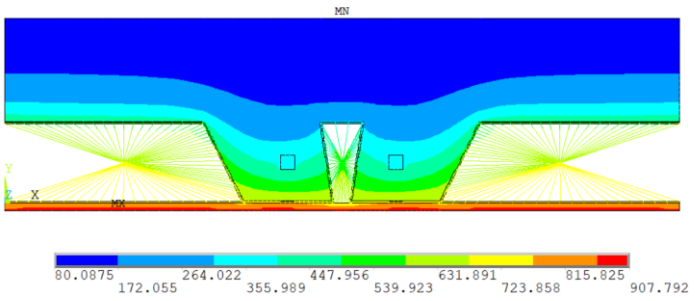

60 (min)

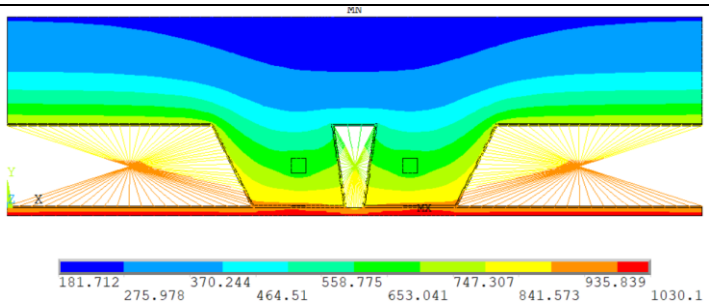

120 (min)

Temperature Graph - R

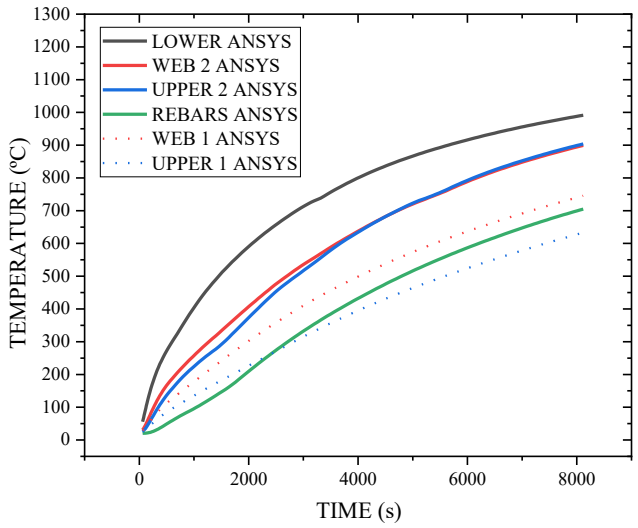

Temperature Graph - I

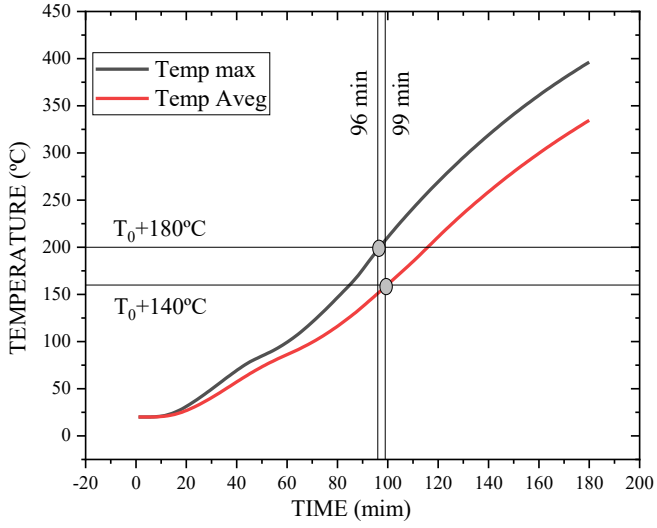

DATA SHEET			
Model 12: Slab 2 – VP50 – h1 = 65 mm			
Model 12 - Basic Data (1/2)			
Experimental type	Title: VP50 – h1 = 65 mm		
Parametric study	Author: Otávio G. N. Ribeiro		Year: 2024
Detailing			
Steel Deck	Concrete	Steel Bars	Insulation type
Geometry: VP-50 Thickness: 0.8mm Grade: ISQ 230 Steel galvanized 275	Density: Normal Weight Class: 25/30 Moisture: 3.0%	Description: 2Ø10 Grade: S450	Mineral wool plate hi = 10 mm $\rho = 70 \frac{kg}{m^3}$
Cross – Section			

L1 R (mm)	30
L2 R (mm)	55
L3 R (mm)	25
L1 T (mm)	165
L2 T (mm)	115
L3 T (mm)	250
h1 (mm)	65
h2 T (mm)	50
h2 R (mm)	50

Mesh size

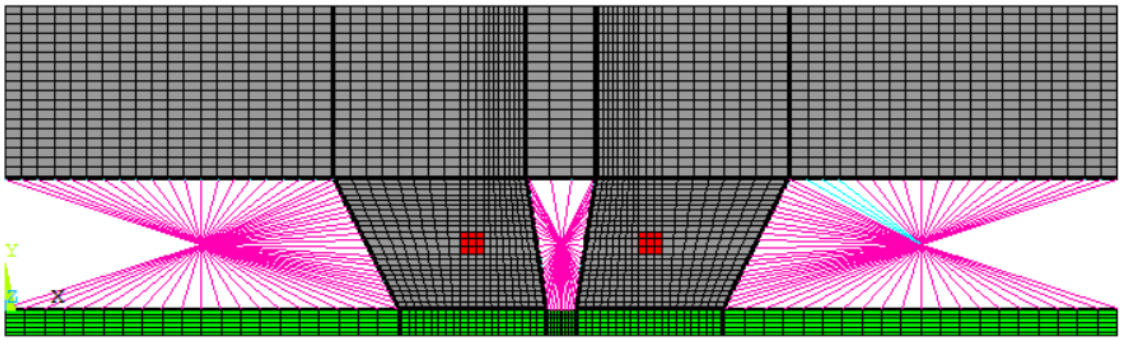

Model 12 - Basic Data (2/2)				
Ansys element	Convection Coef. (αc)	View Factor (Ø)		Temperature Curve
Plane 55: Steel, concrete, mineral wool and air convection. Link 31: radiation. Link 34: convection.	Exposed Surface: 25 W/(m² K) Unexposed Surface: 9 W/(m² K)	$Ø_{LOWER}$	1	Exposed Surface: ISO-834 Unexposed Surface: 20ºC
		$Ø_{WEB\ 2}$	0.6974	
		$Ø_{UPPER\ 2}$	0.9301	
		$Ø_{WEB\ 1}$	0.058	
		$Ø_{UPPER\ 1}$	0.064	

Temperature field

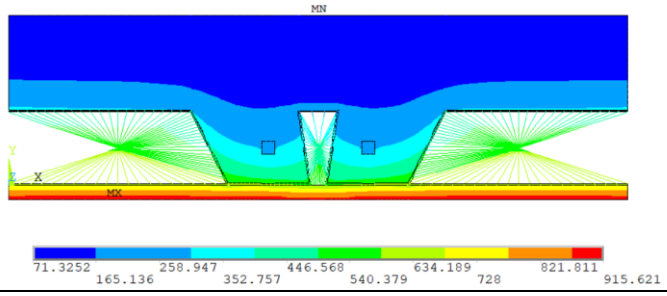

60 (min)

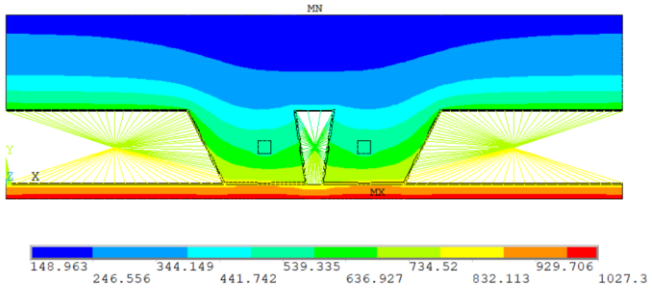

120 (min)

Temperature Graph - R

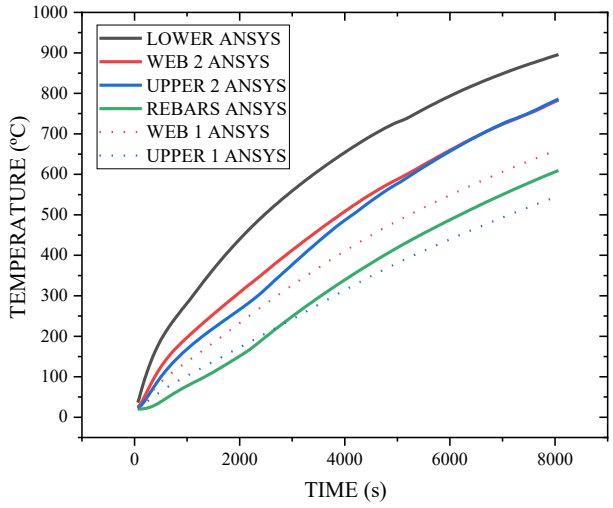

Temperature Graph - I

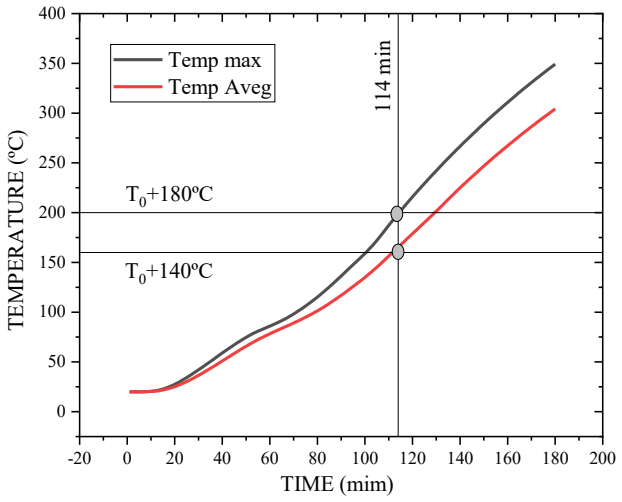

DATA SHEET			
Model 13: Slab 2 – VP50 – h1 = 65 mm			
Model 13 - Basic Data (1/2)			
Experimental type	Title: VP50 – h1 = 65 mm		
Parametric study	Author: Otávio G. N. Ribeiro		Year: 2024
Detailing			
Steel Deck	Concrete	Steel Bars	Insulation type
Geometry: VP-50 Thickness: 0.8mm Grade: ISQ 230 Steel galvanized 275	Density: Normal Weight Class: 25/30 Moisture: 3.0%	Description: 2Ø10 Grade: S450	Mineral wool plate hi = 20 mm $\rho = 70 \frac{kg}{m^3}$

Cross – Section

L1 R (mm)	30
L2 R (mm)	55
L3 R (mm)	25
L1 T (mm)	165
L2 T (mm)	115
L3 T (mm)	250
h1 (mm)	65
h2 T (mm)	50
h2 R (mm)	50

Mesh size

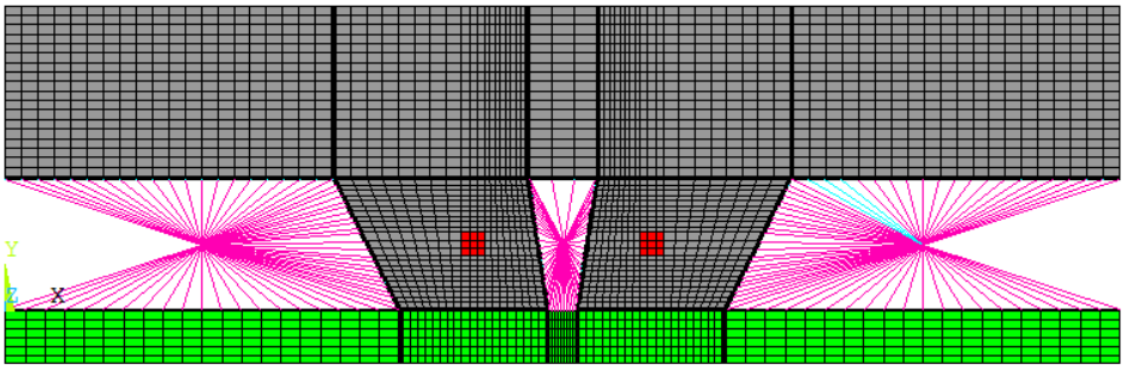

Model 13 - Basic Data (2/2)				
Ansys element	Convection Coef. (αc)	View Factor (Ø)		Temperature Curve
Plane 55: Steel, concrete, mineral wool and air convection. Link 31: radiation. Link 34: convection.	Exposed Surface: 25 W/(m² K) Unexposed Surface: 9 W/(m² K)	$Ø_{LOWER}$	1	Exposed Surface: ISO-834 Unexposed Surface: 20ºC
		$Ø_{WEB\ 2}$	0.6974	
		$Ø_{UPPER\ 2}$	0.9301	
		$Ø_{WEB\ 1}$	0.058	
		$Ø_{UPPER\ 1}$	0.064	

Temperature field

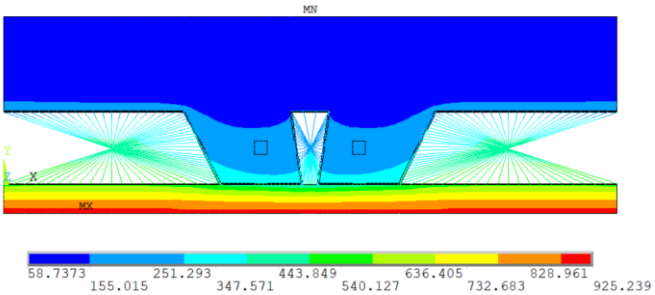

60 (min)

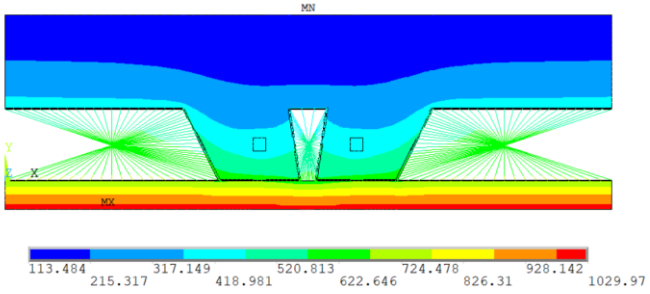

120 (min)

Temperature Graph - R

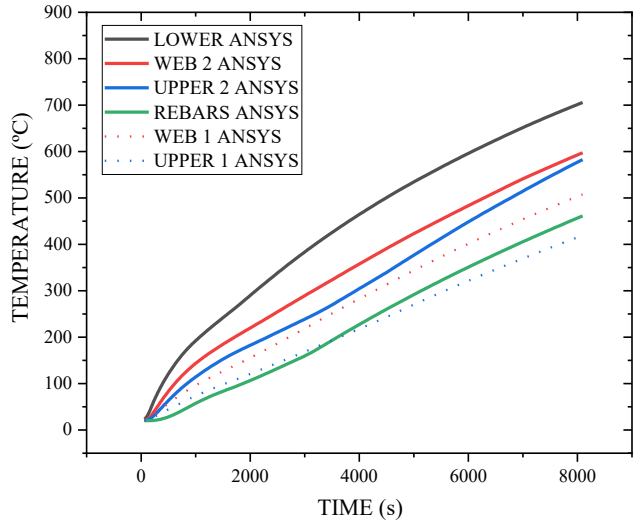

Temperature Graph - I

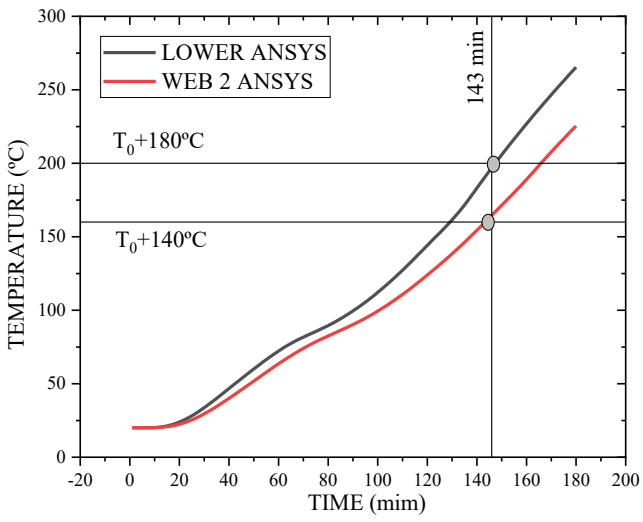

DATA SHEET			
Model 14: Slab 2 – VP50 – h1 = 65 mm			
Model 14 - Basic Data (1/2)			
Experimental type	Title: VP50 – h1 = 65 mm		
Parametric study	Author: Otávio G. N. Ribeiro		Year: 2024
Detailing			
Steel Deck	Concrete	Steel Bars	Insulation type
Geometry: VP-50 Thickness: 0.8mm Grade: ISQ 230 Steel galvanized 275	Density: Normal Weight Class: 25/30 Moisture: 3.0%	Description: 2Ø10 Grade: S450	Mineral wool plate hi = 30 mm $\rho = 70 \frac{kg}{m^3}$

Cross – Section

L1 R (mm)	30
L2 R (mm)	55
L3 R (mm)	25
L1 T (mm)	165
L2 T (mm)	115
L3 T (mm)	250
h1 (mm)	65
h2 T (mm)	50
h2 R (mm)	50

Mesh size

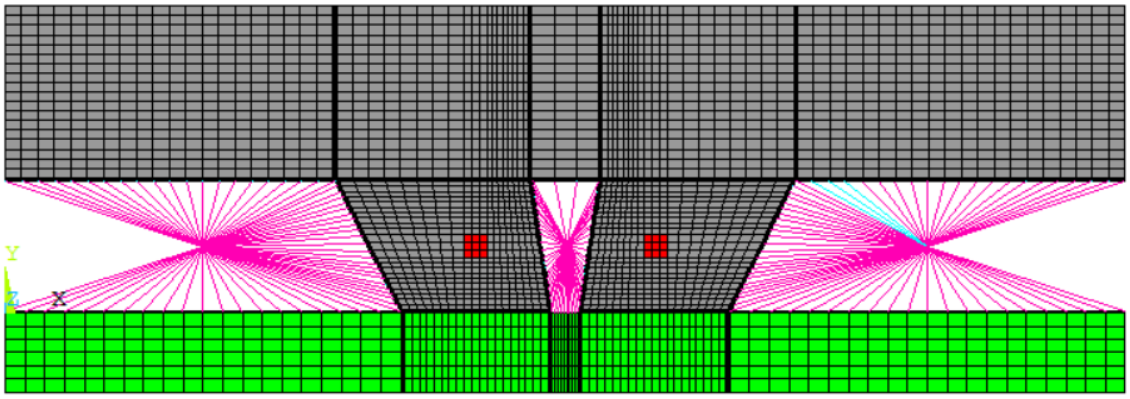

Model 14 - Basic Data (2/2)				
Ansys element	Convection Coef. (αc)	View Factor (Ø)		Temperature Curve
Plane 55: Steel, concrete, mineral wool and air convection. Link 31: radiation. Link 34: convection.	Exposed Surface: 25 W/(m² K) Unexposed Surface: 9 W/(m² K)	$Ø_{LOWER}$	1	Exposed Surface: ISO-834 Unexposed Surface: 20ºC
		$Ø_{WEB\ 2}$	0.6974	
		$Ø_{UPPER\ 2}$	0.9301	
		$Ø_{WEB\ 1}$	0.058	
		$Ø_{UPPER\ 1}$	0.064	

Temperature field

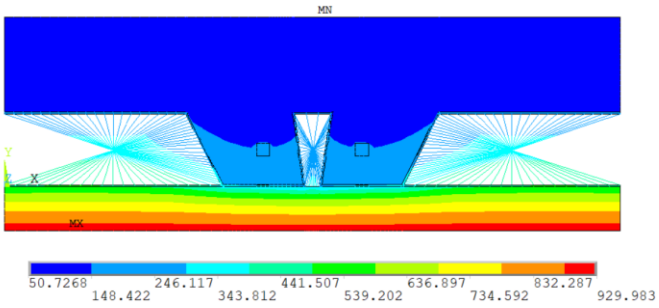

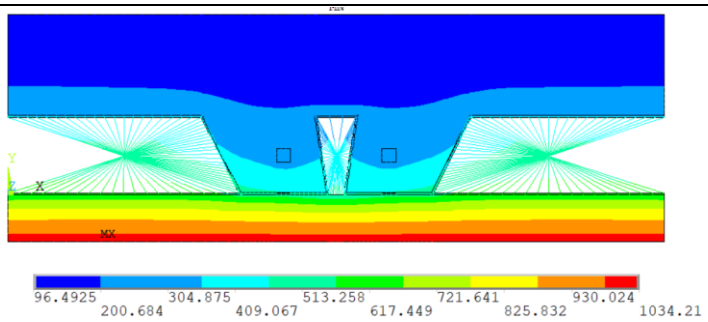

60 (min) | 120 (min)

Temperature Graph - R

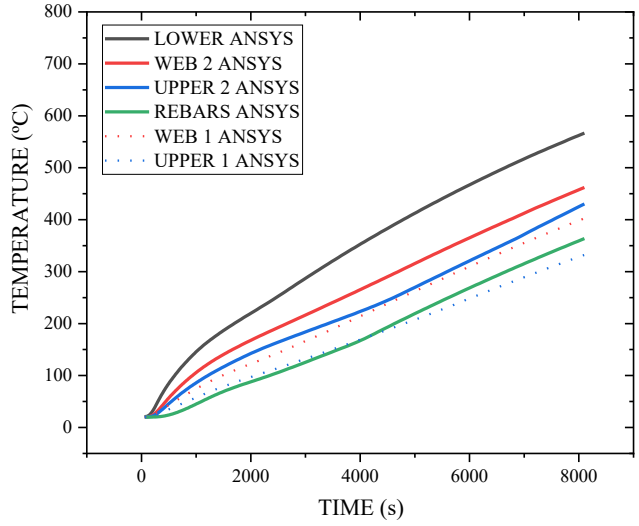

Temperature Graph - I

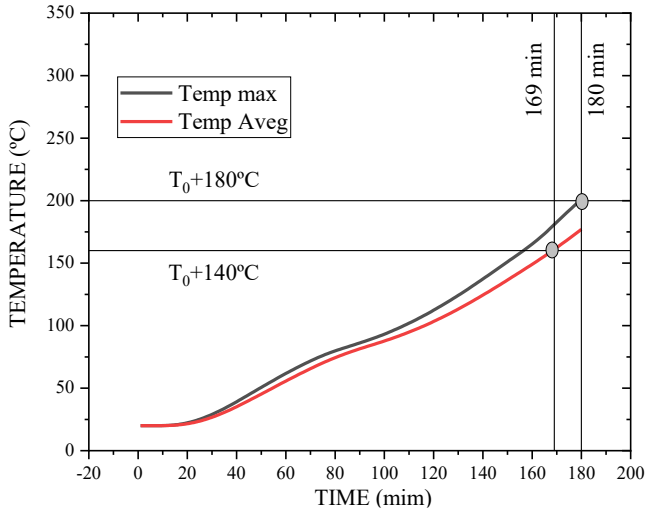

DATA SHEET			
Model 15 Slab 3 – VP200 – h1 = 65 mm			
Model 15 - Basic Data (1/2)			
Experimental type	Title: VP200 – h1 = 65 mm		
Parametric study	Author: Otávio G. N. Ribeiro		Year: 2024
Detailing			
Steel Deck	Concrete	Steel Bars	Insulation type
Geometry: VP-200 Thickness: 0.8mm Grade: ISQ 230 Steel galvanized 275	Density: Normal Weight Class: 25/30 Moisture: 3.0%	Description: 2Ø10 Grade: S450	steel shield
Cross – Section			

L1 R (mm)	85
L2 R (mm)	110
L3 R (mm)	25
L1 T (mm)	300
L2 T (mm)	230
L3 T (mm)	460
h1 (mm)	65
h2 T (mm)	200
h2 R (mm)	50

Mesh size

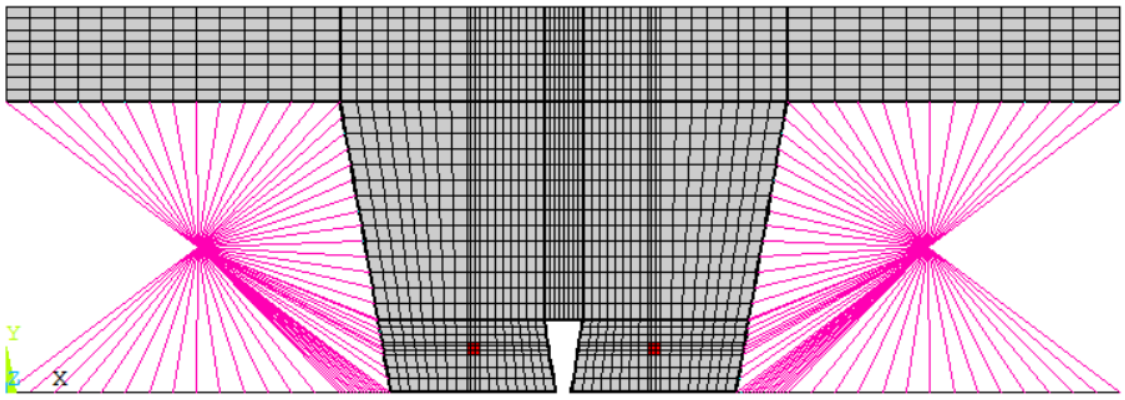

Model 15 - Basic Data (2/2)				
Ansys element	Convection Coef. (αc)	View Factor (Ø)		Temperature Curve
Plane 55: Steel, concrete and air convection. Link 31: radiation. Link 34: convection.	Exposed Surface: 25 W/(m² K) Unexposed Surface: 9 W/(m² K)	$Ø_{LOWER}$	1	Exposed Surface: ISO-834 Unexposed Surface: 20ºC
		$Ø_{WEB\ 2}$	0.48	
		$Ø_{UPPER\ 2}$	0.7125	
		$Ø_{WEB\ 1}$	0.058	
		$Ø_{UPPER\ 1}$	0.064	

Temperature field

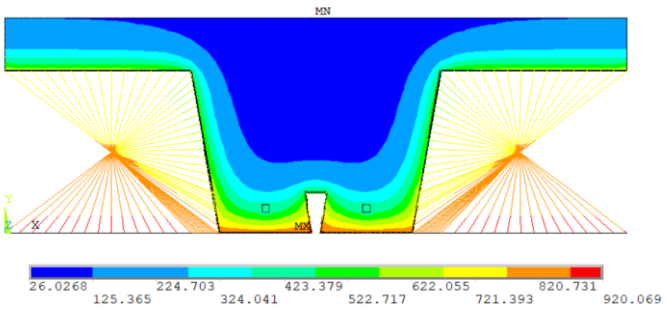

60 (min)

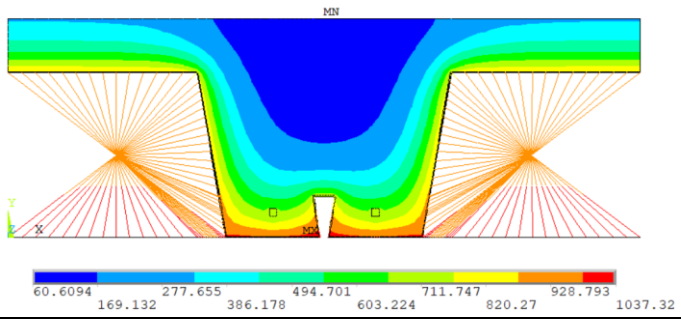

120 (min)

Temperature Graph - R

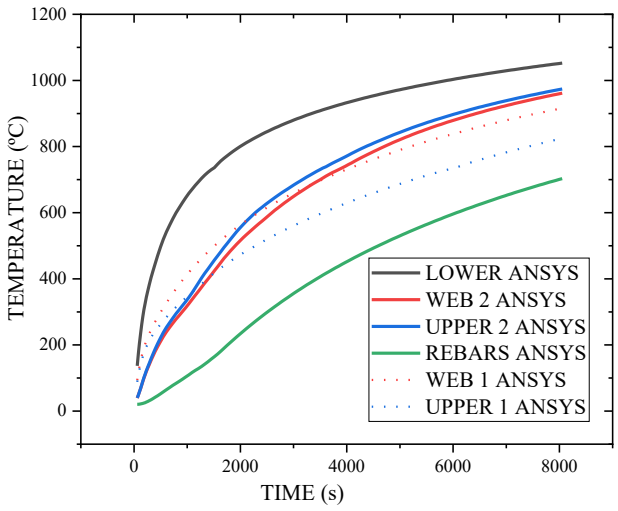

Temperature Graph - I

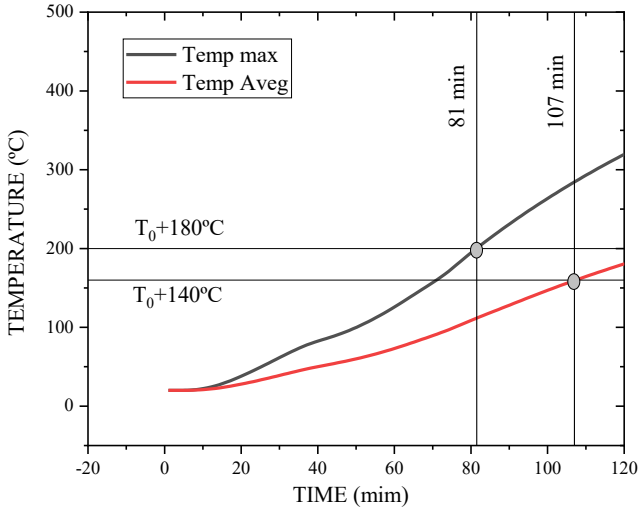

DATA SHEET			
Model 16 Slab 3 – VP200 – h1 = 65 mm			
Model 16 - Basic Data (1/2)			
Experimental type	Title: VP200 – h1 = 65 mm		
Parametric study	Author: Otávio G. N. Ribeiro		Year: 2024
Detailing			
Steel Deck	Concrete	Steel Bars	Insulation type
Geometry: VP-200 Thickness: 0.8mm Grade: ISQ 230 Steel galvanized 275	Density: Normal Weight Class: 25/30 Moisture: 3.0%	Description: 2Ø10 Grade: S450	Without insulation
Cross – Section			

L1 R (mm)	85
L2 R (mm)	110
L3 R (mm)	25
L1 T (mm)	300
L2 T (mm)	230
L3 T (mm)	460
h1 (mm)	65
h2 T (mm)	200
h2 R (mm)	50

Mesh size

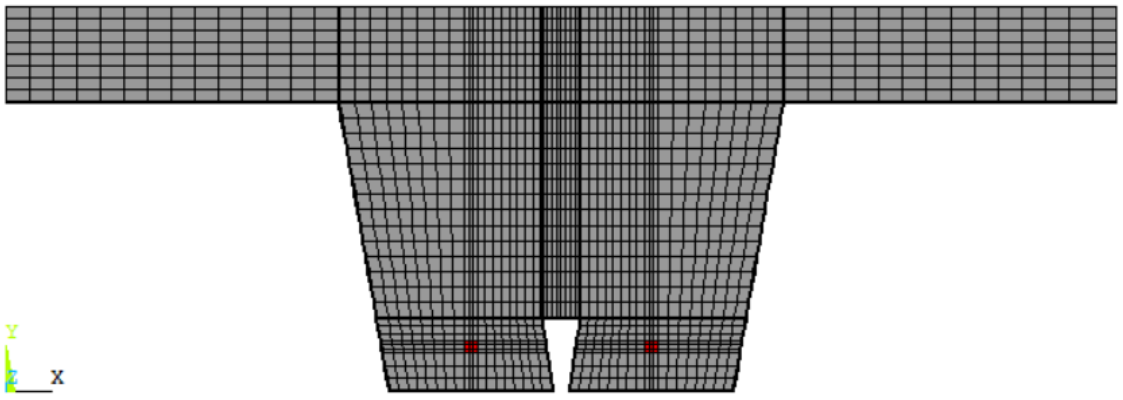

Model 16 - Basic Data (2/2)				
Ansys element	Convection Coef. (αc)	View Factor (Ø)		Temperature Curve
Plane 55: Steel, concrete and air convection.	Exposed Surface: 25 W/(m² K) Unexposed Surface: 9 W/(m² K)	$Ø_{LOWER}$	1	Exposed Surface: ISO-834 Unexposed Surface: 20ºC
		$Ø_{WEB\ 2}$	0.48	
		$Ø_{UPPER\ 2}$	0.7125	
		$Ø_{WEB\ 1}$	0.058	
		$Ø_{UPPER\ 1}$	0.064	

Temperature field

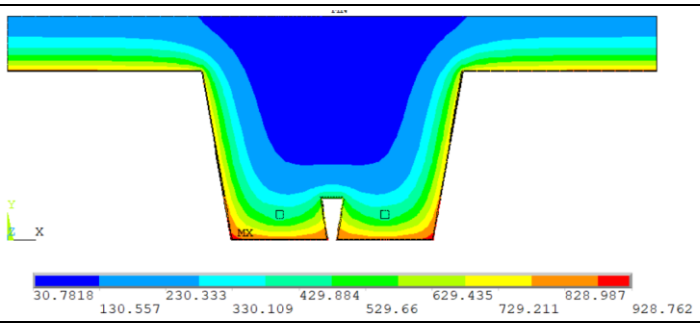

60 (min)

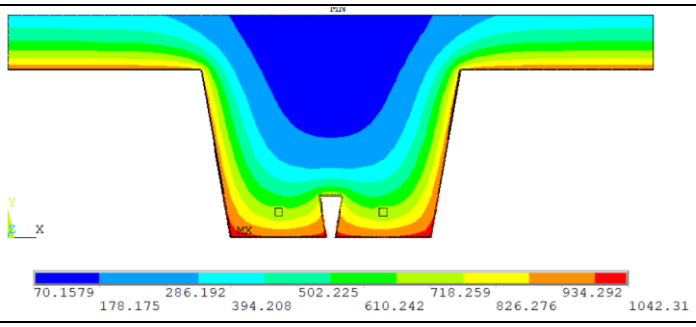

120 (min)

Temperature Graph - R

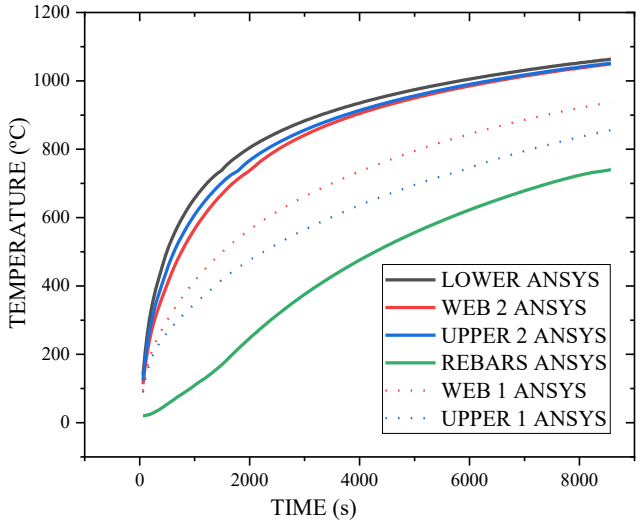

Temperature Graph - I

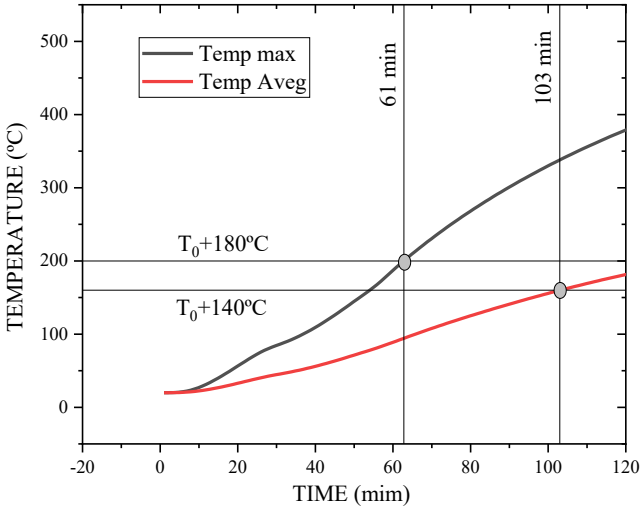

DATA SHEET			
Model 17 Slab 3 – VP200 – h1 = 65 mm			
Model 17 - Basic Data (1/2)			
Experimental type	Title: VP200 – h1 = 65 mm		
Parametric study	Author: Otávio G. N. Ribeiro		Year: 2024
Detailing			
Steel Deck	Concrete	Steel Bars	Insulation type
Geometry: VP-200 Thickness: 0.8mm Grade: ISQ 230 Steel galvanized 275	Density: Normal Weight Class: 25/30 Moisture: 3.0%	Description: 2Ø10 Grade: S450	Mineral wool
Cross – Section			

L1 R (mm)	85
L2 R (mm)	110
L3 R (mm)	25
L1 T (mm)	300
L2 T (mm)	230
L3 T (mm)	460
h1 (mm)	65
h2 T (mm)	200
h2 R (mm)	50

Mesh size

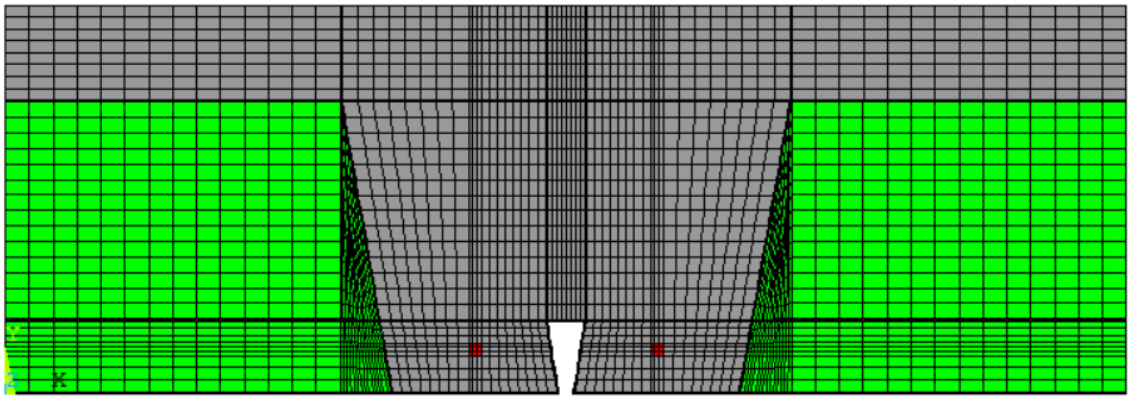

Model 17 - Basic Data (2/2)				
Ansys element	Convection Coef. (αc)	View Factor (Ø)		Temperature Curve
Plane 55: Steel, concrete, mineral wool and air convection.	Exposed Surface: 25 W/(m² K) Unexposed Surface: 9 W/(m² K)	$Ø_{LOWER}$	1	Exposed Surface: ISO-834 Unexposed Surface: 20ºC
		$Ø_{WEB\ 2}$	0.48	
		$Ø_{UPPER\ 2}$	0.7125	
		$Ø_{WEB\ 1}$	0.058	
		$Ø_{UPPER\ 1}$	0.064	

Temperature field

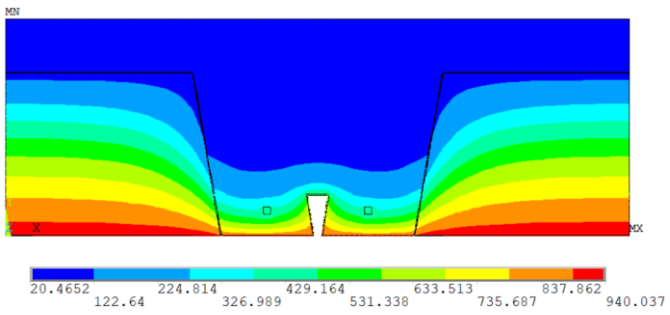

60 (min)

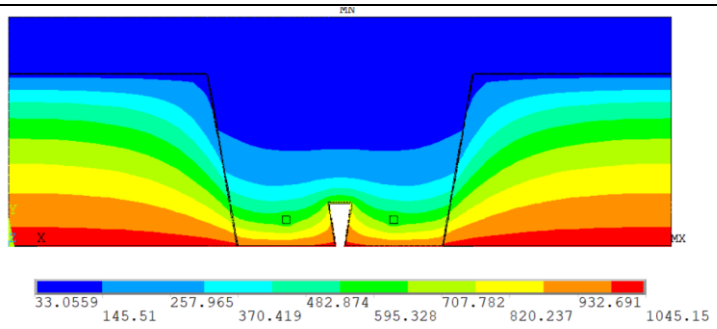

120 (min)

Temperature Graph - R

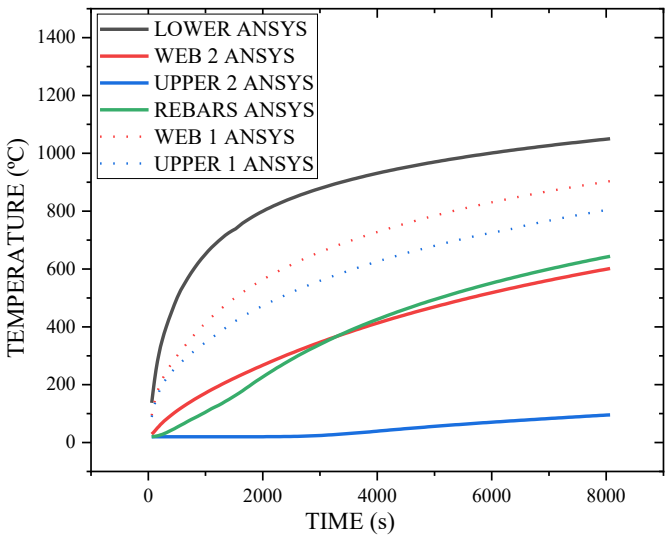

Temperature Graph - I

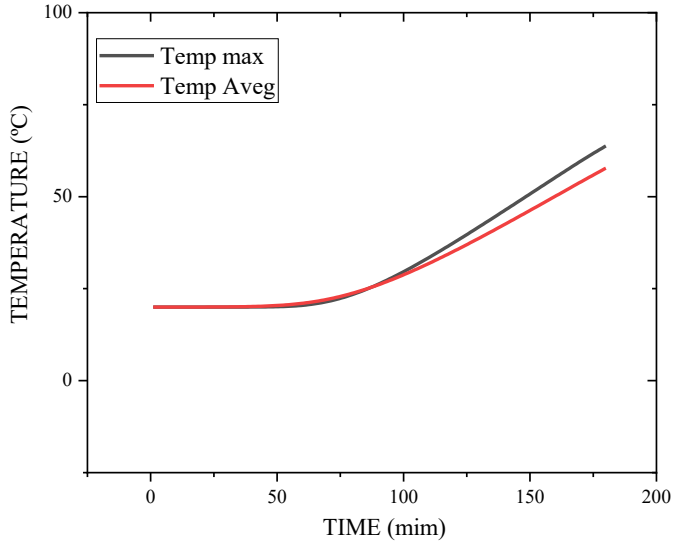

DATA SHEET			
Model 18 Slab 3 – VP200 – h1 = 65 mm			
Model 18 - Basic Data (1/2)			
Experimental type	Title: VP200 – h1 = 65 mm		
Parametric study	Author: Otávio G. N. Ribeiro		Year: 2024
Detailing			
Steel Deck	Concrete	Steel Bars	Insulation type
Geometry: VP-200 Thickness: 0.8mm Grade: ISQ 230 Steel galvanized 275	Density: Normal Weight Class: 25/30 Moisture: 3.0%	Description: 2Ø10 Grade: S450	Mineral wool plate hi = 5 mm $\rho = 70 \frac{kg}{m^3}$

Cross – Section

L1 R (mm)	85
L2 R (mm)	110
L3 R (mm)	25
L1 T (mm)	300
L2 T (mm)	230
L3 T (mm)	460
h1 (mm)	65
h2 T (mm)	200
h2 R (mm)	50

Mesh size

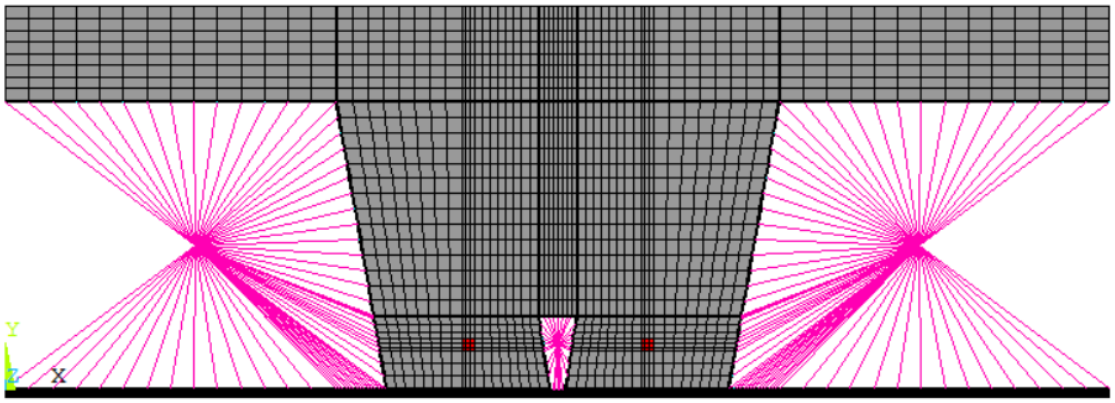

Model 18 - Basic Data (2/2)				
Ansys element	Convection Coef. (αc)	View Factor (Ø)		Temperature Curve
Plane 55: Steel, concrete, mineral wool and air convection. Link 31: radiation. Link 34: convection.	Exposed Surface: 25 W/(m² K) Unexposed Surface: 9 W/(m² K)	$Ø_{LOWER}$	1	Exposed Surface: ISO-834 Unexposed Surface: 20ºC
		$Ø_{WEB\ 2}$	0.48	
		$Ø_{UPPER\ 2}$	0.7125	
		$Ø_{WEB\ 1}$	0.058	
		$Ø_{UPPER\ 1}$	0.064	

Temperature field

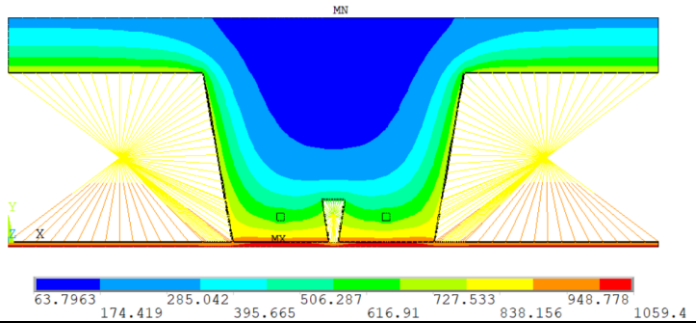

60 (min)

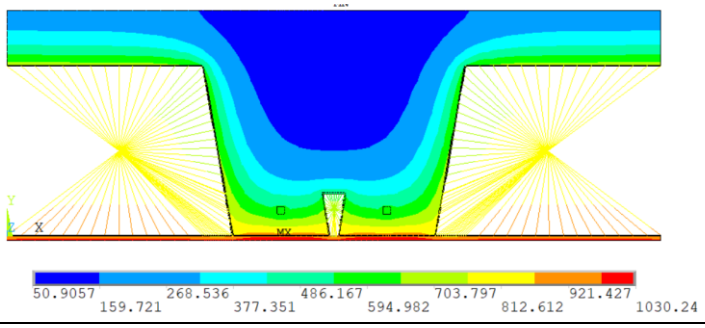

120 (min)

Temperature Graph - R

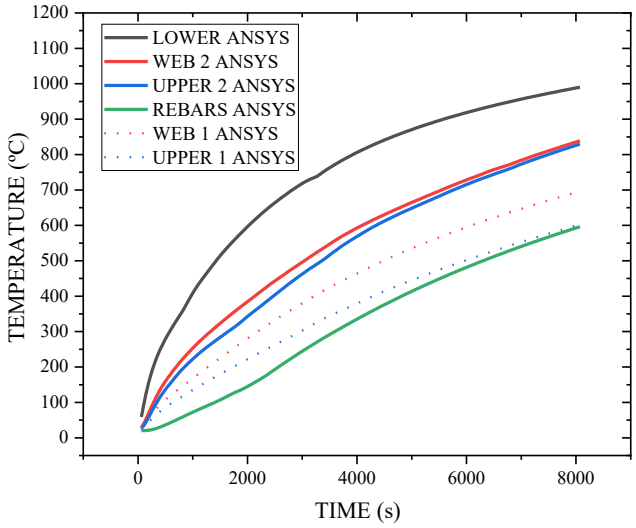

Temperature Graph - I

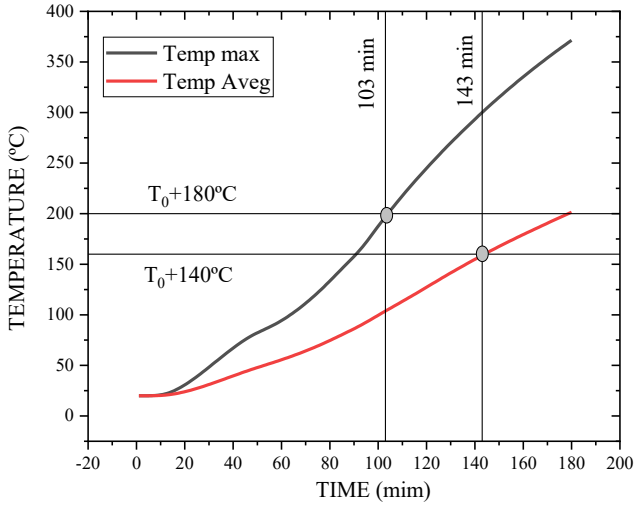

DATA SHEET			
Model 19 Slab 3 – VP200 – h1 = 65 mm			
Model 19 - Basic Data (1/2)			
Experimental type	Title: VP200 – h1 = 65 mm		
Parametric study	Author: Otávio G. N. Ribeiro		Year: 2024
Detailing			
Steel Deck	Concrete	Steel Bars	Insulation type
Geometry: VP-200 Thickness: 0.8mm Grade: ISQ 230 Steel galvanized 275	Density: Normal Weight Class: 25/30 Moisture: 3.0%	Description: 2Ø10 Grade: S450	Mineral wool plate hi = 10 mm $\rho = 70 \frac{kg}{m^3}$
Cross – Section			

L1 R (mm)	85
L2 R (mm)	110
L3 R (mm)	25
L1 T (mm)	300
L2 T (mm)	230
L3 T (mm)	460
h1 (mm)	65
h2 T (mm)	200
h2 R (mm)	50

Mesh size

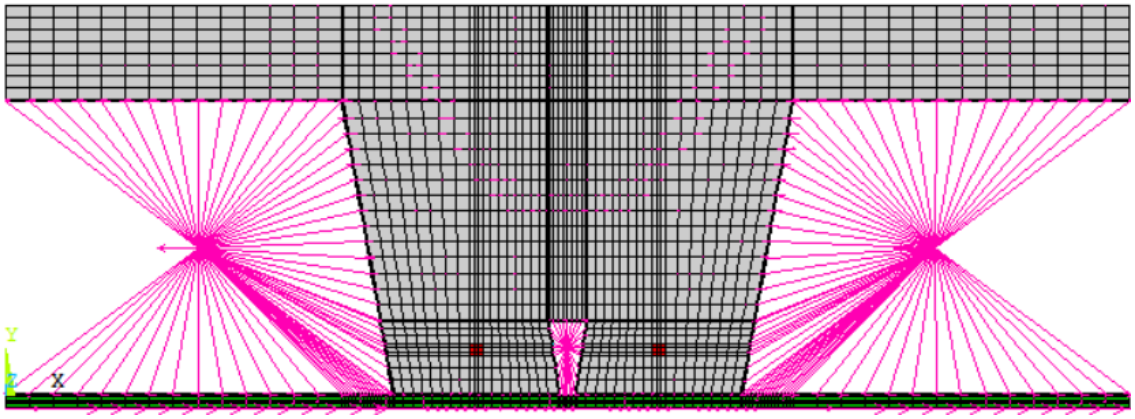

Model 19 - Basic Data (2/2)				
Ansys element	Convection Coef. (αc)	View Factor (Ø)		Temperature Curve
Plane 55: Steel, concrete, mineral wool and air convection. Link 31: radiation. Link 34: convection.	Exposed Surface: 25 W/(m^2 K) Unexposed Surface: 9 W/(m^2 K)	$Ø_{LOWER}$	1	Exposed Surface: ISO-834 Unexposed Surface: 20ºC
		$Ø_{WEB\ 2}$	0.48	
		$Ø_{UPPER\ 2}$	0.7125	
		$Ø_{WEB\ 1}$	0.058	
		$Ø_{UPPER\ 1}$	0.064	

Temperature field

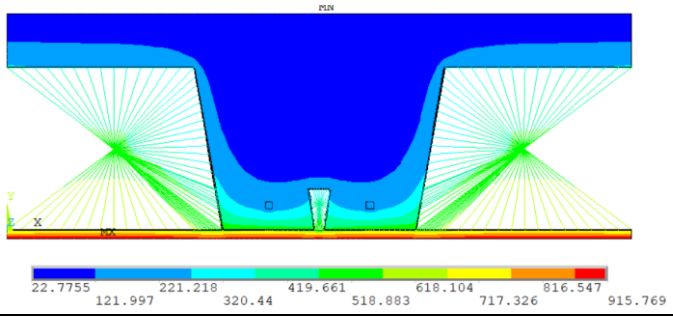

60 (min)

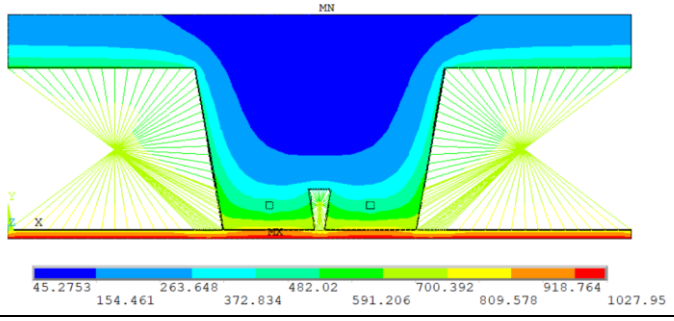

120 (min)

Temperature Graph - R

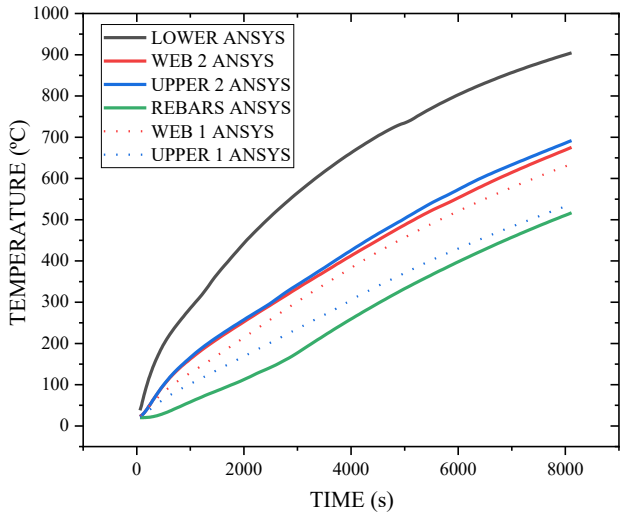

Temperature Graph - I

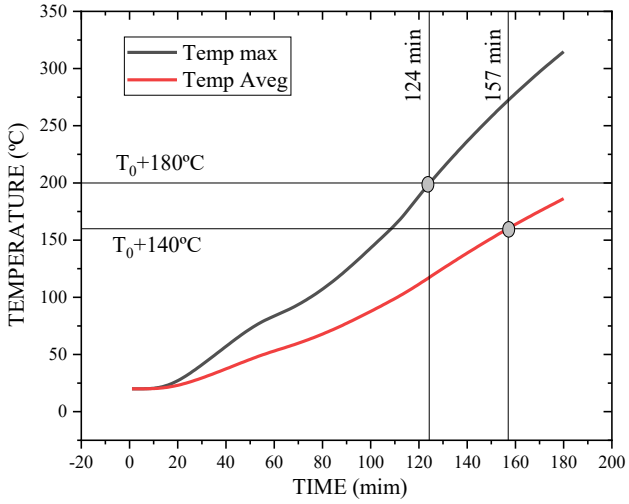

DATA SHEET			
Model 20 Slab 3 – VP200 – h1 = 65 mm			
Model 20 - Basic Data (1/2)			
Experimental type	Title: VP200 – h1 = 65 mm		
Parametric study	Author: Otávio G. N. Ribeiro		Year: 2024
Detailing			
Steel Deck	Concrete	Steel Bars	Insulation type
Geometry: VP-200 Thickness: 0.8mm Grade: ISQ 230 Steel galvanized 275	Density: Normal Weight Class: 25/30 Moisture: 3.0%	Description: 2Ø10 Grade: S450	Mineral wool plate hi = 20 mm $\rho = 70 \frac{kg}{m^3}$

Cross – Section

L1 R (mm)	85
L2 R (mm)	110
L3 R (mm)	25
L1 T (mm)	300
L2 T (mm)	230
L3 T (mm)	460
h1 (mm)	65
h2 T (mm)	200
h2 R (mm)	50

Mesh size

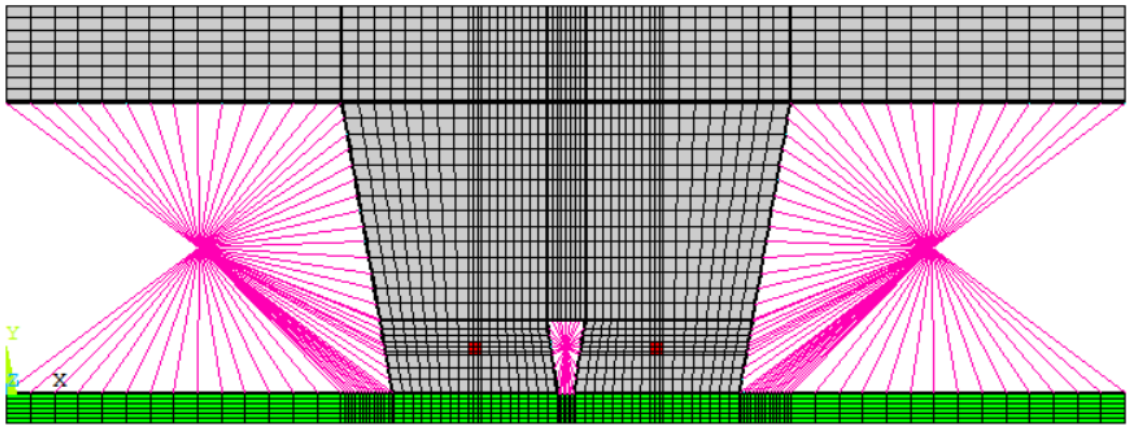

Model 20 - Basic Data (2/2)				
Ansys element	Convection Coef. (αc)	View Factor (Ø)		Temperature Curve
Plane 55: Steel, concrete, mineral wool and air convection. Link 31: radiation. Link 34: convection.	Exposed Surface: 25 W/(m² K) Unexposed Surface: 9 W/(m² K)	$Ø_{LOWER}$	1	Exposed Surface: ISO-834 Unexposed Surface: 20ºC
		$Ø_{WEB\ 2}$	0.48	
		$Ø_{UPPER\ 2}$	0.7125	
		$Ø_{WEB\ 1}$	0.058	
		$Ø_{UPPER\ 1}$	0.064	

Temperature field

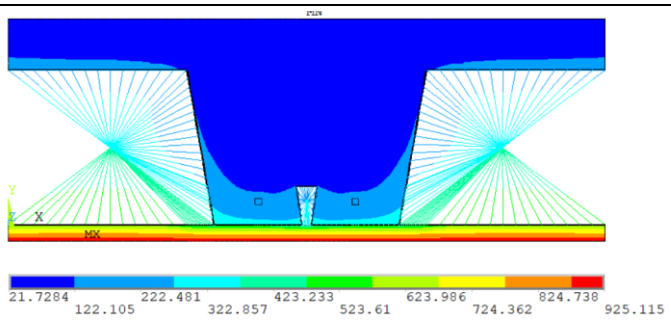

60 (min)

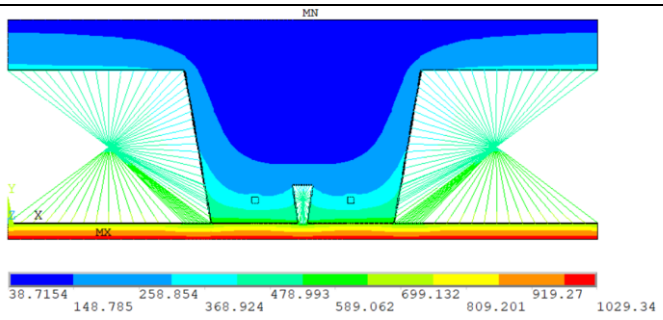

120 (min)

Temperature Graph - R

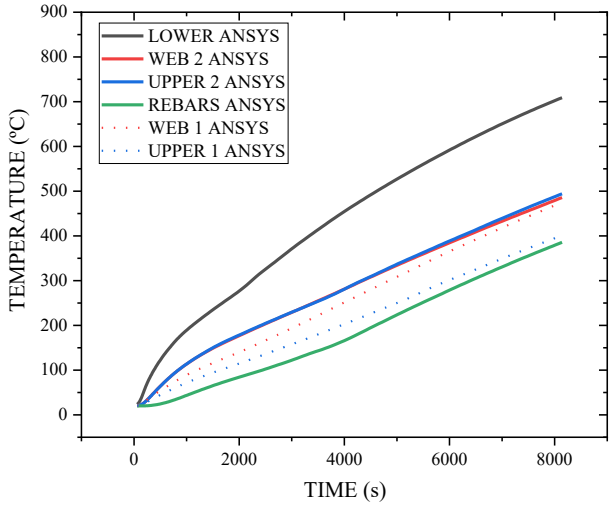

Temperature Graph - I

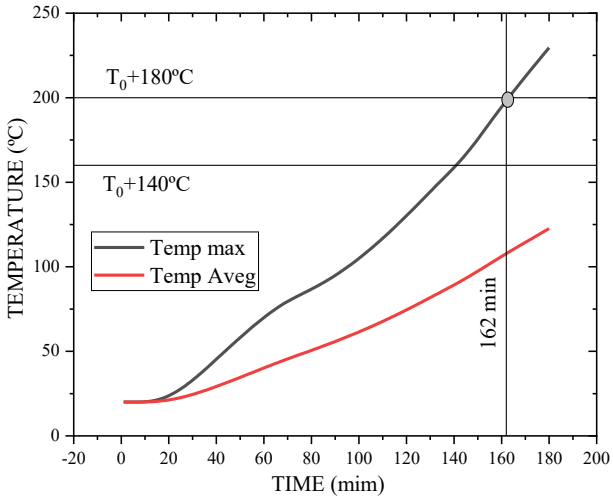

DATA SHEET			
Model 21 Slab 3 – VP200 – h1 = 65 mm			
Model 21 - Basic Data (1/2)			
Experimental type	Title: VP200 – h1 = 65 mm		
Parametric study	Author: Otávio G. N. Ribeiro		Year: 2024
Detailing			
Steel Deck	Concrete	Steel Bars	Insulation type
Geometry: VP-200 Thickness: 0.8mm Grade: ISQ 230 Steel galvanized 275	Density: Normal Weight Class: 25/30 Moisture: 3.0%	Description: 2Ø10 Grade: S450	Mineral wool plate hi = 30 mm $\rho = 70 \frac{kg}{m^3}$
Cross – Section			

L1 R (mm)	85
L2 R (mm)	110
L3 R (mm)	25
L1 T (mm)	300
L2 T (mm)	230
L3 T (mm)	460
h1 (mm)	65
h2 T (mm)	200
h2 R (mm)	50

Mesh size

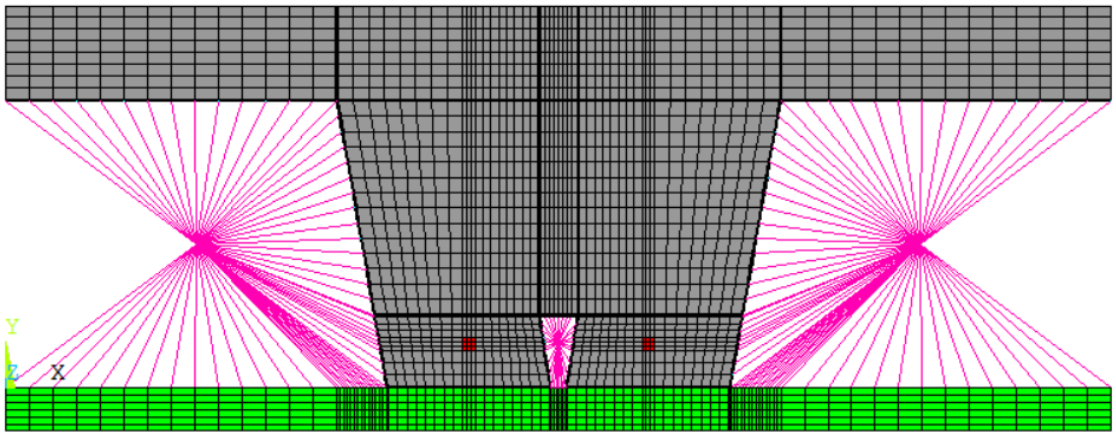

Model 21 - Basic Data (2/2)				
Ansys element	Convection Coef. (αc)	View Factor (Ø)		Temperature Curve
Plane 55: Steel, concrete, mineral wool and air convection. Link 31: radiation. Link 34: convection.	Exposed Surface: 25 W/(m² K) Unexposed Surface: 9 W/(m² K)	$Ø_{LOWER}$	1	Exposed Surface: ISO-834 Unexposed Surface: 20ºC
		$Ø_{WEB\ 2}$	0.48	
		$Ø_{UPPER\ 2}$	0.7125	
		$Ø_{WEB\ 1}$	0.058	
		$Ø_{UPPER\ 1}$	0.064	

Temperature field

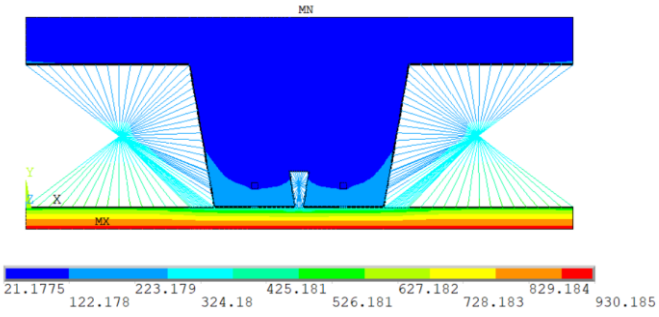

60 (min)

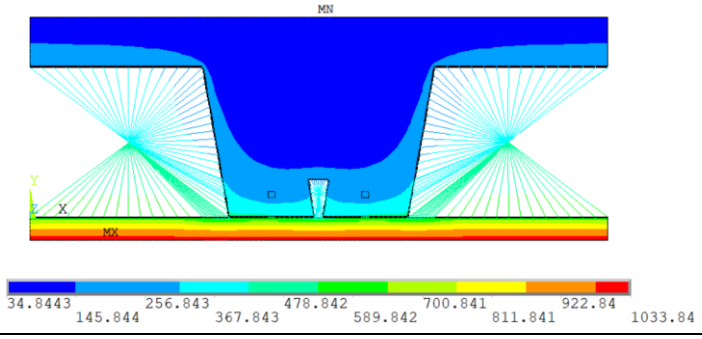

120 (min)

Temperature Graph - R

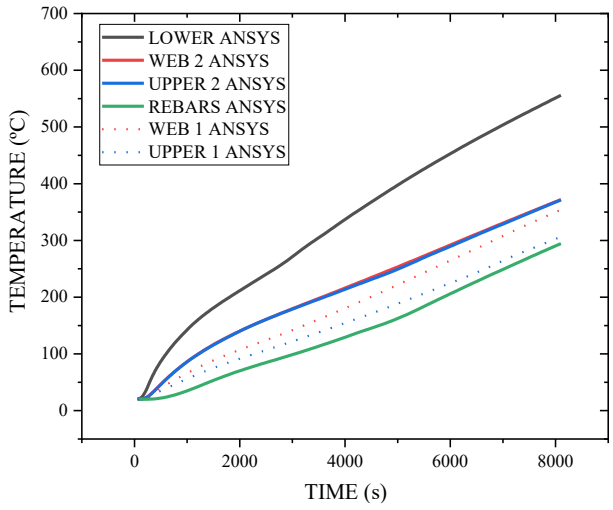

Temperature Graph - I